

KRAS-dependent Extracellular Vesicles in Colorectal Cancer: Cargo, Biogenesis, and Function

By  
Scott A. Hinger

Dissertation

Submitted to the Faculty of the  
Graduate School of Vanderbilt University

in partial fulfillment of the requirements

for the degree of

DOCTOR OF PHILOSOPHY

in

Biological Sciences

January 31, 2020

Nashville, Tennessee

Approved:

Todd R. Graham, Ph.D.

James G. Patton Ph.D.

Robert J. Coffey, M.D.

Lauren P. Jackson, Ph.D.

Jared T. Nordman, Ph.D.

This work is dedicated to the following loved ones:

To my loving parents, Dan and Sue Hinger, for the continuous love and support of both my education and well-being.

To my brother Matt Hinger, for the continuous brotherly support and love.

To my amazing Ohioan friends, Matt, Steve, Trevor, John, Arslan, Ameya, Jake, Anthony, Daniel F., Daniel K., Marissa, Wes, Aaron, and Suraj, for unbelievable love, support, and friendship, without which I could not have made it this far.

To my IGP friends, Justine, Andy, Rachel, Jordan, Sean, David, Greg, James, and Hunter, for the newly found friendships I have made here over the last six years.

To my previous scientific mentors, Dr. Juan D. Alfonzo and Dr. Mary Anne Rubio, for giving me an early opportunity to find joy and happiness in research science. Without you this work would have not come to fruition.

## Acknowledgements

This work would not have been possible without the financial support of Vanderbilt University Department of Biological Sciences. It is without question that I am here because of my advisor, Dr. James Patton, who has always aided and encouraged scientific independence and has pushed me to grow in all aspects of my research career. I would like to further acknowledge Dr. Juan Alfonzo and Dr. Mary Anne Rubio, who, as a bright-eyed freshman at Ohio State University, took me under their scientific wings, and gave me every opportunity to learn and grow, establishing my current love for science. I am grateful for the many collaborators I have had here at Vanderbilt University, especially Dr. Robert Coffey, Dr. Alissa Weaver, Dr. Jeffrey Franklin, Dr. Kasey Vickers, Dr. Qi Liu, and Dr. John Karijovich. Your mentorship and support were imperative to the completion of all work described here. Further, I am grateful for all of the members, current and past, of the Patton Laboratory, especially Dr. Diana Cha, Dr. Mahesh Rao, Dr. Dominic Didiano, and Jessica Abner, both for your friendship and constructive criticism throughout my graduate school experience.

This work was supported by grants from the National Institutes of Health, U19CA17951.

## Table of Contents

	Page
Dedication.....	ii
Acknowledgements.....	iii
List of Tables .....	viii
List of Figures .....	ix
 <b>Chapter</b>	
1. Introduction .....	1
1.1 Extracellular vesicle biogenesis .....	3
1.1.1 Microvesicle biogenesis .....	4
1.1.2 Exosome biogenesis .....	5
1.1.3 Rab proteins in extracellular vesicle biogenesis .....	9
1.1.3.1 Rab13 and its intracellular role .....	13
1.2 Extracellular vesicle cargo .....	16
1.2.1 Extracellular RNA.....	17
1.2.1.1 mRNAs.....	17
1.2.1.2 lncRNAs.....	18
1.2.1.3 miRNAs.....	21
1.2.2 Extracellular proteins.....	25
1.3 Functional significance of extracellular vesicles.....	27
1.3.1 Functional significance in cancer.....	28
1.4 Conclusions.....	33
2. Diverse long-RNAs are differentially sorted into extracellular vesicles secreted by colorectal cancer cells.....	35
2.1 Abstract.....	35
2.2 Introduction.....	36
2.3 Results .....	38
2.3.1 Comparison of long RNAs in cells versus EVs .....	38
2.3.2 Differential RNA export and KRAS status.....	42
2.3.3 Differential enrichment of ncRNAs and mRNAs in EVs .....	43
2.3.4 mRNA export into EVs .....	44
2.3.5 lncRNA export into EVs.....	45

2.3.6 Extracellular transfer of mRNA .....	45
2.3.7 Extracellular transfer of lncRNA .....	47
2.4 Discussion .....	52
2.4.1 Selective export and functional transfer of RNA .....	52
2.4.2 Size limitations on EV transfer.....	53
2.4.3 Mechanisms of RNA export.....	54
2.5 Methods .....	55
2.5.1 EV isolation .....	55
2.5.2 RNA purification .....	56
2.5.3 mRNA library preparation and sequencing.....	56
2.5.4 Read mapping.....	57
2.5.5 Gene ontology.....	57
2.5.6 Data availability .....	57
2.5.7 RT-PCR and RT-qPCR .....	58
2.5.8 Plasmid construction .....	59
2.5.9 Transfection .....	59
2.5.10 Protein collection and western blotting .....	60
2.5.11 Transwell co-culture assays .....	60
2.6 Acknowledgements .....	62
2.7 Author contributions.....	62
2.A Appendix.....	63
2.A.1 Pairwise replicate analysis.....	63
2.A.2 Effects of serum starvation and ionomycin treatment on cellular RNA profiles.....	64
2.A.3 Table. Top 100 KRAS independent upregulated EV RNAs .....	65
2.A.4 Gene ontology .....	68
2.A.5 mRNA RNA-seq read profiles .....	69
2.A.6 Validation of RNA-seq .....	70
2.A.7 Extracellular transfer of <i>Rab13</i> mRNA .....	71
2.A.8 RT-PCR of gRNAs in DKO-1 EVs.....	72
3. Rab13 regulates sEV secretion in mutant <i>KRAS</i> colorectal cancer cells .....	73
3.1 Abstract .....	73
3.2 Introduction.....	74
3.3 Results .....	77
3.3.1 Rab13 regulates sEV secretion in a KRAS-dependent manner.....	77
3.3.2 Rab13 regulates anchorage-independent growth via sEVs .....	78
3.3.3 Rab13 regulates the secretion of sEV markers .....	79

3.3.4 Rab13 and $\beta$ 1-integrin co-localize at the plasma membrane .....	79
3.3.5 $\beta$ 1-integrin is enriched in EVs.....	80
3.3.6 $\beta$ 1-integrin+ EVs are distinct from CD63+ exosomes .....	84
3.4 Discussion.....	86
3.4.1 Rab13 regulates EV secretion in mutant KRAS cells.....	86
3.4.2 Heterogeneity in sEV populations. ....	87
3.4.3 Rab13 localization and cell confluency.....	88
3.4.4 EV heterogeneity and extracellular RNA .....	88
3.5 Methods .....	89
3.5.1 Cell culture .....	89
3.5.2 Isolation of EVs .....	89
3.5.3 Nanoparticle tracking analysis (NTA) .....	90
3.5.4 Direct immunoaffinity capture of sEVs.....	90
3.5.5 Plasmid construction .....	91
3.5.6 Protein collection and western blotting .....	91
3.5.7 Transfection of shRNA plasmids and Rab13HA expression plasmids .....	92
3.5.8 Three-dimensional culturing of DKO-1 cells in type-1 collagen.....	92
3.5.9 Transwell proliferation assays .....	93
3.5.10 Transwell luciferase reporter assays .....	93
3.5.11 Proliferation assays.....	94
3.5.12 Soft agar assays .....	94
3.5.13 Immunocytochemistry .....	94
3.5.14 Transmission electron microscopy of EVs.....	95
3.6 Acknowledgements .....	95
3.7 Author contributions.....	96
3.A Appendix.....	97
3.A.1 NTA analysis of sEVs collected from DKO-1 and DKs-8 cells under Rab13 knockdown conditions.....	97
3.A.2 Proliferation of cells under Rab13 knockdown conditions.....	98
3.A.3 Transwell assay schematic.....	99
3.A.4 Rab13 regulates growth in type-1 collagen via sEV secretion.....	100
4. exRNA and cetuximab resistance .....	101
4.1 Abstract .....	101
4.2 Introduction.....	102
4.3 Results .....	105
4.3.1 <i>miR-100</i> and <i>miR-125b</i> are highly expressed in EVs derived from CTX resistance	

CRC Cells .....	105
4.3.2 CC-CR EVs can promote CTX resistance in CC cells .....	105
4.4 Discussion .....	106
4.5 Methods .....	107
4.5.1 Cell culture .....	107
4.5.2 EV isolation .....	108
4.5.3 RT-qPCR .....	108
4.5.1 Three-dimensional culturing of CC and CC-CR cells in type-1 collagen .....	109
4.A Appendix .....	110
4.A.1 miR-125b and miR-100 levels in CRC cell-derived EVs .....	110
5. Discussion .....	111
5.1 Limitations of long RNAs in EVs .....	112
5.2 Intracellular vs extracellular roles of Rab13 .....	116
5.3 Alternative mechanisms for EV-mediated CTX resistance in the CC/CC-CR model .....	120
References .....	123

## List of Tables

<b>Table</b>	<b>Page</b>
1. Known vesicle classes .....	3
2. Rab proteins in EV biogenesis .....	12
3. RNA subtypes found in EVs .....	19
4. Top 10 long RNAs enriched in EVs and KRAS mutant and WT cells. ....	46



## List of Figures

Figure	Page
1. Rab proteins in intracellular trafficking.....	11
2. Rab13 expression linked to decreased survival probability .....	15
3. Functional role of EVs in cancer .....	29
4. Evs as potential mediators of cancer therapeutic resistance .....	32
5. Long RNA-seq analysis of EV and cellular RNA from CRC cell lines.....	41
6. KRAS-dependent sorting of long RNAs into EVs.....	42
7. Extracellular transfer of Rab13 mRNA.....	48
8. Functional transfer of lncRNAs with CRISPR-Display. ....	50
9. Rab13 regulates EV secretion in a KRAS-dependent manner.....	76
10. Rab13 regulates and co-localizes with sEV markers. ....	81
11. Identification of $\beta$ 1-Integrin+, Rab13+ sEVs. ....	83
12. $\beta$ 1-Integrin+/Rab13+ EVs are distinct from CD63+ exosomes .....	85
13. <i>miR-100</i> And <i>miR-125b</i> are enriched in CC-CR EVs. ....	104
14. EVs from CC-CR cells confer CTX resistance to CC Cells. ....	106
15. Potential stoichiometric models for long RNAs in EVs. ....	114
16. Potential functions of Rab13 in epithelial cancer cell progression. ....	118

## Chapter 1

### Introduction

Extracellular vesicles (EVs) are membrane-derived vesicles released through a relatively conserved mechanism from plants to animals (Raposo and Stoorvogel, 2013). Although there has been a recent reemergence of interest in EVs, detection of small secreted vesicles was shown as early as 1971 in algae, with the first demonstration of human cell-derived EVs in 1981 (EBERHARD G. TRAMS, 1981). Human cells have been shown to secrete a variety of EVs and extracellular particles, including microvesicles, apoptotic bodies, exosomes, and exomeres (review, (Colombo et al., 2014b)). Although these vesicles are, for the most part, classified by their size, they can also be classified by their secretion pathway. Two of the most well studied biogenesis pathways include direct blebbing from the plasma membrane (e.g. microvesicles) (Muralidharan-Chari et al., 2009) or through the fusion of the late endosome (multivesicular body) with the plasma membrane, releasing its luminal contents (e.g. exosomes) (Rose M. Johnstone, 1987). Most common purification strategies are based on differential ultracentrifugation to isolate specific sizes of vesicles which limits the ability to distinguish between plasma membrane-derived or late endosome-derived vesicles. For this reason, the preferred nomenclature is to refer to all extracellular vesicles as EVs. Although there are a variety of vesicles, the majority of the focus within the field has been on small extracellular vesicles (sEVs), ranging in size from 30-100nm in diameter, and microvesicles (MVs), ranging in size from 100-1000nm in diameter (Muralidharan-Chari et al., 2009; Raposo et al., 1996). Over the past few years, it has become apparent that EVs play a critical role in cell-to-cell communication, with a heavy focus on how cargo selection is regulated and the mechanisms of biogenesis.

EVs contain diverse RNAs, proteins, and lipids (Colombo et al., 2014b). Extracellular RNA (exRNA) was first detected in 2007 from mouse mast cells which secrete functional mRNAs that can be taken up by recipient cells (Valadi et al., 2007). Since that time, almost all classes of RNA have been found to be secreted into the extracellular space, including mRNAs, long non-coding (lnc)RNAs, microRNAs (mi)RNAs, and other small non-coding RNAs (Cha et al., 2015a; Crescitelli et al., 2013; Dou et al., 2016; Hinger et al., 2018; Nolte-'t Hoen et al., 2012; Valadi et al., 2007).

Proteomic studies of EVs collected from various models has yielded extensive data (Demory Beckler et al., 2013; Kalra et al., 2012; They et al., 1999). EVs are reported to contain a wide range of proteins including cytoskeletal, cytosolic, plasma membrane and vesicular trafficking proteins. Many of these proteins have post-translational modifications that reflect their localization, origin, and, potentially, their mechanism of secretion (Moreno-Gonzalo et al., 2014). Interestingly, EVs have been shown to contain both cell receptors and receptor ligands, suggesting a mechanism for receptor signaling during cell-cell communication (Demory Beckler et al., 2013; Higginbotham et al., 2011; Singh and Coffey, 2014; Skog et al., 2008). This has been shown to be particularly important in neuronal signaling (Sharma et al., 2019), immune evasion (Schorey et al., 2015), and cancer progression in human cell models (Kalluri, 2016).

Cell-to-cell signaling via EVs has also been shown to play an important role in many physiologically relevant models, including development, neuronal disease, immune function, drug resistance, and cancer progression (review, (Colombo et al., 2014b)). Because of these functional findings, there has been an increase in interest in EV biogenesis and associated cargo. Current understanding of EV biogenesis is ongoing but thus far seems to be consistent with context-, cell-, and disease-specific mechanisms. Here, I will focus on what is currently

known about EV biogenesis, EV content, and the functional capacity of EVs, particularly in cancer cell models.

### 1.1 Extracellular vesicle biogenesis

The two most well characterized pathways for EV secretion include budding from the plasma membrane and fusion of late endosomes with the plasma membrane (review, (Abels and Breakefield, 2016)). These pathways lead to the production of what are classically referred to as microvesicles (MVs) and exosomes, respectively. Although there is partial overlap in size, cargo, and functional capacity, the mechanisms for biogenesis for these vesicles are distinct, and will be described below. Additional vesicle classes and their associated biogenesis pathway are described in **Table 1**.

**Table 1. Known Extracellular Particle Classes**

Name	EV Class	Biogenesis	Size
Oncosome	Large	PM budding	1-10 um
Apoptotic body	Large	Apoptosis	1-5 um
Apoptotic vesicle	Variable	Apoptosis	100-1000 nm
Classical microvesicle	Large	PM budding	150-1000 nm
(AARDC1)-mediated microvesicle	Small	PM budding	40-100 nm
Classical exosome	Small	MVB	40-150 nm
Non-classical exosome	Small	MVB	40-150 nm
Exomere	Nanoparticle	Unknown	35-50 nm
Non-vesicular aggregates	Nanoparticle	Unknown	N/A

### 1.1.1 Microvesicle biogenesis

MVs range from 100-1000nm in diameter and are secreted through the outward budding and fission of the plasma membrane (Cocucci et al., 2009; Muralidharan-Chari et al., 2009). These vesicles have also been termed 'ectosomes', or even 'microparticles' (Christoph Hess, 1999). It is important to note that there are cell-, disease-, and growth condition-specific mechanisms for MV secretion, and that the size of plasma-membrane derived vesicles is quite heterogeneous (Colombo et al., 2014b). Currently, there are two well-characterized mechanisms for MV biogenesis. MVs, like many other structural changes induced at the membrane, can be formed through the redistribution of phospholipids and the contraction of cellular cytoskeletal proteins. The formation of asymmetrical micro-domains by aminophospholipid translocases (i.e. flippases and floppases) and redistribution of phosphatidylserine to the outer leaflet leads to budding of the plasma membrane (Bénédicte Hugel, 2005; Edouard M. Bevers, 1999). Following the formation of these asymmetric lipid domains, MV release is completed when actin-myosin interactions lead to the contraction of cytoskeletal structures (McConnell et al., 2009; Muralidharan-Chari et al., 2009). In human melanoma cells, MV release occurs upon activation of ADP-ribosylation factor 6 (ARF6) leading to the activation of phospholipase D (PLD) (Muralidharan-Chari et al., 2009). PLD activation recruits extracellular signal-regulated kinase (ERK) to the plasma membrane, where it activates myosin light change kinase (MLCK) leading to the release of MVs from the plasma membrane (Muralidharan-Chari et al., 2009). In contrast, ARF1, and not ARF6, was found to be the driver of MV secretion in a breast cancer cell model, supporting comments above about cell-specific mechanisms for MV secretion (Schlienger et al., 2014). Why certain cells use one ARF isoform over another to drive MV secretion is not understood. Further, whether or not this system of MV biogenesis is used in other cancers remains to be determined. In fact, a recent study has shown

an ARF-independent mechanism for MV biogenesis where TSG101, an Endosomal sorting complexes required for transport (ESCRT)-I subunit, is recruited to the plasma membrane via association with the arrestin 1 domain-containing protein 1 (ARRDC1), promoting fission of the plasma membrane (Nabhan et al., 2012). TSG101 has also been linked to exosome biogenesis, suggesting overlapping pathways between MV and exosome secretion (Colombo et al., 2013). Because current methods for vesicle isolation rely almost entirely on vesicle size, and because recent work suggests a potential overlap in biogenesis mechanisms as well, understanding the heterogeneity across all EVs is becoming more and more important.

### **1.1.2 Exosome biogenesis**

Exosomes are a class of vesicles ranging from 40-100nm in diameter that are secreted upon the fusion of multivesicular bodies (MVB) with the plasma membrane, releasing intraluminal vesicles (Rose M. Johnstone, 1987). MVBs are formed through dynamic membrane-bound vesicular trafficking as part of the endocytic pathway (Klumperman and Raposo, 2014; Lippincott-Schwartz, 2009). Early endosomes are formed upon internalization of plasma membrane via phagocytosis, pinocytosis, or clathrin-mediated endocytosis. At this point, many extracellular ligands or cellular components are trafficked for recycling to the plasma membrane, others are targeted for degradation, and another subgroup targeted for secretion via exosomes. As early endosomes mature, they internalize intraluminal vesicles (ILVs), leading to the formation of late endosomes and ultimately MVBs (Sotelo and Porter, 1959). The canonical fate of MVBs was previously thought to be fusion with the lysosome, an acidic cellular compartment containing hydrolases that ultimately degrade the material contained within the

MVB (Futter et al., 1996). However, certain MVB populations can, instead, fuse with the plasma membrane, leading the release of exosomes (Jaiswal et al., 2002; Raposo et al., 1996).

Current evidence suggests that there are distinct populations of MVBs destined for plasma membrane fusion. Polarized epithelial cells have been shown to contain morphologically different MVBs at their apical and basolateral surfaces, and later work showed that vesicles secreted from different sides of polarized epithelial cells are distinct in their cargo and function (Tauro et al., 2013; van Niel et al., 2001). HeLa cells have been shown to produce two different MVB populations upon EGF stimulation: EGFR+ MVBs and Lactoferrin binding protein A (LBPA)+ MVBs (White et al., 2006). These two populations are distinct from one another, but both are enriched for CD63, a classical cargo marker of exosomes. Epstein-Barr virus transformed cultured B cells release both cholesterol-negative and cholesterol-positive MVBs, with the cholesterol positive MVBs more often targeted for the plasma membrane than to lysosomes (Ikeda and Longnecker, 2007). Interestingly, exosomes have been suggested to be enriched in cholesterol, strengthening the idea that there are in fact distinct MVB populations (Pfrieger and Vitale, 2018). In addition to the examples describe here, there are other examples of distinct MVB populations (Akers et al., 2013; Hessvik and Llorente, 2018), furthering the idea that mammalian cells somehow target specific MVBs for exosome release rather than trafficking to the lysosome. It is important to note, however, that many of the mechanisms determining the fate of MVBs seem to be heavily tied to cell- or disease-specific models.

The primary pathway for ILV, and thus, exosome formation is through the inward budding of the MVB membrane via ESCRT machinery (review, (Schmidt and Teis, 2012)). This was first hypothesized when proteomic studies detected various ESCRT proteins in secreted vesicles (They et al., 2001). The ESCRT-0 complex has been shown to regulate exosome

secretion in three cell model systems, ranging from neurons (Tamai et al., 2010) to tumor cells (Hoshino et al., 2013). Tumor EVs have also been shown to contain ESCRT proteins, including syntenin, ALIX, and syndecan (Baietti et al., 2012). Syntenin levels have been shown to regulate EV secretion in similar models, dependent on ESCRT-II, ESCRT-III, and VPS4 (Baietti et al., 2012). More recently, a large-scale RNA interference screen was carried out on ESCRT proteins in HeLa cells and identified proteins across all four ESCRT complexes that impact exosome release, further confirming that the ESCRT machinery may be a major driver of ILV and exosome biogenesis and secretion (Colombo et al., 2013). However, there are other ESCRT-independent mechanisms that induce exosome secretion as well, and some mammalian cell models have shown the ability to produce ILVs without the need for major ESCRT components (Trajkovic et al., 2008). Many of these ESCRT-independent mechanisms rely heavily on the localization and accumulation of specific lipids, like ceramide and lysobisphosphatidic acid, at the surface of the MVB (Hirotsami Matsuo, 2004). In fact, it may be the conversions of lipids via neutral sphingomyelinase that promotes the invagination of the MVB, and thus EV formation (Kosaka et al., 2010). Because of their large hydrophobic head groups and small hydrophilic tail groups, these lipids promote inward budding and the formation of ILVs (Trajkovic et al., 2008). Why certain cells use distinct mechanisms for ILV formation, and whether or not ESCRT is truly an important player in exosome biogenesis, remain to be fully determined.

How MVBs carry out fusion with the plasma membrane to facilitate exosome release is arguably the least understood aspect of exosome biogenesis. The most well studied pathway for membrane-membrane fusion is through the use of SNARE proteins (review, (Han et al., 2017)). SNARE proteins facilitate the fusion of vesicles to membranes and organelles throughout the endosomal and intracellular trafficking pathways. Originally, SNARE proteins



were divided into two separate classes: vesicle SNAREs (v-SNAREs), which associate with trafficking vesicles, and target SNAREs (t-SNAREs), which associate with the target membrane. Recent findings suggest that certain SNARE proteins can be associated with both transport vesicles and target membranes, driving a need for reclassification (DIRK FASSHAUER, 1998). A reclassification system takes into account the structure of the SNARE proteins: R-SNAREs, which provide the arginine (R) residue to the SNARE complex, and Q-SNAREs, which provide the glutamine (Q) residue (DIRK FASSHAUER, 1998). R-SNAREs often function as v-SNAREs, and Q-SNAREs often function as t-SNAREs (DIRK FASSHAUER, 1998). Currently, two R-SNARE proteins have been shown to regulate the secretion of exosomes: vesicle-associated membrane protein 7 (VAMP7) and YKT6 (Fader et al., 2009; Marc Ruiz-Martinez, 2016). Overexpression of the VAMP7 N-terminal domain, which is required for association with its Q-SNARE protein, inhibited the secretion of exosomes (Fader et al., 2009). Inhibition of the R-SNARE/Q-SNARE interaction in this model led to the enlargement and mislocalization of MVBs, suggesting that VAMP7 is required for the fusion of MVBs to the plasma membrane, and subsequently release of cargo (Fader et al., 2009). Reduction of YKT6 levels in both HEK293 and A549 human cells models reduced the levels of secreted TSG101, a common marker of exosomes (Gross et al., 2012; Marc Ruiz-Martinez, 2016). It remains to be determined with which Q-SNARE VAMP7 or YKT6 interacts. Two Q-SNAREs, SYX-5 in *C. elegans*, and Syx1A in human cultured cells, have been shown to be required for EV release, but their associated R-SNAREs are unknown (Hyenne et al., 2015; Koles et al., 2012). The changes in EV secretion in these models were measured by secreted levels of TSG101, a common marker for exosomes. However, it has been shown that TSG101 can also mark MVs (Nabhan et al., 2012). More work needs to be done to determine whether SNARE proteins

regulate only a single subtype of EVs, multiple subtypes of EVs, or whether they only regulate the loading of TSG101 into exosomes.

There is evidence that other proteins also influence the biogenesis of exosomes through non-canonical mechanisms that are again cell- and disease state-dependent. Diacyl glycerol kinase  $\alpha$  has been shown to negatively regulate exosome secretion in T cells (Alonso et al., 2011). Both V-ATPase and the Ras-related GTPase homolog (Ral-1) have been linked to exosome biogenesis in *C. elegans* (Hyenne et al., 2015). Increasing the cellular levels of lipid precursors in PC-3 cells also increased the secretion of EVs (Phuyal et al., 2015). These examples illustrate the vast complexity of EV biogenesis, as varying pathways can have a significant effect on EV secretion. Further, each example measured EV regulation via different methods, compounding issues with whether or not these proteins regulate total EV secretion, a subpopulation of EVs, or in fact, just the packaging of particular protein markers into EVs. This issue is further illustrated by the role of Rab GTPase proteins, as discussed below.

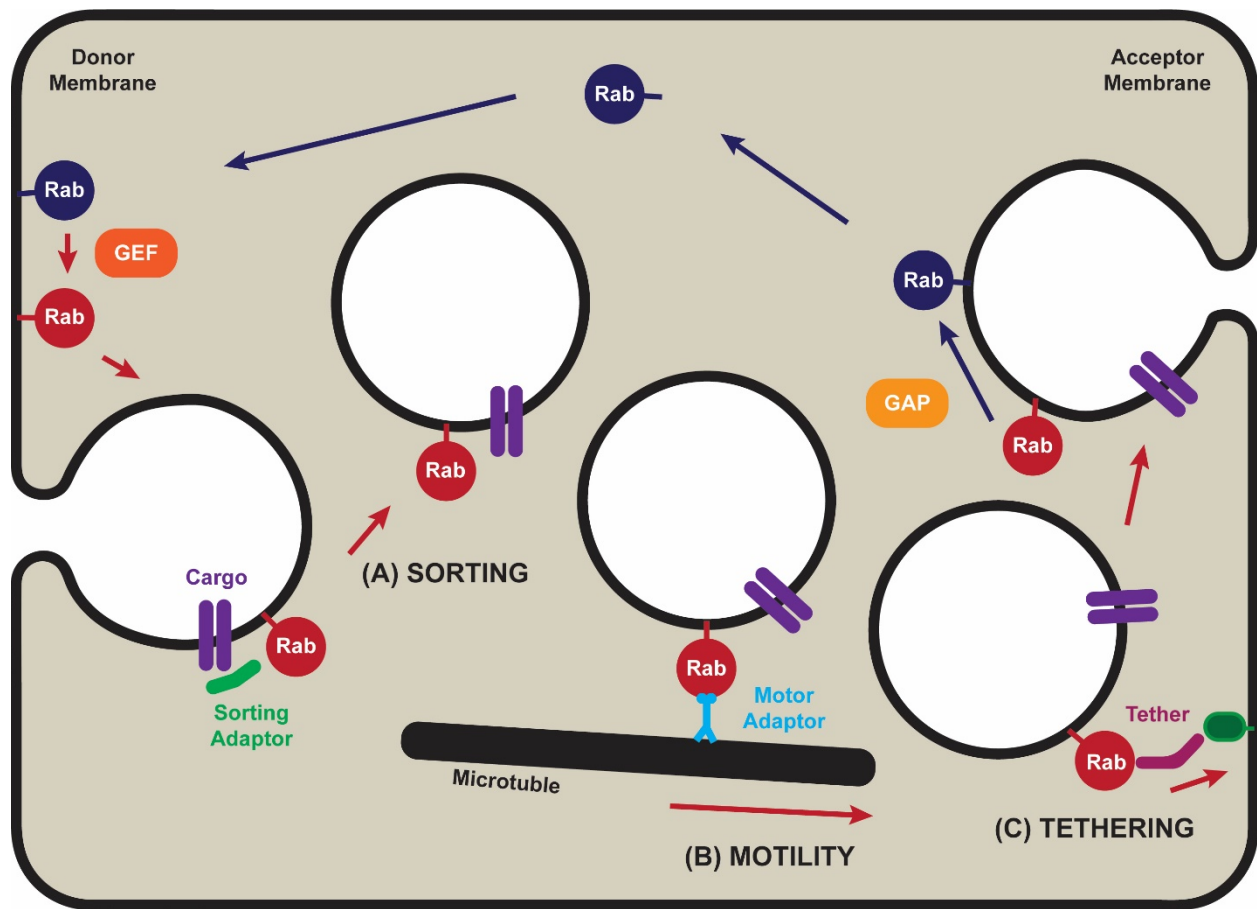
### **1.1.3 Rab proteins in extracellular vesicle biogenesis**

Rab proteins are small GTPases in the Ras protein superfamily that are highly conserved regulators of intracellular vesicle transport ((de Renzis et al., 2002; Lamber et al., 2019; Langemeyer and Barr, 2012; Langemeyer et al., 2014; Wu et al., 2011b; Yoshimura et al., 2010; Zerial and McBride, 2001), **Fig. 1**). There are currently more than 50 known Rab proteins in human cells, with functional roles in almost all aspects of protein trafficking. As with all G proteins, Rab proteins have two conformational forms, a GDP-bound inactive state, and a GTP-bound active state (Stenmark, 2009). GTP/GDP exchange factors (GEFs) catalyze the activation of Rab proteins, incorporating GTP into the inactive Rab protein (Delprato et al.,

2004). Hydrolysis of bound GTP is enhanced by GTPase-activating proteins (GAPs), which inactivate Rab proteins (Haas et al., 2007). In addition to canonical GTP- or GDP- bound states, there may be non-canonical roles for some G proteins that are active even in the GDP bound state (Nakayama, 2006). Rab proteins bind to proteins other than their associated GAPs and GEFs, called Rab effector proteins. Rab effector proteins have been linked to various intracellular trafficking functions, including cargo sorting, vesicular motility, and membrane-membrane tethering (Christoforides et al., 1999; de Renzis et al., 2002; Pfeffer, 2017; Vitale et al., 1998; Yoshimura et al., 2007) (**Fig. 1**). Because of their dominant role in intracellular trafficking, it is not surprising that they play a significant role in EV secretion (**Table 2**).

The first finding that Rab proteins play an important role in EV release was determined using human K562 leukemia cells (Ariel Savina, 2002). Expression of a dominant-negative form of Rab11 decreased the secretion of EVs, as measured by the levels of transferrin receptor and other EV protein makers (Tambini et al., 2010). Rab35 and Rab27 have also been shown to play an important role in regulating the secretion of proteolipid protein+ EVs in an oligodendrocyte cell line (Hsu et al., 2010). In contrast, no effect on EV secretion in *Drosophila* cells was found for Rab35 (Beckett et al., 2013; Hsu et al., 2010). In a large-scale shRNA screen of all Rab proteins in HeLa cells, six Rab proteins were shown to have an impact on EV secretion (Ostrowski et al., 2010). These include Rab2b, Rab5a, Rab9a, Rab27a, Rab27b, and Rab35. Among these, Rab27a/b seems to be the most important for promoting EV release (Ostrowski et al., 2010). In the same screen, Rab27a/b and Rab35 were shown to regulate the docking of MVBs to the plasma membrane, suggesting that Rab proteins may function at different steps throughout the EV biogenesis pathway (Ostrowski et al., 2010). Rab7, which was thought not to be important in HeLa cells, was later shown regulate secretion of ALIX+ and syntenin+ EVs in an MCF7 tumor model (Baietti et al., 2012).

**Figure 1. Rab proteins in intracellular trafficking**



**Figure 1.** Roles of Rab proteins in intracellular vesicle trafficking. (A) Active GTP bound Rab proteins facilitate the sorting of cargo in budding vesicles via associated sorting adaptor proteins (green). (B) Active (shown) and inactive Rab proteins regulate the shuttling of vesicles between cellular compartments along cytoskeletal tracts (black) through either association with motor protein adaptors (light blue), or through direct association with motor proteins. (C) Rab proteins can also facilitate the tethering of vesicles to acceptor membranes through the recruitment of tethering factors (pink) that interact with SNARE proteins, promoting the fusion of vesicles with acceptor membranes. Following trafficking events, Rab proteins are inactivated to their GDP bound state by GAPs (light orange), and shuttled back to their original donor membrane, where they are then activated by GEFs (dark orange) to carry out further trafficking events. Red Rab represents activated Rab proteins, blue Rab represents inactive Rab proteins. Adapted from Stenmark et al. 2009.

**Table 2. Rab proteins in EV Biogenesis**

Name	Cell Line	Cellular Localization	Citation
Rab2b	HeLa	Endoplasmic Reticulum, Golgi Network	(Ostrowski et al., 2010)
Rab5a	HeLa	Plasma Membrane, Early Endosome	(Ostrowski et al., 2010)
Rab9a	HeLa	Late Endosome, Golgi Network	(Ostrowski et al., 2010)
Rab7	MCF-7, HUVEC	Early Endosome, Late Endosome, Lysosome	(Baietti et al., 2012)
Rab11	K562	Golgi Network, recycling vesicles	(Tambini et al., 2010)
Rab27a	Varying	Secretory Granule, Early Endosome, Late Endosome	(Ostrowski et al., 2010)
Rab27b	HeLa, HUVEC	Secretory Granule, Early Endosome, Late Endosome	(Ostrowski et al., 2010)
Rab35	Oli-neu	Recycling Endosome, Late Endosome	(Hsu et al., 2010)
Rab13	DKO-1	Tight Junctions, Early Endosome, Late Endosome, Plasma Membrane	Chapter 3

A major limiting factor in the study of Rab-dependent EV secretion is the lack of global regulation across different species and disease models, and the potential functional redundancy among various Rab proteins. Many early discoveries made in regard to Rab proteins regulating EV secretion used measurement of protein markers associated with EVs and not necessarily vesicle counts. For example, Rab11 has been shown to regulate the secretion of EVs in human K562 leukemia cells (Ariel Savina, 2002), *Drosophila* cells (Beckett et al., 2013), and human retinal epithelial cells (Abrami et al., 2013), but contradicting data has shown that Rab11 does not regulate EV secretion in Hela cells (Ostrowski et al., 2010) or human neurons (Walsh et al., 2019). There are three potential explanations for these conflicting results. First, the authors of each paper relied on the detection of specific EV markers to measure the varying levels of EV secretion. Although it is accepted that certain proteins are used as effective EV markers, Rab proteins may regulate the trafficking of the proteins themselves and may not play a role in the biogenesis of the lipid vesicle. In fact, Rab11 has been shown to regulate the recycling of the transferrin receptor to the plasma membrane (Takahashi et al., 2012), and misregulation of

Rab11 could lead to its accumulation in an incorrect endosomal compartment, leading to its degradation instead of its association with EVs. Second, different cell models may not enrich for the same proteins in their EVs such that the use of specific markers may depend on the model system in question. There are many examples of inconsistencies with known EV markers (Kalra et al., 2012), suggesting that quantifying protein abundance is not an effective way to measure EV secretion. Finally, and more broadly, Rab-dependent EV biogenesis may be heavily tied to disease state, tissue, or the organismal model used to discover players in vesicle secretion mechanisms. This is shown especially with the role of Rab27a, which has been linked to EV secretion in various cancer models (Bobrie et al., 2012; Hoshino et al., 2013; Peinado et al., 2012; Webber et al., 2015), but was not required in other cell-state and disease models (Abrami et al., 2013; Koles et al., 2012). Other Rab proteins have also shown inconsistent association with EV biogenesis when using distinct cell model systems (Jae et al., 2015; Worst et al., 2017). Because of the highly variable regulation of EV secretion by Rab proteins, it has become more important to understand and study novel Rab proteins in their associated models, as they may also be found to play important roles in EV biogenesis. One Rab protein, Rab13, has been shown to play important roles in cancer progression, but has yet to be linked to EV biogenesis, making it an interesting candidate for study in the EV field, particularly in our colorectal cancer (CRC) cell model (**see Chapter 3**).

#### **1.1.3.1 Rab13 and its intracellular role**

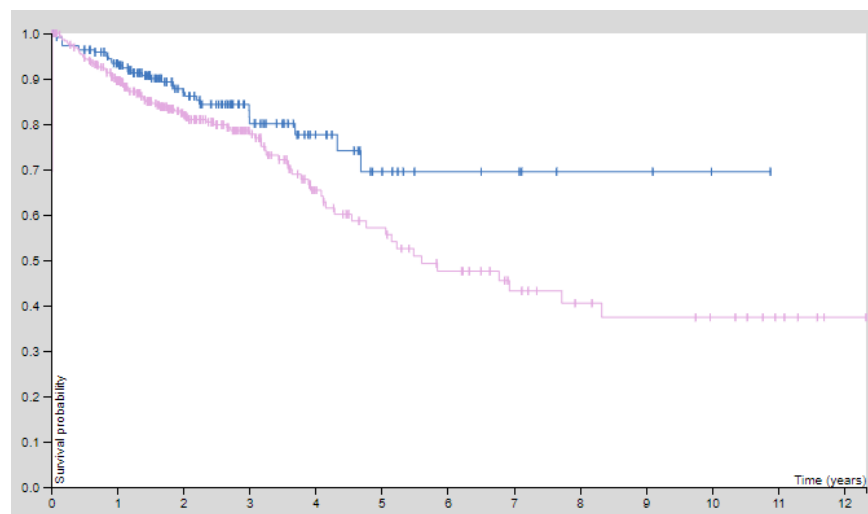
Rab13, like all small GTPases, functions in various trafficking pathways in many cell models with significant links to cancer progression. Rab13 was originally discovered associated with tight junctions in polarized epithelial cells and its proposed mechanism was to regulate the

trafficking of molecules to the basal or apical cell surface, as well as to regulate the stability of tight junctions (TJs) themselves (Yamamura et al., 2008). The association of Rab13 with the plasma membrane has been shown to be regulated by retinal rod rhodopsin-sensitive cGMP 3',5'-cyclic phosphodiesterase subunit delta (PDE6D), and that isoprenylation of Rab13 is required for this interaction (Anne-Marie Marzesco, 1998). Once PDE6D binds to Rab13, it becomes dissociated from the plasma membrane (Marzesco et al., 2002). Further work has shown that Rab13 is recruited to TJs from a cytoplasmic pool at an early stage of TJ assembly (Marzesco et al., 2002), and that active Rab13 may delay the formation of mature TJs (Kohler et al., 2004). This is important in cancer, as misregulation of TJ formation is linked to cancer progression (Martin and Jiang, 2009). Interestingly, active Rab13 directly binds and negatively regulates protein kinase A (PKA) (Kohler et al., 2004). Rab13-PKA signaling has been suggested to regulate the docking of intracellular vesicles near cell-cell junctions, and PKA activity has been shown to be required for membrane trafficking, suggesting a possible link to the secretion of EVs (Van et al., 2004). Further studies have shown Rab13-dependent recycling of occludin-1, ZO-1, Syx, and claudin-1 at TJs, confirming the importance of Rab13 in the regulation of stable, functional cell-cell contact sites (Marzesco et al., 2002; Yamamura et al., 2008). Both occludin-1 and claudin-1 have been detected in cancer EVs (Kalra et al., 2012), furthering the link between Rab13 and EV biogenesis.

Rab13 interacts with specific GEFs, GAPs, and other effector proteins. Interactions between Rab13 and molecules interacting with CasL-like 2 (MICAL-L2) regulates many of the effects of Rab13 on cytoskeletal reorganization (Kanda et al., 2008). Interestingly, the phenotypes observed when the Rab13/MICAL-L2 interaction is disrupted are similar to the disruption of the Rab27/Munc13-4 interaction, which has been shown to play a role in the regulation of EV secretion (Neeft M, 2005). Rab13 has also been shown to interact with two

members of the DENND GEF family: DENND1c (Yoshimura et al., 2010) and DENND2B (Ioannou et al., 2015), both of which have been shown to activate Rab13 at the plasma membrane of epithelial cells. Once Rab13 is trafficked to the cell membrane, it is activated by DENND2B (Ioannou et al., 2015). Upon activation, Rab13 stimulates MICAL-L2, leading to the formation of membrane ruffles, while Rab13 itself promotes the fusion of its associated vesicles with the plasma membrane, supplying new membrane or delivering cargo, such as integrins (Ioannou et al., 2015). This is supported by finding that Rab13 is required for the recycling of  $\beta$ -1 integrin in an epithelial cell model (Sahgal S, 2019). Taken together, the molecular mechanisms of Rab13 are important for regulating cell membrane homeostasis, as well as promoting cell-cell interactions and the secretion of cargo. Since these mechanisms have also been linked to EV biogenesis, one would hypothesize an important role for Rab13 in vesicle secretion.

**Figure 2. Rab13 expression linked to decreased survival probability**



**Figure 2.** Data collected by the Human Protein Atlas project shows a significant link between high Rab13 expression levels (pink) and lower long-term survival probabilities in patients with colorectal cancer. Patients with lower Rab13 expression are shown in blue.



Because of its important role in regulating epithelial cell-cell interactions, Rab13 has also been proposed to play an important role in the development of various cancers (review (McPherson, 2016)). Of particular interest to our laboratory, high Rab13 expression is inversely linked to CRC patient prognosis (**Fig. 2**, Protein Atlas Data). Epidermal growth factor receptor (EGFR) is a tyrosine kinase receptor that is well characterized for its involvement in the development of cancers, particularly CRC. Overexpression of DENND2B, a Rab13 GEF, increases downstream EGFR signaling, and promotes cell growth through cross activation of the ERK signaling pathway (Majidi et al., 1998). A further link between Rab13 and EGFR recycling is through MICAL-L1, a Rab13 effector protein that regulates the recycling of EGFR (Abou-Zeid et al., 2011). Interestingly, MICAL-L1 is also an effector protein of Rab35, suggesting potential overlap in Rab13/Rab35 functionality, particularly in regard to EV biogenesis (Rahajeng et al., 2012). The Rab35/MICAL-L1 interaction is regulated by Arf6, a known regulator of MV secretion, suggesting Rab13 and/or Rab35 may regulate PM-derived EVs (Allaire et al., 2013; Muralidharan-Chari et al., 2009; Rahajeng et al., 2012). In addition to Rab13's role in regulating cell growth through EGFR, Rab13 and its associated effector proteins have been shown to play significant roles in cell-cell adhesion (Yamamura et al., 2008), cell migration and scattering (Kanda et al., 2008), as well as angiogenesis (Wu et al., 2011a). Taken together, Rab13 plays an important role in cancer progression, and because of its potential role in EV secretion, makes it an interesting candidate to study in a CRC cell model.

## 1.2 Extracellular vesicle cargo

EV cargo has continuously been shown to be cell-, disease-, biogenesis pathway-, and growth condition-dependent. From large-scale screens, a large number of proteins and RNAs

have been identified that are secreted into EVs (Kalra et al., 2012)). Despite context-specific differences, there nevertheless appear to be distinct mechanisms for the sorting of specific proteins and RNAs into EVs.

### **1.2.1 Extracellular RNA**

Work in the exRNA field has shown the presence of almost every known coding and non-coding RNA in the extracellular space, including messenger mRNAs (Valadi et al., 2007), long non-coding RNAs (lncRNAs) (Hinger et al., 2018), tRNAs (Bellingham et al., 2012), miRNAs (Cha et al., 2015a), small ncRNAs (e.g. snRNAs, snoRNAs, rRNAs) (Bellingham et al., 2012; Freedman et al., 2016), yRNAs (Balkom et al., 2015), and circular RNAs (ciRNAs) (Dou et al., 2016). For some of these RNAs, distinct functions have been demonstrated after transfer to recipient cells, but a common mechanism governing selective RNA export has not been determined and may also be context specific (Fabbri et al., 2012; Montecalvo et al., 2012; Skog et al., 2008; Zomer et al., 2010). Interestingly, most RNAs found within EVs are less than 200 nucleotides in length, suggesting that there may be a size limitation to the secretion of RNAs (Bellingham et al., 2012; Cha et al., 2015b; Hinger et al., 2018). An overview of all known exRNA subtypes can be found in **Table 3**.

#### **1.2.1.1 mRNAs**

mRNAs are one of the least abundant populations of RNA in the extracellular space, accounting for ~2% of the total amount of secreted RNA (Yuan et al., 2016). However, most of these RNAs are fragments of mRNA and not full length (Unpublished, Patton Laboratory). The first reported detection of full length mRNA being present in EVs was in mouse mast cells, but

follow up studies have not been able to detect full length mRNAs (Valadi et al., 2007). Two groups reported the transfer of Cre mRNAs via EV; however, their data cannot rule out the possibility that Cre protein was transferred (Ridder et al., 2014; Zomer et al., 2015). Multiple studies have reported mRNAs in EVs based on RNA-seq data, but in almost all of these cases, it is not clear if full length mRNAs are present. Detection of mRNAs in EVs has most commonly been based on RNA-seq reads in various cancer cell models, including mutant EGFRvIII reads from glioblastoma patient serum (Skog et al., 2008). Because the majority of these reports have not demonstrated full length transfer, it remains unclear what role mRNA transfer plays in exRNA communication. One possibility is that RNA fragments function in ways other than translation into protein, including interaction of RNA fragments with Toll-like receptors on endosomes (Fabbri et al., 2013; Fabbri et al., 2012; Sato et al., 2009).

### **1.2.1.2 lncRNAs**

lncRNAs are RNAs larger than 200 nucleotides in length that lack open reading frames (Rinn and Chang, 2012). lncRNAs are often 5'-capped, spliced, and polyadenylated, but this is not required, as some lncRNAs have been reported that lack these modifications (Wilusz et al., 2008; Zhang et al., 2014). Much of the human genome is transcribed into lncRNAs, but the exact function of these transcripts remains to be determined. For the few that have been characterized, they play various roles in the cell, including transcriptional regulation, epigenetic changes, miRNA sequestering, and protein complex scaffolding (review, (Rinn and Chang, 2012)). The expression of various lncRNAs is frequently cell-type and disease-state specific with some of the best examples showing roles in modulating oncogenic pathways in cancer (Berrondo et al., 2016; Ellis et al., 2012; Emmrich et al., 2014).

**Table 3. RNA subtypes found in EVs**

<b>Name (abbreviation)</b>	<b>Size range (nt)</b>	<b>Function(s) (reference)</b>
microRNA (miRNA)	19-22	Inhibits protein translation and/or facilitates degradation of mRNA (Eulalio, Tritschler, and Izaurralde 2009); activation of immune response (Fabbri et al. 2012)
Small nucleolar RNA (snoRNA)	60-300	Guides the methylation or pseudouridylation of rRNAs and other RNAs (Matera, Terns, and Terns 2007)
Small nuclear RNA (snRNA)	~150	Modulation of RNA polymerase II activity; splicing (Matera, Terns, and Terns 2007).
Piwi-interacting RNA (piRNA)	20-30	Chromatin modification and transposon silencing (Iwasaki, Siomi, and Siomi 2015)
yRNA fragment (yRF)	27-33	Cell proliferation (C. P. Christov, Trivier, and Krude 2008); apoptosis (Chakraborty et al. 2015).
tRNA-derived fragment (tRF)	19-22	Translational repression, analogous to miRNAs (Haussecker et al. 2010; Y. S. Lee et al. 2009)
tRNA-derived half (tRH, tiRNA)	30-40	Stress-induced translational repression (Yamasaki et al. 2009; P. Ivanov et al. 2011)
Vault RNA fragments	~23	Translational repression, analogous to miRNAs (Persson et al. 2009)
Long ncRNA (lncRNA)	>200	Chromatin remodeling (Meller, Joshi, and Deshpande 2015); translational regulation; mRNA stability (reviewed in Fatica and Bozzoni 2014)
Circular RNA (circRNA)	>80 nt	miRNA sponges (Hansen et al. 2013); transcriptional regulation (Z. Li et al. 2015)

lncRNAs have been shown to play a significant role in EV secretion or as cargo RNAs. *TUC339* is a lncRNA that is selectively exported in hepatocellular cancer cell (HCC) EVs, and plays a significant role in reprogramming recipient cell behavior (Kogure et al., 2013). Three different lncRNAs have been shown to play a role in drug resistance via secretion in EVs. *lncARSR* was shown to promote sunitinib resistance in renal cell carcinoma with resistance capable of being transferred to neighboring cells through the secretion of *lncARSR* in EVs (Qu et al., 2016). *LINC-ROR* has been shown to promote chemoresistance in HCC cells (Takahashi et al., 2014a). Treatment of HCC cells with various chemotherapy agents promotes the secretion of *LINC-ROR* into EVs (Takahashi et al., 2014a). Another lncRNA expressed in chemoresistant-HCC cells is *VLDLR* which is exported into EVs. These EVs have been shown to promote resistance in recipient cells (Takahashi et al., 2014b). In a different model, glial cells expressing high levels of the lncRNA *POU3F3* were able to transfer this lncRNA via EVs to neighboring human brain microvascular endothelial cells leading to increased cell proliferation, migration, and angiogenesis in recipient cells (Hu et al., 2018). Two other lncRNAs, *CCAT2* and *H19*, have both been shown to promote angiogenesis in an EV-dependent mechanism (HAI-LI LANG, 2017; Jia et al., 2016). Together, there is an increasing amount of data to suggest that the transfer of lncRNAs through the extracellular space plays a significant role in the progression of disease and drug resistance. In addition, lncRNAs have been shown to be effective biomarkers in the detection of disease (Berrondo et al., 2016). A key remaining question is whether or not these lncRNAs are functioning as full-length transcripts. The previously described examples suggest the transfer of ncRNAs far exceeding the average size found within EVs (~200 nucleotides). Further work is needed to show whether these lncRNAs are functioning as full-length transcripts, or if they are capable of transferring drug resistance through fragmented, or non-canonical mechanisms.

### 1.2.1.3 miRNAS

miRNAs are one of the most well studied non-coding RNAs, both in the context of cellular and extracellular functionality. miRNAs were initially discovered in *C. elegans*, and have since been shown to play highly significant roles in gene regulation in most animal cells (Lee et al., 1993). miRNAs are ~22 nucleotide small RNAs that bind target mRNAs to repress translation (review, (Bartel and Chen, 2004)). miRNAs are capable of targeting 30-60% of all protein coding mRNAs (Bartel and Chen, 2004; Griffiths-Jones et al., 2006), and more than 24,000 miRNAs have been identified across vertebrate and invertebrate cell models (Griffiths-Jones, 2004).

miRNA biogenesis occurs through two distinct processing events to yield mature ~22 nucleotide miRNAs. Following transcription, primary miRNAs (pri-miRNAs) are incorporated into the microprocessor complex, a protein complex made up of the RNA-binding protein DiGeorge Syndrome Critical Region 8 (DGCR8) and the ribonuclease III enzyme Drosha (Gregory et al., 2004; Lee et al., 2003). Drosha cleaves the pri-miRNA at the base of a characteristic hairpin structure (Lee et al., 2004). Following cleavage, the now precursor miRNA (pre-miRNA) is exported out of the nucleus via the Exportin 5 nuclear membrane pore (Lund et al., 2004; Yi et al., 2003). Upon shuttling to the cytoplasm, the pre-miRNA is processed by DICER which cleaves the terminal loop producing a mature miRNA duplex (Bernstein, 2001; Ketting, 2001; Pasquinelli et al., 2000). Interestingly, both strands of the miRNA duplex, including the 5' (5p) and 3' (3p), can function in gene regulation, with the exact strand apparently driven, at least in part, by 5' end stability and RNA:RNA base pairing (Bernstein, 2001; Ketting, 2001; Pasquinelli et al., 2000). After processing, mature miRNAs are loaded in an ATP-dependent manner into an Argonaute protein (Hammond, 2000; Schwarz, 2003). While the majority of miRNAs follow a

Dicer-dependent pathway, there are other non-canonical pathways that lead to the maturation of miRNAs as well (review, (Ha and Kim, 2014)).

Following maturation and association with an Argonaut (AGO) protein, the miRNA-induced silencing complex, or RISC, is formed (Gregory et al., 2005). AGO proteins function to facilitate the formation of the RNA-RNA binding interaction, and can also function as a nuclease under proper complementation (Liu et al., 2004). This complex, along with an AGO protein, includes the GW182 family of proteins, which provide a scaffold for the recruitment of other proteins required for the deadenylation and degradation of target mRNAs (Ding and Han, 2007). First, the poly(A)-deadenylase complexes, PAN2-PAN3 and CCR4-NOT, are recruited and associate with RISC (Behm-Ansmant et al., 2006). These complexes are required for the deadenylation of the poly(A) tail, which ultimately leads to the destabilization of the target mRNA (Djuranovic et al., 2012; Eulalio et al., 2008). After recruitment of the deadenylase complexes, the decapping protein DCP2 and its associated proteins are recruited to the 5' end of the target mRNA (Behm-Ansmant et al., 2006; Rehwinkel et al., 2005). Following 5' decapping, the target mRNA is degraded 5'-3' via the exoribonuclease 1 (XRN1) (Orban and Izaurralde, 2005).

Because of their small size and their detection in almost every biological fluid (Creemers et al., 2012; Heneghan et al., 2010; Huang et al., 2010; Matsumura et al., 2015), miRNAs have been of great interest in the exRNA and EV field. miRNAs have been shown to be associated with various extracellular complexes, including high density lipoproteins (HDL) (Vickers et al., 2011), AGO-2 complexes (Arroyo et al., 2011), and EVs (Cha et al., 2015a; Valadi et al., 2007). How miRNAs are loaded into EVs is still under debate. Inhibition of the ESCRT complex has been shown to promote the association of RISC to the surface of the MVB, suggesting a possible loading mechanism for miRNAs into exosomes (Gibbings et al., 2009). 3'-uridylylated

miRNAs have been shown to be selectively exported into EVs, suggesting a potential role for non-template-directed nucleotide addition (Koppers-Lalic et al., 2014). However, only a small percentage of total miRNAs secreted into EVs are modified in this manner, indicating other potential targeting mechanisms. A role for sequence motif-dependent secretion of miRNAs has also been suggested (Santangelo et al., 2016; Villarroya-Beltri et al., 2013a). T-lymphocyte cells have been shown to selectively export miRNAs containing a GGAG sequence motif (Booth et al., 2006). The authors hypothesize that hnRNPA2B1 binds GGAG sequences on these miRNAs targeting them for secretion (Booth et al., 2006). However, the ability of hnRNPA2B1 to target miRNAs for secretion is not universal and may be cell-type and disease-state specific (Cha et al., 2015a). AGO phosphorylation has also been shown to regulate miRNA secretion into EVs via a KRAS-dependent mechanism in CRC cells (McKenzie et al., 2016). Lipid-dependent mechanisms for miRNA export have also been reported with inhibition of neutral sphingomyelinase 2 (nSMase2) inhibiting both EV biogenesis and miRNA secretion (Cha et al., 2015a; Kosaka et al., 2010). Sphingosine-1-phosphate, a ceramide metabolite, has also been shown to be an essential player in EV secretion, but it is not clear if this is miRNA-specific (Kajimoto et al., 2013). Interestingly, inhibition of nSMase2 has also been shown to promote the association of miRNAs with HDL (Vickers et al., 2011), suggesting the potential for complementary roles between HDL- and EV-associated miRNAs.

Increasing evidence suggests that miRNAs play significant roles as extracellular RNA (review, (Zhang et al., 2015)). EV-mediated transfer of *miR-105* directly targets tight junction formation in a breast cancer cell model, promoting metastasis (Zhou et al., 2014). Our laboratory has shown that *miR-100* is exported into EVs in a KRAS-mutant dependent mechanism, and that *miR-100* can function to repress translation in recipient cells (Cha et al., 2015a). *miR-21* has also been shown to be enriched in EVs from umbilical cord blood, and



these EVs promote proliferation of fibroblasts, and promote wound healing in the developing embryo (Fang et al., 2016). In an oral cancer cell model, *miR-342* and *miR-1246* have been shown to promote metastasis through their transfer via EVs (Sakha et al., 2016).

Whether or not miRNAs function in recipient cells in a RISC-dependent manner is controversial in the EV field (Chevillet et al., 2014). When studying the presence of miRNAs in prostate cancer patient sera, Chevillet et al (2014) made the striking observation that EV-associated miRNAs make up less than ~2-5% of the total secreted RNA, and that when calculated, EVs contain much less than 1 miRNA copy per vesicle, even when measuring some of the most abundant miRNAs in the extracellular space (Chevillet et al., 2014). This suggests that RISC-mediated gene silencing may not be physiologically plausible, opening the door to possible non-canonical or non-EV-associated functions. A large scale screen of miRNAs detected in patient sera showed that ~90% of detectable miRNAs were found outside of vesicles, with only ~60% of miRNAs associated with EVs, suggesting that EV-associated miRNAs may not be the predominant driver of miRNA-mediated functionality (Kroh et al., 2010). Two major mechanisms that may explain the stoichiometric discrepancy between copy numbers and function include the association of miRNAs with AGO-2 protein aggregates (Arroyo et al., 2011), high density lipoprotein (HDL) particles (Vickers et al., 2011), and the activation of RNA-sensing Toll-like receptors (Fabbri et al., 2012).

In healthy patient sera, ~90% of all *miR-16* and *miR-92a* copies were shown to be circulating, but not in vesicles, rather, associated with AGO-2 protein complexes, suggesting that RISC-mediated gene silencing may be through the transfer of non-vesicular AGO-2 protein aggregates (Arroyo et al., 2011). HDL is another potential player in the extracellular transfer of miRNAs, and may explain the functional ability to regulate gene silencing by cell-cell

communication due to their high abundance and association with miRNAs in patient serum (Tabet et al., 2014; Vickers et al., 2011). *miR-223* has been shown to associate with HDL in the extracellular space (Tabet et al., 2014), and has further been shown to be functionally transferred via HDL-dependent mechanisms (Tabet et al., 2014). Because miRNAs seem to more heavily associate with non-vesicular proteins and aggregates, it may be that the RISC-mediated gene silencing may occur, just not through vesicle mediated transfer. Instead, it may be through the secretion of protein aggregates and HDL particles that function as carriers of miRNAs through the extracellular space, and upon internalization, function in gene silencing.

Recently, a new non-canonical role for miRNAs in the extracellular space has been proposed (Fabbri et al., 2013). *miR-21* and *miR-29a* are secreted by tumor cells and can bind to and activate RNA sensing Toll-like receptors (TLRs) in immune cells thereby triggering an inflammatory response (Fabbri et al., 2012). EV associated *miR-21* and *miR-29a* were shown to be taken up into endosomal compartments of recipient cells, where they activated TLR8, leading to downstream activation of NF- $\kappa$ B, secretion of pro-inflammatory and pro-metastatic cytokines, and an increase in the metastatic potential of cancer cells (Fabbri et al., 2012). Large scale receptor activation via EV-mediated miRNA transfer is enticing from a functional standpoint, as it allows for robust changes in recipient cells by transfer of a small concentration of miRNAs.

### **1.2.2 Extracellular proteins**

Protein cargo within EVs consist of a common group of proteins enriched in EVs regardless of cell type, as well as numerous proteins expressed in a cell- or disease-specific manner (Jeppesen et al., 2019). Proteins from the endosome, plasma membrane, and cytosol

are most commonly enriched in EVs, while proteins from the nucleus, mitochondria, and endoplasmic reticulum are less common (Thery, 2011). Comparison of protein cargo from MVs and exosomes are often distinct, suggesting specific sorting mechanisms (Haraszti et al., 2016). MV-associated proteins are more often subject to posttranslational modifications, like glycosylation, compared to exosome enriched proteins (Williams et al., 2018). Consistent with their biogenesis, exosomes contain proteins from the ESCRT machinery, including Alix, TSG101, HSC70, and HSP90 (Colombo et al., 2013). Exosomes are also enriched in tetraspanins, particularly CD63, CD81, and CD9 (Bobrie et al., 2012). Indeed, all of the proteins mentioned above are now considered classical EV markers by the International Society for Extracellular Vesicles (Thery et al., 2018).

The transfer of oncogenic material, particularly oncogenic proteins, has been of great interest in the EV field. Previous work has shown the functional transfer of various oncogenes via EV-mediated trafficking, including EGFRvIII in glioblastoma (Skog et al., 2008), H-ras and c-myc in a transfected fibroblast model, and KRAS in a CRC cell model (Demory Beckler et al., 2013). Many receptor ligands, especially those associated with EGFR, have been shown to be enriched in EVs (Higginbotham et al., 2011), and can even impact recipient cells via EV-mediated transfer (Higginbotham et al., 2011; Zhang et al., 2019). Transfer of oncogenic proteins and receptor ligands could lead to changes in the tumor microenvironment and may even promote changes in non-cancerous cells. Whether or not transfer of oncogenic proteins can mediate long term effects on non-cancerous cells is unknown.

With the advancement and refinement in vesicle isolation techniques, the precise protein composition of distinct EV subtypes needs to be carefully reconsidered. For example, earlier work reported the presence of AGO proteins in EVs from mutant KRAS cells, but after more

rigorous purification, Ago proteins were not found in all EVs (Jeppesen et al., 2019; McKenzie et al., 2016). EVs have been reported to contain not only Ago proteins, but the entire machinery for miRNA processing, although these findings have been highly contested in the field (Melo et al., 2014). Other than Ago proteins, earlier work had suggested that DNA and histones are incorporated within exosomes, but neither DNA nor histones were detected in high resolution density gradient-purified EVs by Jeppesen et al. 2019 (Jeppesen et al., 2019). Instead, these proteins were part of non-vesicular aggregates that co-purify with EVs unless density gradients are utilized (Jeppesen et al., 2019). The use of immuno-affinity capture against vesicle markers like CD63, CD81, and CD9 has also helped define the exact protein composition of EVs (Jeppesen et al., 2019). As more refined approaches are adopted, the previous classification of different subclasses of EVs will need to be reassessed.

### **1.3 Functional significance of extracellular vesicles**

EVs play a novel role in cell-to-cell signaling through autocrine and paracrine mechanisms, both locally, and far from the cell of origin. Cell-to-cell communication by EVs has been demonstrated in various systems and diseases, including autoimmune disorders (Robbins and Morelli, 2014), inflammation (Okoye et al., 2014), infection (Schorey et al., 2015), cancer (Kalluri, 2016), neurological diseases including Alzheimer's (Jiang et al., 2019), and even through the human microbiome (Fritz et al., 2016). The mechanisms of EV-dependent, cell-to-cell communication include receptor signaling (Skog et al., 2008), protein and RNA cargo transfer (Cha et al., 2015a; Demory Beckler et al., 2013; Hinger et al., 2018), and immune activation (Okoye et al., 2014).

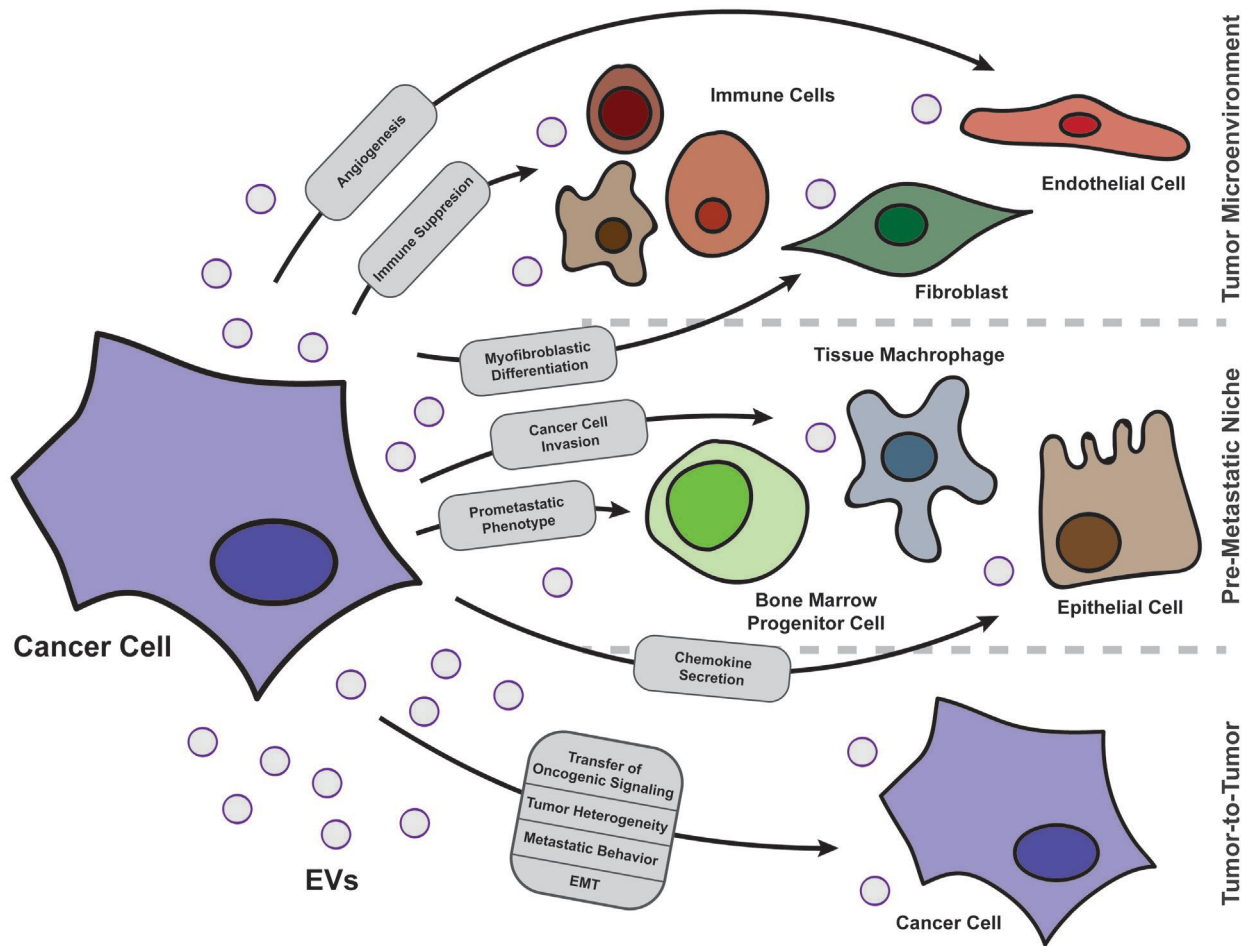
### 1.3.1 Functional significance in cancer

Although all cells secrete EVs, cancer cells secrete more EVs on average, with links to many oncogenic mechanisms including tumor-microenvironment interactions (Hu et al., 2018), angiogenesis (Huang and Feng, 2017), metastasis (Wortzel et al., 2019), proliferation (Demory Beckler et al., 2013), invasiveness (Hoshino et al., 2013; Sakha et al., 2016), and therapeutic resistance (Ciravolo et al., 2012; Hon et al., 2019; Qu et al., 2016; Takahashi et al., 2014b; Zhang et al., 2017) (**Fig. 3**).

Tumor and cancer cell-derived EVs can mediate escape from immune surveillance mechanisms (Clayton et al., 2007). EVs regulate T cells and induce apoptosis in T lymphocytes, leading to suppressed immunity in cancer patients (Huber et al., 2005). EVs can also suppress monocyte maturation (Valenti et al., 2006). PD-L1+ EVs have been shown to promote tumor-specific immune suppression in the tumor microenvironment (Chen et al., 2018). Transfer of *miR-21-5p* and *miR-155-5p* by tumor-associated macrophages promotes migration and invasion in CRC (Lan et al., 2019). Together, EV release is an effective way for cancer cells to escape host immune responses, promoting the growth and spread of cancer.

Cancer-derived EVs also play an important role in metastasis. EV-associated integrins have been shown to regulate organ-specific metastasis at distant sites, in almost all organs, including lung, liver, brain, and bone (Ono et al., 2014; Peinado et al., 2012). EV-associated proteins, like fibronectin, promote cytoskeletal reorganization and increased cell adhesion and motility in a CRC cell model (Abdouh et al., 2019).

**Figure 3. Functional Role of EVs in Cancer**



**Figure 3.** EVs have been shown to play significant roles in various cancer pathways, including (A) regulating the tumor microenvironment, (B) promoting and facilitating the creation of pre-metastatic niches, and (C) tumor cell-cell transfer of oncogenic material to promote growth and metastasis. Cancer EVs have also been shown to impact neighboring cells, including immune cells, fibroblasts, endothelial cells, progenitor cells, and epithelial cells. Adapted from Bebelman et al., 2018.

EV-associated matrix metalloproteinase-9 (MMP9) was also shown to promote metastasis by activating the TGF- $\beta$  signaling cascade, leading to extracellular matrix (ECM) degradation (Redzic et al., 2013). There are many ncRNAs that also promote metastasis through EV-mediated transfer, many of which have been discussed previously. Other than lncRNAs, *miR-210*, *miR-200c*, and *miR-141* have all been shown to promote metastasis via EV transfer in CRC cell models (Korpál et al., 2008). *miR-34a-5p* transfer via EVs from cancer-associated fibroblasts (CAFs) promoted not only metastasis, but also proliferation and epithelial to mesenchymal transition (EMT) in recipient oral squamous cell carcinoma cells (Li et al., 2018). Although the idea that EVs can promote the formation of distant metastatic sites, or pre-metastatic niches, is a highly cited example of a biological function in the EV field, the experimental design and physiological relevance have been heavily criticized. During mouse metastasis experiments, animals were injected with 5 to 15  $\mu\text{g}$  of small EVs, which is approximately  $1.0 \times 10^8$  to  $1.0 \times 10^9$  vesicles per mouse with up to 21 days of constant daily EV treatment (Costa-Silva et al., 2015; Hoshino et al., 2015; Plebanek et al., 2017). Collection of this magnitude of EVs requires anywhere from  $0.5 \times 10^7$  to  $5.0 \times 10^7$  cells (data from our laboratory), a number vastly higher than would be found in an *in vivo* tumor model. Because of this experimental discrepancy, it is not known whether these findings are truly biologically relevant, but recent studies using tumor xenograft models suggest that tumor cells can induce changes in distant tissues via transfer of EVs at a physiological level, suggesting that the findings in previous publications may hold true in an *in vivo* tumor environment (Fu et al., 2018).

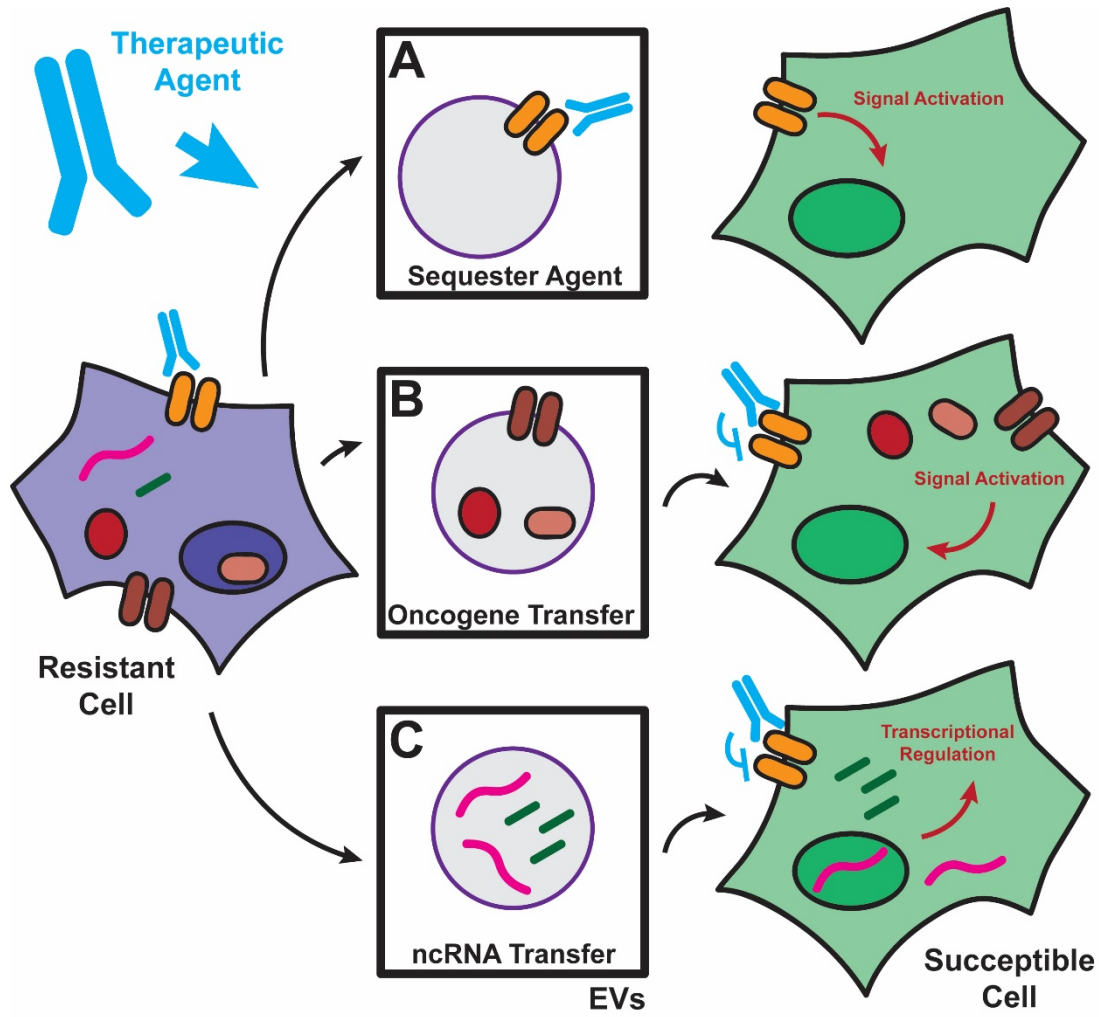
The ability of cells to grow independently of adhesion to the extracellular matrix (ECM) is a key step in the transformation of cancer cells, and correlates strongly with tumorigenic potential in tumor models (Guadamillas et al., 2011). The current standard for testing the tumorigenicity of cancer cells *in vitro* is through the use of anchorage-independent growth

assays, where cells are grown in three-dimensions lacking the necessary signals via integrins to proliferate and grow (Guadamillas et al., 2011; Paolillo and Schinelli, 2017). Because EVs contain a multitude of integrins and associated ECM proteins, one could postulate that EVs drive tumorigenesis through induction of anchorage independent growth. EVs have been linked to *in vitro* anchorage-independent growth in both a breast cancer model (Ochieng et al., 2009) and in the transformation of fibroblasts (Rai et al., 2019), suggesting a strong role in modulating the tumor microenvironment. Related to Chapter 3 below, CRC cell-derived EVs can promote anchorage-independent growth, indicating a link between EVs and tumorigenesis in the CRC model (Demory Beckler et al., 2013). More recently,  $\beta$ 1-integrin+ EVs have been shown to promote anchorage-independent growth in a pancreatic tumor model, further suggesting that EVs can provide the required integrins and ECM proteins to support the growth of cells in environments with misregulated ECM formation, like that of a tumor (DeRita et al., 2019).

Drug and chemotherapeutic resistance is a significant problem in many cancers, and recent evidence suggests that EVs may mediate resistance via cell-to-cell communication (**Fig. 4**) (Kahlert and Kalluri, 2013). MCF-7 breast cancer cells develop resistance to docetaxel when exposed to EVs from resistant MCF-7 cells (Lv et al., 2014). Also, breast cancer cells secrete EGF2+ EVs that are able to sequester Trastuzumab and lower its overall effectiveness (Ciravolo et al., 2012). The transfer of extracellular lncRNA *ROR* in a hepatocellular cancer cell model led to increased chemoresistance through TGF- $\beta$  signaling activation, suggesting that resistance can potentially be driven through extracellular RNA-mediated mechanisms (Takahashi et al., 2014a). Cetuximab (CTX), a monoclonal antibody that targets the ectodomain of the EGFR, is used to treat late stage metastatic CRC in patients without KRAS mutations.



**Figure 4. EVs as Potential Mediators of Cancer Therapeutic Resistance**



**Figure 4.** Tumor cells secrete EVs that can promote therapeutic resistance in recipient susceptible cells via various mechanisms. (A) EVs may contain proteins, like receptors, that sequester therapeutic agents away from susceptible cells, reducing drug efficacy, and promoting growth under treatment conditions. (B) The transfer of oncogenic proteins via EVs can induce proliferation. (C) Non-coding RNAs can change transcriptional regulation in recipient cells by inhibiting the efficiency of various therapeutic agents or promoting the activation of signaling cascades not directly targeted by treatment.

Recent work in a CRC cell model suggests that EVs may mediate CTX resistance via the PTEN/Akt signaling cascade (Zhang et al., 2017). Further, the transfer of circRNAs has also been shown to promote CTX resistance in CRC (Hon et al., 2019). Interestingly, the Coffey laboratory has shown that CTX resistance can be induced via the overexpression of two miRNAs, *miR-100* and *miR-125b*, through targeting of negative regulators of Wnt signaling (Lu et al., 2017). Preliminary findings have shown that these miRNAs are enriched in CRC cell-derived EVs, suggesting that EV transfer of functional miRNAs may induce CTX resistance (see **Chapter 4**). Because of the well-known link between the PTEN/Akt and Wnt signaling pathway (Anderson and Wong, 2010), it may be that the EV-driven resistance found by Zhang et al. (2017) is mediated by the functional transfer of *miR-100* and *miR-125b* through the extracellular space. In fact, extracellular *miR-125b* has already been shown to play an important role in cancer progression (Vu et al., 2019).

#### **1.4 Conclusions**

The recent focus on EV research has shown that EV-mediated cell-to-cell communication plays a key role in normal cells and tissues, as well as in a variety of diseases, especially cancer. Understanding the biogenesis and mechanisms controlling cargo loading into EVs may help identify future therapeutic targets for cancer, or may aid in the development of drugs that can prevent or circumvent EV-mediated chemotherapeutic resistance. Although the biogenesis of EVs seem to be regulated in cell-type and disease-state specific mechanisms, Rab proteins have consistently been shown to be key players, not only in intracellular trafficking, but also in controlling the secretion of EVs. Thus, it is important to investigate if other Rab proteins play a role in EV secretion, and under what conditions. It will also be important to better understand the

heterogeneity of secreted vesicles, and to what extent that heterogeneity affects biogenesis, cargo loading, and function. Regulated loading of exRNAs may also drive EV-dependent cancer progression. How cancer cells regulate the export of RNA is not well understood and how these RNAs function in recipient cells remains to be determined. Understanding the molecular mechanisms underlying how EVs participate in cell-to-cell communication is likely to increase our understanding of both normal cell physiology and pathophysiology.

## Chapter 2

### **Diverse long-RNAs are differentially sorted into extracellular vesicles secreted by colorectal cancer cells**

Scott A. Hinger<sup>1</sup>, Diana J. Cha<sup>1</sup>, Jeffrey L. Franklin<sup>3,4,5</sup>, James N. Higginbotham<sup>3,4,5</sup>, Yongchao Dou<sup>2</sup>, Jie Ping<sup>2</sup>, Lihua Shu<sup>1</sup>, Nripesh Prasad<sup>6</sup>, Shawn Levy<sup>6</sup>, Bing Zhang<sup>2</sup>, Qi Liu<sup>2</sup>, Alissa M. Weaver<sup>3</sup>, Robert J. Coffey<sup>3,4,5</sup>, and James G. Patton<sup>1</sup>

Departments of Biological Sciences<sup>1</sup>, Biomedical Informatics<sup>2</sup>, Cell and Developmental Biology<sup>3</sup>, Medicine<sup>4</sup>, Vanderbilt University Medical Center, Nashville, TN, 37235, Veterans Affairs Medical Center<sup>5</sup>, Nashville, TN 37235, HudsonAlpha<sup>6</sup>, Huntsville, AL, and Vanderbilt University, Nashville, TN 37235.

Published, 2018 (Hinger et al., 2018).

#### **2.1 Abstract**

Although much is known about extracellular miRNA, the identity, regulation, and functional roles of secreted coding and long noncoding RNAs (lncRNAs, >200nt) are largely unknown. We have previously shown that mutant *KRAS* colorectal cancer (CRC) cells release EVs containing distinct proteomes, miRNAs, and circular RNAs. Here, we comprehensively identify the broad and diverse classes of CRC extracellular long RNAs secreted in EVs and demonstrate differential export of specific RNAs. We show that distinct noncoding RNAs including antisense transcripts and transcripts derived from pseudogenes are enriched in EVs compared to cellular profiles. Among coding mRNAs, we detected strong enrichment of *Rab13* in mutant *KRAS* EVs

## Chapter 2

and demonstrate functional delivery of *Rab13* mRNA to recipient cells in Transwell culture assays. To assay functional transfer of lncRNAs, we implemented a novel CRISPR/Cas9 based RNA-tracking system to monitor delivery to recipient cells. We show that gRNAs containing export signals from secreted RNAs, but not control gRNAs, are transferred from donor to recipient cells. Our data support the existence of cellular mechanisms to selectively export diverse classes of RNA.

### 2.2 Introduction

The majority of the human genome is transcribed into RNA but only ~2-3% encodes protein (Hangauer et al., 2013). Only a small fraction of noncoding RNA transcripts have been characterized, but they appear to play important regulatory roles in multiple biological contexts. Recently, numerous studies have demonstrated the presence of distinct types of extracellular RNA (exRNA) in diverse biological fluids, adding yet another surprise to the overall role of RNA in gene expression (Colombo et al., 2014a; Tkach and They, 2016). Because extracellular fluids display abundant ribonuclease activity, exRNA must be protected from degradation, either in protein complexes (Arroyo et al., 2011; Turchinovich et al., 2011), lipid complexes (Tabet et al., 2014; Vickers et al., 2011), or EVs (Ratajczak et al., 2006b; Skog et al., 2008; Valadi et al., 2007). EVs refer to membrane limited nanovesicles including exosomes, microvesicles, and other secreted vesicles (Raposo and Stoorvogel, 2013). Each class of vesicle is unique in its origin and/or size, and thus differs in its composition of lipid, protein, RNA, and potential DNA cargo (Colombo et al., 2014b; Mateescu et al., 2017).

EVs are released by all cell types and can serve as vehicles for transport of protein and RNA cargo between cells representing a novel mechanism for intercellular communication (Ratajczak et al., 2006b; Skog et al., 2008; Valadi et al., 2007). Local and systemic cargo transfer via EVs has been associated with tumor microenvironment interactions, aggressiveness and metastasis (Becker et al., 2016; Kalluri, 2016; Shurtleff et al., 2016). This potentially allows secretion of proteins and RNAs that could inhibit local growth and simultaneously “educate” distant tissues for metastasis (Peinado et al., 2012). Circulating RNAs encased in vesicles or protein complexes are often altered in cancer and bear tumor type-specific ‘signatures’, making them attractive candidates as clinical biomarkers for disease diagnosis and prognosis (Quinn et al., 2015).

Many exRNA studies have focused on miRNAs because they are well characterized, small, relatively stable, and well annotated (Cha et al., 2015a; Mittelbrunn et al., 2011; Valadi et al., 2007; Vickers et al., 2011). However, the diversity of exRNA is extensive and miRNAs are not the most abundant class of RNA found in EVs (Fritz et al., 2016; Mateescu et al., 2017). Analysis of cellular versus extracellular RNA has repeatedly demonstrated selective biogenesis, export, and/or stability of specific RNAs (Cha et al., 2015a; Dou et al., 2016; Kosaka et al., 2010; Santangelo et al., 2016; Skog et al., 2008; Squadrito et al., 2014; Valadi et al., 2007; Villarroya-Beltri et al., 2013b; Wei et al., 2017). Elucidation of the mechanisms for selective sorting of cargo into EVs is critical to understanding extracellular signaling by RNA.

In our ongoing efforts to understand the biological and pathological role of exRNAs regulated by oncogenic signaling, we utilized three isogenic CRC cell lines that differ only in the mutational status of the *KRAS* gene (Shirasawa et al., 1993). These lines are regularly checked to confirm their original *KRAS* status and mutation, and are passaged a limited number of times

to prevent further mutations from occurring. *KRAS* mutations occur in approximately 34-45% of colon cancers (Wong and Cunningham, 2008). The parental DLD-1 cell line contains both wild-type and G13D mutant *KRAS* alleles, while the isogenically-matched derivative cell lines contain only one mutant *KRAS* allele (DKO-1) or one WT *KRAS* allele (DKs-8) (Shirasawa et al., 1993). We previously showed that EVs from mutant *KRAS* CRC cells can be transferred to wild type cells to induce cell growth, migration, and invasiveness (Demory Beckler et al., 2013; Higginbotham et al., 2011). Additionally, we found that the miRNA profiles of EVs from all three cell lines are distinct from the parental cells, segregate dependent on *KRAS* status, and that specific miRNAs can be functionally transferred from mutant *KRAS* cells to wild type cells (Cha et al., 2015a). We also found that specific intracellular oncogenic signaling events can regulate trafficking of miRNAs through phosphorylation of Argonaute (AGO) proteins (McKenzie et al., 2016). More recently, we identified a global downregulation of circular RNAs (circRNAs) in mutant *KRAS* cells with an inverse upregulation in EVs (Dou et al., 2016). Here, we report comprehensive analysis of EV long RNAs (>200nt) and show that, similar to miRNA export, there is selective export of long RNAs to EVs. We also show that both mRNAs and lncRNAs can be functionally transferred between cells.

## **2.3 Results**

### **2.3.1 Comparison of long RNAs in cells versus EVs**

We previously isolated EVs through a series of differential ultracentrifugation steps and showed that the vesicles were approximately 40-130 nm in diameter with the typical cup shaped EM morphology and the expected pattern of protein markers consistent with endosome derived exosomes (Demory Beckler et al., 2013; Higginbotham et al., 2011). Protein and RNA was

isolated from these vesicles for proteomics, small RNA-seq, and circular RNA analysis (Cha et al., 2015a; Demory Beckler et al., 2013; Dou et al., 2016). In all cases, we found that EVs derived from mutant *KRAS* cell lines have distinct proteomes, miRNA profiles, and circular RNA profiles, compared to their parental cellular patterns and compared to EVs from WT *KRAS* cells. Here, we analyzed long RNA-seq (>200 nucleotides) libraries generated from the same vesicle and RNA preparations to determine whether long RNAs are selectively sorted into EVs from CRC cells. Long RNA-seq was performed on rRNA-depleted total cellular RNA and then the cellular RNA profiles were compared to EV RNA profiles. Without rRNA depletion, the majority of RNA-seq reads were derived from rRNA whereas depletion allowed more ready comparison of other differentially enriched RNAs. Comparison of RNA-seq libraries with or without rRNA depletion showed no significant effect on the detection of up-or down-regulated long RNA reads (data not shown). In our previous papers, we referred to our vesicle preparations as exosomes but we are aware that our preparations contain mixtures of lipoproteins and other protein complexes. Moving forward, we will refer to these vesicles as EVs. Regardless of nomenclature, all of our analyses are derived from the same preparations, allowing direct comparison to previous proteomic, small RNA-seq, and circular RNA-seq data (Cha et al., 2015a; Demory Beckler et al., 2013; Dou et al., 2016).

As a first analysis of the long RNA-seq data, we mapped reads to the human genome against both annotated and unannotated regions, allowing a maximum of 2 total mismatches. Alignment in this manner revealed that the mapping percentages were higher in the cellular datasets compared to the EV data sets. For all cellular profiles, ~70% of paired reads mapped to unique sequences in the human genome, while in EVs, the mapping percentages were much lower (30-50%)(**Fig. 5A**). The decreased abundance of unique mappable reads in the EV libraries was not due to amplification and sequencing of contaminating RNAs, but rather

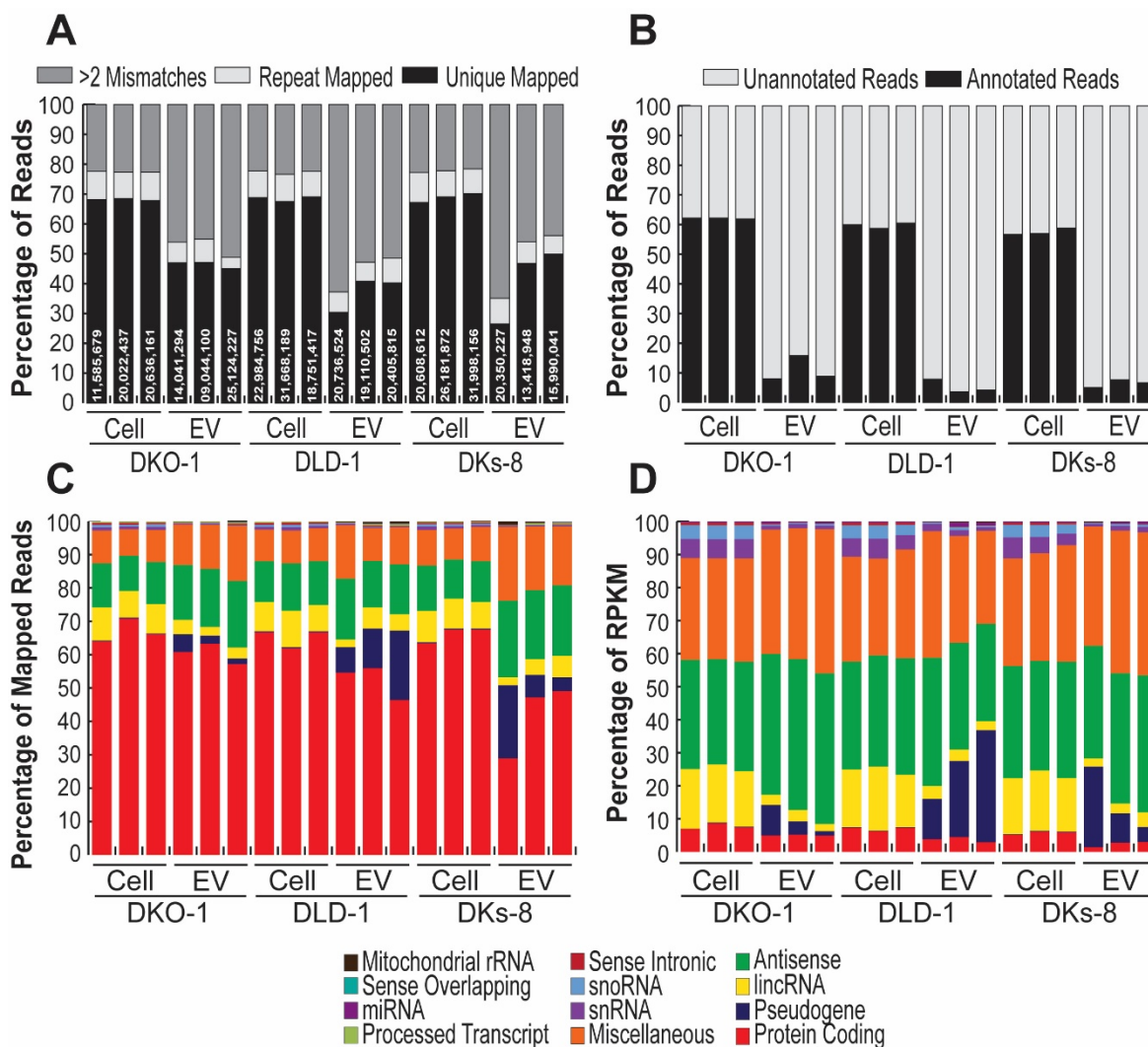


because multiple mismatches were more prevalent in EV RNA compared to parental cellular RNA. One possible explanation for the increase in mismatched reads is the presence of substantially more modified RNAs in EVs, which could alter base incorporation during library construction (Unpublished, Patton Laboratory).

We next restricted read mapping to unambiguous annotated genomic regions and then performed pairwise analyses between samples. In this case, the cell replicates showed high correlation ( $r=0.91-0.94$ ), while the EV replicates showed more variation between triplicate samples ( $r=0.76-0.95$ ) (**2.A.1**). We did not observe as much variability when analyzing extracellular small RNAs or for our proteomic analyses, but for unknown reasons, more variability was observed for the long RNA libraries. The variability was not due to differential quality of the input RNA and was not due to lower sequencing depth. Nevertheless, when we compared the RNA profiles from EVs to their parental cells focusing only on annotated genes, the analysis showed that specific RNAs are selectively exported into EVs, consistent with low correlation between EVs and cells (DKO-1  $r=0.68-0.72$ , DKs-8  $r=0.68-0.78$ , DLD-1  $r=0.66-0.73$ ) (**2.A.1**). In the cellular datasets, a majority of reads corresponded to unique annotated gene regions (~60%) while a much smaller percentage of reads in the EV profiles mapped to unique annotated genes (~5-15%) (**Fig. 5B**). The remaining unassigned reads in both the cellular and EV datasets represent novel RNA species that map to unannotated loci. This is supported by the difference in the percentage of unique mapped reads in both the cellular (~70%) and EV samples (~30-50%) when mapping was not restricted to annotated gene regions (**Fig. 5A**).

Although the majority of annotated long RNA-seq reads mapped to known protein coding sequences in both the cellular and EV datasets, we discovered differential enrichment of specific RNAs between cells and EVs (**Fig. 5C**).

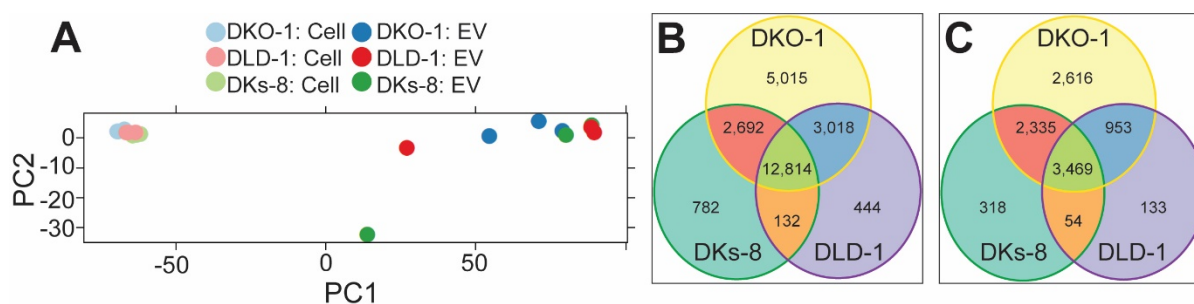
**Figure 5. Long RNA-seq Analysis of EV and Cellular RNA from CRC Cell Lines.**



**Figure 5.** RNA-seq libraries were prepared from transcripts greater than 200 nucleotides from isogenic CRC cell lines and EVs that differ only in KRAS status. The parental DLD-1 cells contain both wild type and mutated KRAS (G13D) alleles, Dks-8 cells contain only a wild type KRAS allele, and DKO-1 cells contain only a mutated KRAS allele. (A) Percentage of reads that map to repeat regions (white), unique regions (black), or reads that contained >2 mismatches (grey) and could therefore not be uniquely mapped to the human genome. Read mapping was to both annotated and unannotated regions of the human genome and the results are plotted as a percentage of total reads per library (white text). (B-C) The unique mapped reads in A were further broken down as percentages of reads that map to unique annotated reads expanded by RNA subtype (B; color scheme at bottom) or plotted as a percentage of total reads (C). When mapping percentages were calculated based on total reads, coding transcripts constitute the largest percent of reads in both cellular and EV samples. (D) Unique annotated mapped reads expanded by RNA subtype (color key at bottom) but plotted as percentage of RPKM. Normalizing by RPKM shows the relative composition of noncoding RNAs in the RNA-seq data sets.

In cells, a higher percentage of transcripts corresponded to protein coding genes and known lncRNAs as compared to EVs. For EVs, we observed enrichment of transcripts derived from pseudogenes and antisense RNAs, with pseudogene transcripts being almost undetectable in cellular samples ( $\leq 0.3\%$ ) (**Fig. 5C**). To better approximate the expression levels of RNAs as opposed to individual read counts, RNAs were plotted by subtype normalized to RPKM. As expected with such normalization, smaller RNAs became more prevalent in both the cellular and extracellular samples, but the relative differential enrichment was unaffected (**Fig. 5D**).

**Figure 6. KRAS Dependent Sorting of Long RNAs Into EVs.**



**Figure 6.** Long RNA-seq profiles were analyzed to identify differentially enriched transcripts in both cells and EVs. (A) Principal Component Analysis comparing cellular (opaque) and EV (solid) RNA-seq data sets. The long RNA composition in cells differed significantly from exosomes indicating that selective sorting mechanisms control export to EVs. Compared to similar miRNA profiles that could readily identify KRAS status. KRAS status could not be readily inferred when comparing long RNA-seq profiles. (B) Number of unique long RNAs upregulated in EVs versus cells differing in KRAS status. (C) Number of unique long RNAs upregulated in cells versus EVs differing in KRAS status.

### 2.3.2 Differential RNA export and KRAS status

To further analyze whether the overall long RNA profiles are distinct between cells and EVs and between wild-type and mutant KRAS, we performed Principal Component Analysis (PCA). PCA analysis revealed that the repertoire of long RNAs is clearly distinct when comparing parental cellular RNA profiles and their secreted EV RNAs (**Fig. 6A**). Across the

three cell lines, RNA expression patterns clustered together and were distinct from EVs, indicating that KRAS-driven differential RNA expression is less pronounced when comparing patterns across cells, as opposed to comparing patterns between EVs and their cognate cell lines. However, if the cellular RNA expression patterns are compared alone, the profiles segregate by KRAS status under a variety of culture conditions (**2.A.2**).

### **2.3.3 Differential enrichment of ncRNAs and mRNAs in EVs**

Differential gene expression analyses were performed comparing cellular RNAs to their cognate EVs, comparing cellular RNAs between the three cell lines differing in KRAS status (mutant cell/WT cell), and comparing EV RNA profiles differing in KRAS status (mutant EV/WT EV). The top differentially expressed RNAs in either wild type or mutant KRAS cells and exosomes are shown in **Table 4** (more extensive list in **2.A.3**). When comparing EVs to their parent cells, we found that DKO-1 mutant KRAS EVs were enriched for a dramatically different population of RNAs compared to EVs from either WT (DKs-8) or heterozygote (DLD-1) KRAS EVs (**Fig. 6B**). A similar trend was observed when comparing cellular RNA patterns in mutant versus wild type or heterozygote cell lines (**Fig. 6C**). Thus, the diversity of RNAs targeted for export is much greater in mutant KRAS cells, especially cells with a single mutant allele and no wild type KRAS allele (DKO-1). It is important to note that the vast majority of long RNAs upregulated in EVs are shared across all three isogenic lines (12,814 RNAs), suggesting export mechanisms for these RNAs are largely KRAS-independent (**Fig. 6B**). This is in contrast to what we observed in previous miRNA profiles where the majority of RNAs were upregulated in DKO-1 EVs (Cha et al., 2015a). Proteomic profiles from DKO-1 and DLD-1 derived EVs were more similar to each other when compared to Dks-8 derived EVs (Demory Beckler et al., 2013).

Gene ontology analysis of unique upregulated exRNAs was carried out to better

understand the possible impact of EV RNA signaling (**2.A.4**). Interestingly, about 5,000 EV RNAs could not be uniquely assigned to specific GO categories, indicating that a large population of unannotated RNAs are specifically exported into EVs, and that their potential function is yet to be understood.

### **2.3.4 mRNA export into EVs**

We detected numerous reads derived from mRNAs that were enriched in EVs. Several of these have known roles in oncogenesis including *Rab13*, *NET1*, and *NEDD4* (Ioannou et al., 2015). Some mRNAs had exosomal read distribution patterns consistent with intact, full-length mRNA, meaning abundant reads mapping across all exons with nearly undetectable reads across introns (**2.A.5**). For example, the data for *Rab13* and *BMI1* supported the presence of mature, intact mRNA due to the distribution and quantity of reads spanning the entire coding sequence in both cellular and EV datasets. In contrast, EV reads from other mRNAs (e.g. *Rab3b*) showed not only reads derived from exons, but also abundant reads across introns, suggesting export of either unprocessed, unspliced mRNA transcripts, or, more likely, RNA fragments (**2.A.5**).

Because RNA-seq cannot distinguish between full-length or fragmented sequences, we used RT-qPCR and RT-PCR to both validate the level of mRNAs in EVs and also to test whether full-length transcripts are present in EVs (**2.A.6**, **2.A.7**). With the caveat that technical difficulties might inhibit reverse transcription of long RNAs, we were not able to amplify most mRNAs greater than 1kb suggesting that the majority of longer mRNAs are probably not present as intact mRNAs in EVs, consistent with previous work (Wei et al., 2017). Interestingly, mRNAs that displayed a mature, spliced read distribution pattern could not always be detected as full-length RNA in EVs by RT-PCR. For example, we could not detect full length *BMI1* transcripts by

RT-PCR whereas we were able to detect full length *Rab13* and *β-actin* mRNAs (**2.A.7**).

Interestingly, Rab13 protein was upregulated >21-fold in DKO-1 EVs, whereas in DKs-8 EVs, enrichment for Rab13 protein was <4-fold (Demory Beckler et al., 2013). This trend was also observed for *Rab13* mRNA, which is upregulated in EVs from all three cell lines, but most upregulated in DKO-1 EVs (**2.A.6**). Actin levels were not enriched in any of the EV preparations compared to cellular profiles.

### **2.3.5 lncRNA export into EVs**

For differential EV enrichment of lncRNA, we found numerous lncRNAs enriched in EVs compared to their matched cognate cells, including anti-sense RNAs, and transcripts derived from pseudogenes. The majority of highly upregulated lncRNAs are either unannotated or haven't been previously studied, suggesting possible novel roles for these RNAs through their export into EVs (**Table 4, 2.A.3**).

### **2.3.6 Extracellular transfer of mRNA**

We previously showed that miRNAs could be transferred extracellularly between donor and recipient cells using Transwell assays (Cha et al., 2015a). As with miRNAs, transfer of long coding and noncoding RNAs could serve as an important intercellular communication mechanism, (Tkach and They, 2016). *Rab13* is upregulated in mutant *KRAS* DKO-1 EVs compared to both cellular profiles and EVs from wild type *KRAS* cells (**2.A.6**). Further, we detected full length *Rab13* mRNA within DKO-1 EVs (**2.A.7**). To test whether *Rab13* mRNA could undergo extracellular transfer from donor to recipient cells, we again utilized Transwell assays. For these assays, DKO-1 (*KRAS* mutant) or DKs-8 (*KRAS* wildtype) donor cells were separately transfected with a vector expressing an HA-tagged version of *Rab13*.

**Table 4. Top 10 Long RNAs Enriched in EVs and KRAS Mutant and WT Cells.**

**MUTANT KRAS**

EV UPREGULATION		
Gene name	RNA Subtype	Log(2) Fold Change
<b>NON-CODING</b>		
CTD-2328D6.1	lincRNA	11.43
REXO1L1P	Pseudogene	9.05
ERVH-1	endogenous retrovirus group H member 1	8.47
LINC01609	lincRNA	8.21
ESRG	embryonic stem cell related (non-protein coding)	7.98
LINC00504	Antisense RNA	7.34
LINC02503	lincRNA	7.15
AC087473.1	lincRNA	7.07
AL671511.1	lincRNA	6.96
UGDH-AS1	UGDH antisense RNA 1	6.14
<b>CODING</b>		
HHLA1	HERV-H LTR-associating 1	7.51
CYSLTR1	cysteinyl leukotriene receptor 1	7.47
MAB21L3	mab-21 like 3	7.23
TMEM212	transmembrane protein 212	6.74
CFAP54	cilia and flagella associated protein 54	6.71
ABCC9	ATP binding cassette subfamily C member 9	6.66
TRIM22	tripartite motif containing 22	6.63
C12orf50	chromosome 12 open reading frame 50	6.62
ADAMTSL3	ADAMTS like 3	6.58
RAB13	member RAS oncogene family	6.12

CELLULAR UPREGULATION		
Gene name	RNA Subtype	Log(2) Fold Change
<b>NON-CODING</b>		
AL356488.2	lincRNA	-6.89
SNORA46	small nucleolar RNA, H/ACA box 46	-6.50
RNU2-6P	RNA, U2 small nuclear 63, pseudogene	-6.39
SNORA53	small nucleolar RNA, H/ACA box 53	-6.19
SNORD3A	small nucleolar RNA, C/D box 3A	-6.07
MIR3609	miRNA host RNA	-6.02
SNHG3	small nucleolar RNA host gene 3	-5.98
7SK	Miscellaneous RNA	-5.76
RNVU1-6	RNA, variant U1 small nuclear 6	-5.76
SNORD3B-2	small nucleolar RNA, C/D box 3B-2	-5.75
<b>CODING</b>		
FNIP1	folliculin interacting protein 1	-6.00
SUPT4H1	SPT4 homolog, DSIF elongation factor subunit	-4.94
CCNL2	cyclin L2	-4.78
HEATR3	HEAT repeat containing 3	-4.66
ZBED5	zinc finger BED-type containing 5	-4.59
ACSL5	acyl-CoA synthetase long chain family member 5	-4.54
TSN	translin	-4.49
OAT	ornithine aminotransferase	-4.45
FBXW11	F-box and WD repeat domain containing 11	-4.31
APH1A	aph-1 homolog A, gamma-secretase subunit	-4.17

**WILDTYPE KRAS**

EV UPREGULATION		
Gene name	RNA Subtype	Log(2) Fold Change
<b>NON-CODING</b>		
CTD-2328D6.1	pseudogene	11.67
REXO1L1P	REXO1 like 1, pseudogene	9.30
LINC01609	lincRNA	7.69
ESRG	embryonic stem cell related (non-protein coding)	7.15
LINC00504	lincRNA	7.08
AL590867.1	lincRNA	7.06
LINC02503	lincRNA	6.70
LACTB2-AS1	LACTB2 antisense RNA 1	6.47
TPTEP1	TPTE pseudogene 1	6.28
AC126768.3	lincRNA	5.71
<b>CODING</b>		
CYSLTR1	cysteinyl leukotriene receptor 1	7.05
HHLA1	HERV-H LTR-associating 1	7.30
TTN	titin	7.14
MAB21L3	mab-21 like 3	6.90
SPINK9	serine peptidase inhibitor, Kazal type 9	6.82
CFAP54	cilia and flagella associated protein 54	6.32
TRIM22	tripartite motif containing 22	6.27
ABCC9	ATP binding cassette subfamily C member 9	6.26
KIAA1328	KIAA1328	5.75
TBC1D8B	TBC1 domain family member 8B	5.09

CELLULAR UPREGULATION		
Gene name	RNA Subtype	Log(2) Fold Change
<b>NON-CODING</b>		
AL356488.2	lincRNA	-6.77
SNORD3A	small nucleolar RNA, C/D box 3A	-6.26
SNORD15B	small nucleolar RNA, C/D box 15B	-5.91
SNORD17	small nucleolar RNA, C/D box 17	-5.57
SNORA23	small nucleolar RNA, H/ACA box 23	-5.48
SCARNA10	small Cajal body-specific RNA 10	-5.39
SNORA12	small nucleolar RNA, H/ACA box 12	-5.27
SNORA74A	small nucleolar RNA, H/ACA box 74A	-5.22
RNU2-63P	RNA, U2 small nuclear 63, pseudogene	-5.01
SNORD3B-2	small nucleolar RNA, C/D box 3B-2	-4.95
<b>CODING</b>		
SLC12A2	solute carrier family 12 member 2	-5.43
FOS	Fos proto-oncogene, AP-1 transcription factor subunit	-4.84
SLC16A1	solute carrier family 16 member 1	-4.84
ACSL1	acyl-CoA synthetase long chain family member 1	-4.56
OAT	ornithine aminotransferase	-4.53
HMGCR	3-hydroxy-3-methylglutaryl-CoA reductase	-4.52
SIK1	salt inducible kinase 1	-4.45
VMP1	vacuole membrane protein 1	-4.45
TFRC	transferrin receptor	-4.35
ATCB1	ATP binding cassette subfamily B member 1	-4.32

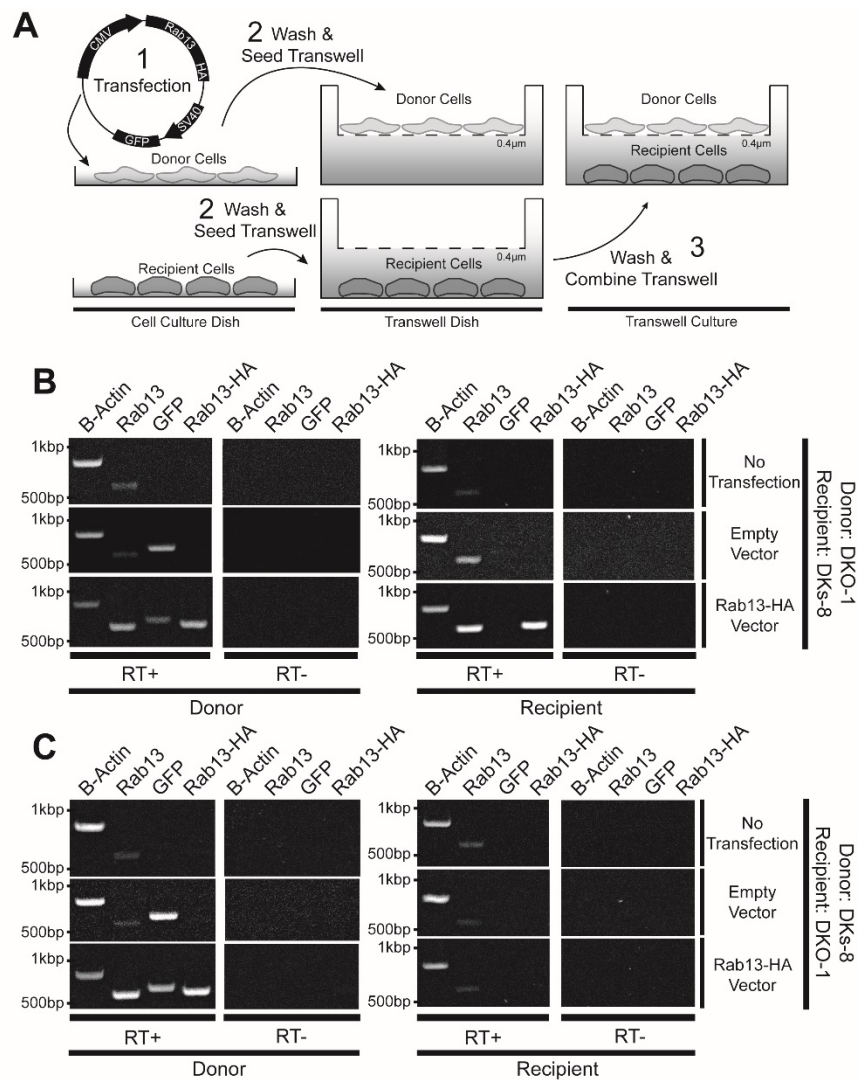
Transfected cells were then trypsinized, washed extensively, and seeded as donor cells on top of a 0.4µm polyester membrane in Transwell dishes (**Fig. 7A**). Recipient cells were separately cultured underneath the membrane. Subsequently, the Transwell dishes were combined and co-cultured for 48 hours, after which RNA and protein were isolated from the respective dishes. By RT-PCR, we were able to detect an approximate 5-fold increase in full length *Rab13-HA* mRNA in recipient cells only when the donor cell carried a KRAS mutation (DKO-1) (**Fig. 7B, Fig. 2.A.7**). In contrast, no detectable transfer of *Rab13-HA* mRNA was observed when we flipped the experiment and used wild type KRAS DKs-8 cells as the donor cells (**Fig. 7C**). This suggests that functional transfer of *Rab13-HA* mRNA is driven by a KRAS-dependent mechanism. To eliminate the possibility of plasmid contamination or transfer, RT-PCR experiments were carried out with or without DNase I treatment and with or without reverse transcriptase in the RT reaction, all of which supported extracellular transfer of *Rab13-HA* mRNA. *Rab13-HA* protein was also detectable in recipient cells (**2.A.7**), but again, only when DKO-1 cells served as the donor cells. In this case, the tagged protein could have been transferred in EVs or *Rab13-HA* mRNA could have been transferred and subsequently translated in the recipient cells.

### **2.3.7 Extracellular transfer of synthetic lncRNAs**

The functional role of most lncRNA remains to be discovered, making the measurement of their transfer by EVs less straightforward. To test for transfer of lncRNAs, we developed a modified version of the CRISPR-Display system (**Fig. 8A**) (Shechner et al., 2015). This system was designed to target lncRNAs to specific genomic loci via gRNAs with an accompanying transcriptional read out. We adapted this technique to quantify analysis of RNA transfer. The system uses a gRNA with an engineered loop that allows insertion of any RNA sequence of



**Figure 7. Extracellular Transfer of Rab13 mRNA.**



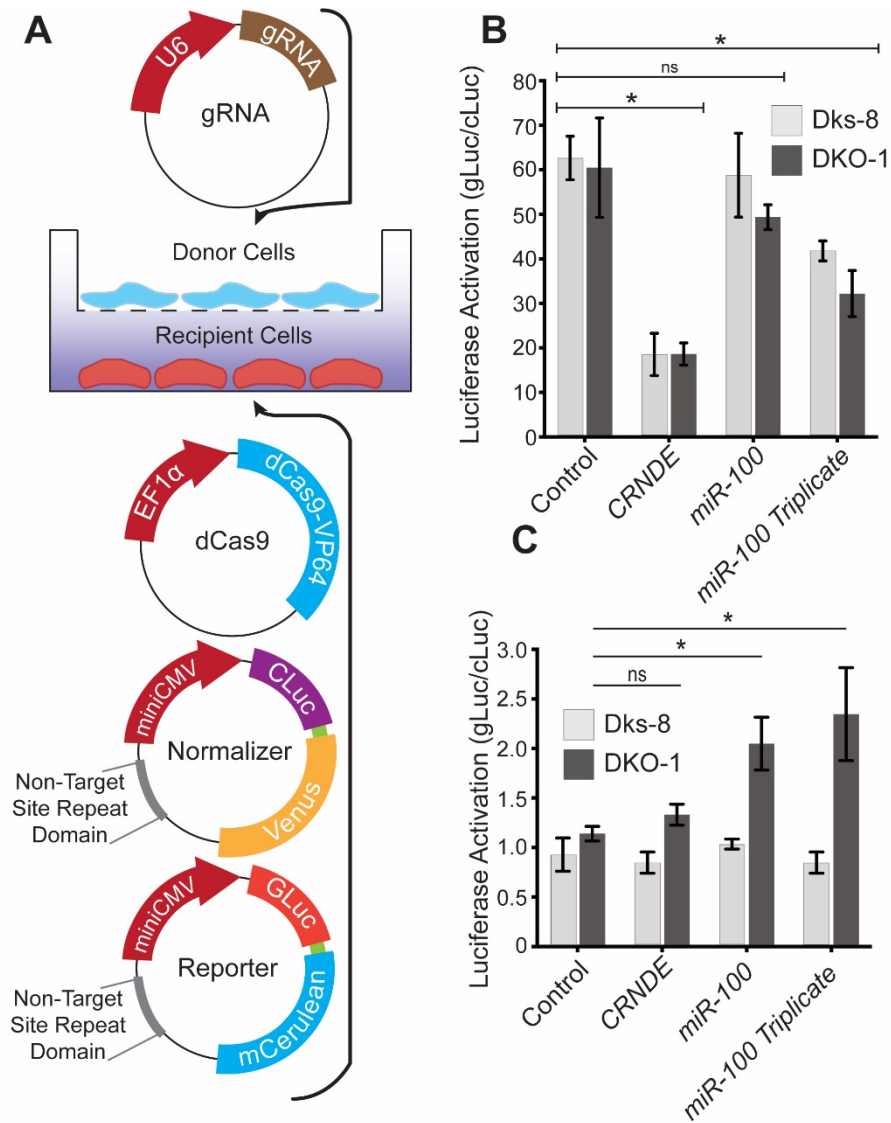
**Figure 7.** (A) Schematic of Rab13-HA transwell assay. (1) Donor cells were separately transfected with the Rab13-HA plasmid. (2) Transfected donor cells were trypsinized and washed extensively before seeding into Transwell dishes. Recipient cells were also cultured separately before trypsinizing, washing and seeding into Transwell dishes. Donor cells were seeded on top of a 0.4µm membrane and recipient cells are seeded below the membrane. (3) After 24 hours to allow adherence, cells were washed with PBS, the media was changed, and the Transwell dishes were combined and allowed to co-culture for 48 hours after which protein and RNA collection was performed. (B-C) RT/PCR of Transwell cultures. RNA was collected under three distinct conditions: (1) No transfection, (2) empty vector transfection, or (3) transfection of the Rab13-HA vector. PCR was carried out on two cDNA populations in the presence (RT+) or absence of RT (RT-), as indicated. RT/PCR was carried out on β-Actin, cellular Rab13 mRNA, GFP mRNA, or Rab13-HA mRNA. (B) RT-PCR of Transwell assays with DKO-1 donor cells and DKs-8 recipient cells. (C) RT-PCR of Transwell assays with DKs-8 donor cells and DKO-1 recipient cells.

interest. The gRNA then targets a dead Cas9 (dCas9) protein fused to the transcriptional activator VP64 to a specific DNA sequence, allowing activation of reporters encoding luciferase, fluorescent proteins, and selectable markers (Shechner et al., 2015). To test for transfer of gRNAs as a proxy for longer noncoding RNAs, we inserted candidate RNAs within the gRNA and expressed unmodified and modified guide RNAs in donor cells in Transwell cultures. Secretion of gRNAs from donor cells that traverse the Transwell membrane and are internalized in recipient cells activate reporter expression in recipient cells. Transfer is quantified based on secreted luciferase (gLuc) levels, production of unique fluorescent proteins, or the development of antibiotic resistance.

We first verified the system by expressing all components in the same cells (i.e. no extracellular transfer) and observed robust activation of luciferase with both unmodified gRNAs or gRNAs containing an insertion of 1 or 3 copies of *miR-100*, which is 22 nucleotides in length (**Fig. 8B**). We chose *miR-100* due to previous experiments demonstrating that *miR-100* is trafficked into mutant KRAS EVs and is capable of functional extracellular transfer in a KRAS-dependent manner (Cha et al., 2015a). We also tested gRNAs containing an insertion of the 700nt lncRNA CRNDE which was not significantly enriched in EVs (Ellis et al., 2012). Expression of all components in the same cells showed that unmodified gRNAs and gRNAs containing either 1 or 3 copies of *miR-100* could properly target dCas9-VP64 to the reporter promoter, resulting in ~50-60-fold increase in gLuc levels. By comparison, insertion of CRNDE lncRNA inhibited gRNA function but still resulted in a ~15-fold increase in gLuc levels.

To test extracellular transfer of modified gRNAs, we used the Transwell system similar to the *Rab13-HA* mRNA experiments and with the same controls (**Fig. 8A**). Donor cells were separately transfected with the various gRNA constructs, while recipient cells were separately transfected with the dCas9~VP64, gLuc, and cLuc reporter constructs.

**Figure 8. Functional Transfer of lncRNAs With CRISPR-Display.**



**Figure 8.** To detect transfer of lncRNAs, we adapted the CRISPR-Display system for use in Transwell cultures. (A) Schematic of modified CRISPR-Display to quantify lncRNA transfer. Donor cells were separately transfected with vectors expressing either wild type gRNAs or gRNAs containing an insertion of the indicated noncoding RNA. Recipient cells were separately transfected with vectors expressing dCas9-VP-64 transcriptional activator, a reporter encoding a secreted form of gLuciferase, and a reporter expressing cLuciferase for normalization. Following the same protocol as in Fig. 3, Transwell dishes were co-cultured for 48 hours and secreted luciferase levels were normalized and quantified. (B) Activation of luciferase in the absence of extracellular gRNA delivery. Dks-8 or DKO-1 cells were transfected with all the CRISPR Display plasmids shown at left. (C) Activation of luciferase after extracellular gRNA delivery. After 48 hours in Transwell cultures, luciferase levels were normalized and quantified with donor cells expressing either unmodified donor gRNAs (control) or gRNAs containing insertions of CRNDE, 1 copy of *miR-100* or 3 copies of *miR-100* (\*  $p < 0.05$ ). Experiments were performed with either Dks-8 or DKO-1 donor cells.

Transfected cells were extensively washed, and then plated in Transwell cultures for 48 hours. Baseline activation of luciferase was measured in recipient cells (either DKO-1 or DKs-8) co-cultured with donor cells (either DKO-1 or DKs-8) expressing unmodified gRNAs (gRNA-CTL). Little to no luciferase activation was observed under these conditions, indicating no extracellular transfer of unmodified gRNA (**Fig. 8C**). However, insertion of either 1 or 3 copies of *miR-100* into the gRNA resulted in a statistically significant 2-fold increase in luciferase activity, but only when the donor cells carried a mutant KRAS allele (DKO-1) (**Fig. 8C**). We did not observe activation of luciferase when wild type KRAS donor cells (DKs-8) were used. Insertion of CRNDE lncRNA did not lead to increased luciferase levels when extracellular transfer was required, regardless of what cell type served as the donor cell. The fact that reporter activation with *miR-100* was only observed with mutant KRAS donor cells is consistent with previous data (Cha et al., 2015a). Together, the data demonstrate that noncoding gRNAs can not only be transferred between cells but, remarkably, be imported into the nuclei of recipient cells to functionally activate transcription of reporters. They also demonstrate that *miR-100* contains an export signal(s) that can drive extracellular transfer.

Consistent with transfer via EVs, we were able to detect full length modified gRNAs in the EV pellet (**2.A.7**). The decrease in GLuc activation between expression of all components in the same cells versus after extracellular RNA transfer probably reflects the relative efficiency of exRNA transfer, but could also be a dramatic underestimate due to variable transfection efficiencies of the four different vectors in the two cell types.

## 2.4 Discussion

### 2.4.1 Selective export and functional transfer of RNA

Our data support the hypothesis that long RNA export into EVs is a selective process and that RNA expression profiles from EVs do not simply reflect cellular RNA abundance (Kosaka et al., 2010; Santangelo et al., 2016; Skog et al., 2008; Squadrito et al., 2014; Valadi et al., 2007). Since original studies suggesting horizontal transfer of mRNAs and proteins (Ratajczak et al., 2006a; Skog et al., 2008; Valadi et al., 2007), almost all known classes of RNA have been detected in extracellular fluids (Fritz et al., 2016). However, definitive studies demonstrating functional long coding and noncoding RNA transfer are limited (Ridder et al., 2014; Skog et al., 2008). We show that long coding and noncoding RNAs can be transferred between donor and recipient cells and that KRAS status plays a role in regulating this transfer.

From quantitative stoichiometric analysis of RNA levels in EVs (Chevillet et al., 2014; Wei et al., 2017), it remains unclear what effect extracellular RNA signaling can have on recipient cells. Our data support the idea that exRNA transfer is indeed possible, but dramatic changes in gene expression in recipient cells would seem to require direct, continuous targeting of EVs from donor to recipient cells. These effects will be different for long versus short range EV transfer or for direct membrane-membrane transfer between cells, as in the immune synapse (Ortega-Carrion and Vicente-Manzanares, 2016). The Transwell system mimics systemic delivery but lacks the full range of possible recipient cells that would be present *in vivo*. Using Transwell assays, we previously showed that we could achieve a 34% increase in *miR-100* after transfer from donor to recipient cells (Cha et al., 2015a). Given the half-life of most miRNAs and their ability to repress multiple targets, such transfer could be biologically significant. Here, we show that transcripts from pseudogenes are enriched in EVs which could

not only alter gene expression patterns in donor cells, but also recipient cells. Pseudogene transcripts have been shown capable of titrating miRNA levels due to binding sites in their 3'UTRs (Poliseno et al., 2010). The tumor suppressor gene *PTEN* and the oncogene *KRAS* both have pseudogenes, *PTENP1* and *KRAS1P*, respectively (McGrath JP, 1983; Poliseno et al., 2010). *PTENP1* can regulate *PTEN* levels and exert a growth-suppressive role and down regulation of *PTEN* expression is associated with focal copy number losses at the *PTENP1* locus in sporadic colon cancer patient samples (Poliseno et al., 2010). A similar relationship was observed between *KRAS* and its pseudogene *KRAS1P*, where transcript levels are positively correlated in different tumors suggesting a proto-oncogenic role for *KRAS1P* (Poliseno et al., 2010). Transcripts from both *PTENP1* and *KRAS1P* were detected in *KRAS* mutant EVs, while transcripts from *PTENP1* were upregulated in EVs regardless of *KRAS* status. This suggests a possible role in transcriptional regulation through cell-cell transfer of pseudogene derived lncRNAs by extracellular delivery, potentially through modulation of miRNA activity.

For mRNA transfer, even relatively small increases in recipient cells could substantially alter gene expression, dependent on the activity and half-life of a given mRNA/protein. Rab13 is a member of the Rab family of GTPases that regulate vesicle trafficking and has been implicated in controlling multiple proteins with roles in cancer (McPherson, 2016). Increased Rab13 expression has been detected in radiotherapy resistant cells such that local transfer of *Rab13* mRNA in tumors could significantly alter the outcome of radiation treatment (Kim et al., 2012). It will be interesting to identify what signals drive export of specific mRNAs in EVs.

#### **2.4.2 Size limitations on EV transfer**

It remains unknown whether there is a strict RNA size limitation for inclusion into EVs. From a variety of biofluids, it was reported that the majority of EV-associated RNAs fall within a

size distribution of 25-700nt (Noerholm et al., 2012; Pegtel et al., 2010). When we compared RNA profiles from EVs to cells, we found that the size distribution of annotated transcripts was similar, suggesting that smaller RNAs are not preferentially exported into EVs. However, identification of mapped reads within EV profiles does not guarantee that these RNAs are full length. In fact, it appears by RT-PCR that intact longer RNAs are generally less than 1000nt (data not shown)(Wei et al., 2017). In addition to size limitations, it is unknown whether secreted long RNAs are characterized by a specific fragmentation or cleavage pattern. In certain contexts, EV-associated mRNAs are enriched for 3'-UTR fragments (Batagov and Kurochkin, 2013; Wei et al., 2017). This may have important implications in regulating gene expression in target cells since the 3'-UTRs of mRNAs are rich in regulatory sequences, similar to the effects of pseudogene transcripts described above (McGrath JP, 1983; Poliseno et al., 2010). Although the precise mechanisms for how 3'UTRs are selected for secretion are unknown, one possibility is that mRNAs undergo post-transcriptional cleavage to produce 3'UTR fragments (Mercer et al., 2010). Another possibility is that EV-associated mRNAs undergo degradation after secretion via extracellular RNases and/or that RISC complexes (RNA Induced Silencing Complexes) are exported into EVs and mRNAs are therefore subject to deadenylation and decay via RISC components (McKenzie et al., 2016; Melo et al., 2014).

### **2.4.3 Mechanisms of RNA export**

Previously, we showed KRAS-dependent selective export of miRNAs (Cha et al., 2015a). For longer RNAs, Principal Component Analysis (PCA) allows segregation between EV and cellular profiles, but KRAS-dependent sorting is not as obvious for EVs. When we restricted PCA analysis to specific long RNA subtypes, the same trends were observed but we noticed much greater variation between exosomal profiles. Together, the data seem to indicate that

mechanisms regulating export of longer RNAs are distinct from those regulating export of miRNAs. One possibility is that among the wide diversity of long RNAs being exported to EVs, some are being secreted simply as part of normal cellular decay whereas others might be more tightly regulated. Potentially, miRNAs are more tightly regulated as a subtype of RNA because they are exported largely intact whereas the range of long RNAs may encompass both intact and fragmented RNAs. This is consistent with the fact that miRNAs are more frequently being examined as potential biomarkers in various extracellular fluids, but as sequencing of such fluids continues, specific long RNAs might be identified that are subject to tightly regulated export and therefore more likely to serve as useful biomarkers of disease (Freedman et al., 2016; Matsumura et al., 2015; Quinn et al., 2015).

## **2.5 Methods**

### **2.5.1 EV isolation**

EVs were isolated from conditioned medium of DKO-1, Dks-8, and DLD-1 cells (Higginbotham et al., 2011). Pooled media was centrifuged for 10 min at  $300 \times g$  and the supernatant was filtered through a 0.22- $\mu$ m polyethersulfone filter (Nalgene, Rochester, NY). The filtrate was concentrated  $\sim 300$ -fold with a 100,000 molecular-weight cutoff centrifugal concentrator (Millipore) and then subjected to high-speed centrifugation at  $150,000 \times g$  for 2 hours. The resulting EV-enriched pellet was resuspended in PBS containing 25 mM HEPES (pH 7.2) and washed by centrifuging at  $150,000 \times g$  for 3 hours. The wash steps were repeated a minimum of 3 times. The resulting pellet was resuspended in PBS containing 25 mM HEPES (pH 7.2).



### **2.5.2 RNA purification**

Total RNA from EVs and cells was isolated using TRIzol (Life Technologies). For EV RNA isolation, TRIzol was incubated with 100  $\mu$ l or less of concentrated EVs for an extended 15 min incubation prior to chloroform extraction. RNA pellets were resuspended in 60  $\mu$ l of RNase-free water and were then re-purified using the miRNeasy kit (QIAGEN).

### **2.5.3 mRNA library preparation and sequencing**

Total RNA was extracted from EVs or cell lines using TRIzol followed by miRNeasy Kit purification. Final elution was in 60  $\mu$ l RNase free sterile distilled water. The concentration and integrity of the extracted total RNA was estimated by Qubit<sup>®</sup> 2.0 Fluorometer (Invitrogen, Carlsbad, California), and Agilent 2100 Bioanalyzer (Applied Biosystems, Carlsbad, CA), respectively. RNA samples with a RIN value of at least 7.0 or higher were used for further processing for cellular RNAs. Approximately 500 ng of total RNA were required for proceeding to downstream RNA-seq applications. Ribo-zero Magnetic Gold rRNA removal kits (Epicenter, Illumina Inc.) were used to remove ribosomal RNA from the total RNA. First strand synthesis was performed using NEBNext RNA first strand synthesis module (New England BioLabs Inc., Ipswich, MA, USA). Directional second strand synthesis was performed using NEBNext Ultra Directional second strand synthesis kit. Resulting cDNAs were used for library preparation using NEBNext<sup>®</sup> DNA Library Prep Master Mix Set for Illumina<sup>®</sup> with slight modifications. Briefly, end-repair was performed followed by poly-A addition and custom adapter ligation. Post-ligated materials were individually barcoded with unique in-house genomics service lab (GSL) primers. Library quality was assessed by Qubit 2.0 Fluorometer, and the library concentration was estimated by utilizing a DNA 1000 chip on an Agilent 2100 Bioanalyzer. Accurate quantification for sequencing applications was

determined using qPCR-based KAPA Biosystems Library Quantification kits (Kapa Biosystems, Inc., Woburn, MA). Each library was diluted to a final concentration of 12.5 nM and pooled equimolar prior to clustering. Paired-End (PE, 150bp) sequencing was performed on all samples. Raw reads were de-multiplexed using a bcl2fastq conversion software v1.8.3 (Illumina, Inc.) with default settings.

#### **2.5.4 Read mapping**

Read sequencing quality checks were performed using FastQC (v0.11.2). Reads were mapped to the human genome hg19 (UCSC) using tophat2 (v2.0.13) with gene annotation from Gencode version 19. Htseq-count (version 0.6.1p1) was used for counting with the same annotation as mapping. DESeq2 was used to perform differential analysis and PCA analysis. The trimmed mean of M values (TMM) was used for normalization. The cutoffs for log<sub>2</sub> fold change (log<sub>2</sub>FC) and PDR were |log<sub>2</sub>FC| >= 1 and FDR <= 0.001. Functional enrichment analysis was analyzed using WebGestalt (Wang et al., 2017).

#### **2.5.5 Gene ontology**

Reads were mapped as above with two differences: DESeq2 was used to detect differential expression between exosomes and cells, and reads were aligned to the reference genome hg19 using STAR, followed by analysis using WebGestalt (for more in-depth methodology on GO, visit [www.webgestalt.org](http://www.webgestalt.org)).

#### **2.5.6 Data availability**

Raw RNA-sequencing data for all cellular and EV replicates, including all FASTQ files, are available at <http://exrna-atlas.org/genboreeKB/projects/extracellular-rna-atlas->

[v2/exat/datasets#EXRJFRAN16VDqI8AN](https://data.mendeley.com/datasets/9pd453pm7k/draft?a=abd2b83b-da41-4db4-9821-ec5994747355). RNA-sequencing quality control, total mapped read counts, total fold enrichment data, and all data associated with the Gene Ontology analysis can be found at <https://data.mendeley.com/datasets/9pd453pm7k/draft?a=abd2b83b-da41-4db4-9821-ec5994747355>.

### 2.5.7 RT-PCR and RT-qPCR

Accuscript RT (Agilent Technologies) was used to convert and amplify long RNAs to cDNAs with 500 ng of RNA used per RT reaction. Random hexamer RT primers were used to amplify cDNA for RT-qPCR while oligo-dT primers were used for RT-PCR assays. 1  $\mu$ L cDNA product was used to amplify full length RNAs using a 25  $\mu$ L Phusion DNA polymerase reactions. Taqman RNA assays (Life Technologies) were performed as indicated. Briefly, 10 ng of total RNA was used per individual RT reaction; 0.67  $\mu$ L of the resultant cDNA was used in 10  $\mu$ L qPCR reactions. 1  $\mu$ L of the resultant cDNA was used in a 10  $\mu$ L qPCR reaction. qRT-PCR reactions were conducted in 384-well plates using the Biorad CFX384 Real-Time System. All C(t) values were  $\leq 40$ . Triplicate C(t) values were averaged and normalized against b-actin. Fold-changes were calculated using the  $\Delta\Delta C(t)$  method, where  $\Delta = C(t)_{RNA} - C(t)_{U6\ snRNA/B-Actin}$ , and  $\Delta\Delta C(t) = \Delta C(t)_{tumor} - \Delta C(t)_{control}$ , and  $FC = 2^{-\Delta\Delta C(t)}$ . In some cases, RT-PCR bands were electrophoresed and band intensity measured using AlphaView.

#### *Primers:*

Rab13HA\_F: 5'-ATGGCCAAAGCCTACGAC

Rab13HA-R: 5'-TCAAGCGTAATCTGGAACATC

ACTB\_F: 5'-ATGTTTGAGACCTTCAACACCC

ACTB\_R: 5'-TGTGCAATCAAAGTCCTCG

Rab13\_ORF\_F: 5'-ATGGCCAAAGCCTACGACC

Rab13\_ORF\_R: 5'-GCCCAGGGAGCACTTGTTG

GFP\_F: 5'-ATGGAGAGCGACGAGAGC

GFP\_R: 5'-TTATTCTTCACCGGCATCTG

### 2.5.8 Plasmid construction

Human Rab13 cDNA was synthesized using Accuscript RT (Agilent Technologies). Rab13HA cDNA was inserted into the CMVMIR plasmid using BamHI and EcoRV (New England Biolabs). CRISPR-Display plasmids were a gracious gift from David Shechner of the Rinn Laboratory at Harvard University. All plasmids were confirmed by sequencing (Genewiz, South Plainfield, NJ, USA).

*Primers:*

Rab13HA\_F: 5'-ATACGGATCCATGCCAAAGCCTACGAC

Rab13HA\_R: 5'- ATACGCGGCCGCTCAAGCGTAATCTGGAACATC

### 2.5.9 Transfection

*CRISPR-Display.* Cells were plated in 12-well plates (Corning, 3513, Corning, NY, USA) at a density of  $1.25 \times 10^5$  cells/well and left overnight at 37°C to reach ~70% confluency. The following day, cells were transfected with 250ng each (1µg total DNA) of the following constructs: Gaussia Luciferase (GLuc), Cypridinia Luciferase (Cluc), dCas9-VP64, and empty gRNA vector (sg-CTL), or gRNAs containing CRNDE (sg-CRNDE), one copy of *miR-100* (sg-*miR-100-1*), or three tandem copies of *miR-100* (sg-*miR-100-3*). Transfection used Lipofectamine 2000 reagent. Cells were incubated for 24-hours in Dulbecco's Modified Eagle's Medium (DMEM) (Sigma-Aldrich, D5546, pen/strep, and non-essential amino acids (NEAA) at 37°C. Afterwards, cells were washed thrice with PBS and incubated with serum-free DMEM for

another 48 hours. Media was then collected for EV collection.

#### **2.5.10 Protein collection and western blotting**

Protein was collected concurrently with RNA through TRIzol extraction (Life Technologies).

Following isolation, protein was resuspended in 1x RIPA buffer with 1% SDS (Life

Technologies). Protein concentration was quantified by BCA assay (BIO-RAD). 10µg of total

protein was loaded onto a 12% MINI-PROTEAN TGX® 12 by 50µL well pre-casted gel (BIO-

RAD). Gels were transferred using the Trans-Blot® Turbo Transfer System (BIO-RAD).

Membranes were blocked in 5% milk in TBS-T for 1 hour at room temperature. Primary antibody

was incubated overnight in 5% milk in TBS-T at 4°C. Secondary antibodies were incubated in

5% milk in TBS-T for 1 hour at room temperature. Membranes were treated with SuperSignal™

West Femto Maximum Sensitivity Substrate for 60 seconds (Thermo Scientific). Blots were then

exposed to film and developed for ~1 second to ~1 minute depending on band intensity.

Antibodies:

Mouse anti-β-Actin Antibody: 1:1000 (Abcam, ab6276)

Mouse anti-HA Antibody: 1:1000 (Sigma-Aldrich, 12CA5)

Anti-mouse ECL Antibody: 1:5000 (GE Healthcare, NA931)

#### **2.5.11 Transwell co-culture assays**

*CRISPR-Display*. Recipient cells were plated in 12-well Transwell (Corning, 3450, Corning, NY,

USA) plates at a density of  $\sim 6 \times 10^4$  cells/well and cultured in DMEM supplemented with 10%

FBS for 24 hours until about 70% confluent. Cells were transfected with 125ng of each of the

following constructs: Gaussia Luciferase (GLuc), Cypridina Luc (CLuc), and dCas9 plasmids,

complexed with 2 $\mu$ L of Lipofectamine 2000. Donor cells were plated in separate 12-well dishes at  $\sim 2.25 \times 10^4$  cells/well. Cells were transfected with either no guide RNA (no sgRNA), an empty gLuc guide RNA control plasmid (sg-CTL), or gLuc guide RNAs containing CRNDE (sg-CRNDE), one copy of *miR100* (sg-miR-100-1), or three tandem copies of *miR-100* (*miR-100-3*) sequences. 24-hours post transfection, cells were trypsinized, seeded into Transwell dishes, and allowed to adhere for 24 hours. Cells were then washed three times with PBS, co-cultures were initiated in FBS-free growth medium. Media from co-cultures was collected at 48 hours post co-culture. Co-culture media was subject to gLuc and cLuc reporter assays (NEB, E3300, E3309). Fold activation was calculated as follows: [(gLuc/cLuc) sgRNA] / [(gLuc/cLuc) no sgRNA] by comparing gLuc activation normalized to cLuc expression between cells with sgRNAs or without guide RNA (no sgRNA).

*Rab13-HA*. Donor cells were plated in 12-well dishes at  $\sim 1.0 \times 10^5$  cells/well and cultured in DMEM supplemented with 10% FBS for 24 hours until about 70% confluent. Cells were then transfected with either no vector, 500ng cmvMIR; empty construct, or 500ng cmvMIR; Rab13HA construct complexed with  $\sim 2$ -5 $\mu$ L of Lipofectamine 2000. Donor cells were incubated with DNA complexes for 24 hours. Recipient cells were plated in 12-well Transwell (Corning, 3450, Corning, NY, USA) plates at a density of  $\sim 1.5 \times 10^5$  cells/well and cultured in DMEM supplemented with 10% FBS. Transfected cells were washed and seeded into 12-well (114 mm<sup>2</sup>), 0.4 $\mu$ m-pore polyester membrane Transwell filters. (Corning, 3450, Corning, NY, USA) 24-hours post seeding, media from donor Transwells and recipient wells were replaced with FBS-free growth medium, and co-cultured. Cellular RNA and protein was collected from both donor and recipient cell, in pooled triplicates, and purified through previously described means.

## **2.6 Acknowledgements**




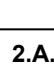
This work was supported by grants from the National Institutes of Health, U19CA179514, RO1 CA163563 to RJC, and a GI Special Program of Research Excellence (SPORE) P50 95103. The authors would like to thank Dr. David Shechner from the Rinn lab for the CRISPR-Display vectors and Dr. Kasey Vickers from Vanderbilt for helpful suggestions.

## **2.7 Author contributions**

SAH, DJC, LS, and JLF designed and performed most of the experimental work with help from JNH. NP and SL performed the sequencing analyses. YD, QL, PJ, and BZ performed computational, bioinformatics, and statistical analyses. JGP, RJC, AMW conceived and directed the project. SAH, DJC, JLF, AMW, and JGP wrote the manuscript.

## 2.A Appendix

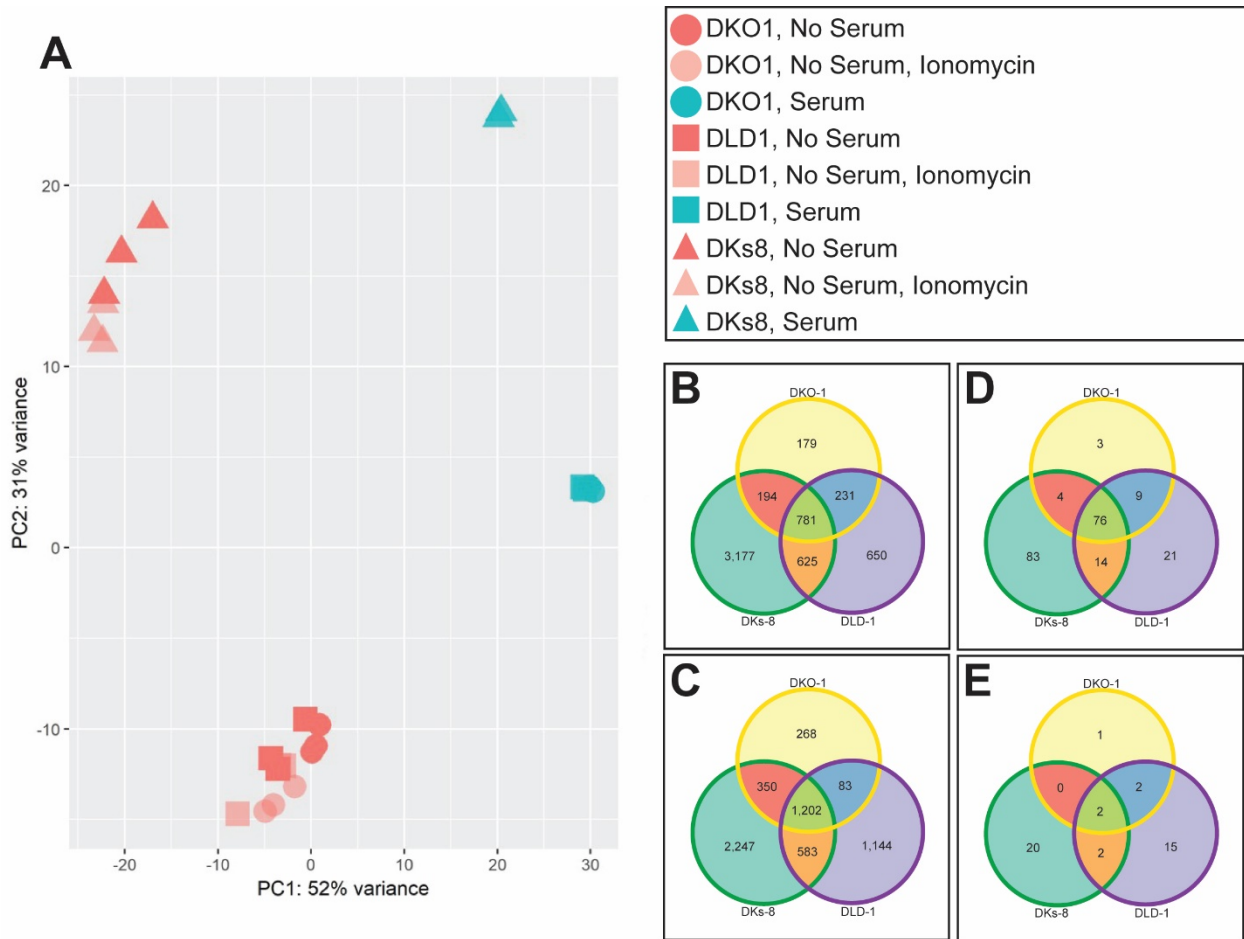
### 2.A.1 Pairwise replicate analysis.

DKO-1 Cell 1	0.92	0.91	0.68	0.71	0.70	0.92	0.91	0.91	0.73	0.66	0.66	0.91	0.91	0.91	0.78	0.69	0.67
 DKO-1 Cell 2	0.91	0.69	0.71	0.71	0.92	0.91	0.92	0.73	0.67	0.66	0.91	0.91	0.91	0.78	0.70	0.68	
 DKO-1 Cell 3	0.69	0.72	0.71	0.91	0.91	0.91	0.73	0.68	0.67	0.90	0.90	0.90	0.78	0.70	0.68		
 DKO-1 EV 1	0.94	0.92	0.68	0.69	0.69	0.83	0.93	0.93	0.70	0.69	0.69	0.77	0.94	0.95			
 DKO-1 EV 2	0.91	0.71	0.72	0.71	0.84	0.92	0.92	0.72	0.72	0.71	0.78	0.93	0.94				
 DKO-1 EV 3	0.71	0.71	0.71	0.83	0.91	0.91	0.72	0.71	0.71	0.77	0.91	0.92					
 DLD-1 Cell 1	0.91	0.91	0.73	0.67	0.66	0.91	0.91	0.91	0.78	0.70	0.68						
 DLD-1 Cell 2	0.91	0.73	0.68	0.67	0.90	0.91	0.91	0.78	0.70	0.68							
 DLD-1 Cell 3	0.73	0.67	0.67	0.90	0.91	0.91	0.78	0.70	0.68								
 DLD-1 EV 1	0.82	0.82	0.73	0.73	0.73	0.78	0.84	0.83									
 DLD-1 EV 2	0.93	0.68	0.68	0.67	0.76	0.93	0.94										
 DLD-1 EV 3	0.67	0.67	0.67	0.75	0.93	0.94											
 DKs-8 Cell 1	0.92	0.92	0.78	0.71	0.69												
 DKs-8 Cell 2	0.93	0.78	0.71	0.69													
 DKs-8 Cell 3	0.78	0.70	0.68														
 DKs-8 EV 1	0.78	0.76															
 DKs-8 EV 2	0.95																
 DKs-8 EV 3																	

**2.A.1.** Pairwise analysis comparing triplicates of each cell and EV RNA-seq library (18 samples in total). Spearman correlations are shown between the cell replicates ( $R=0.90-0.93$ ), between EVs and their cognate cells ( $R=0.67-0.73$ ), and between EV replicates ( $R=0.82-0.94$ ).



## 2.A.2 Effects of serum starvation and ionomycin treatment on cellular RNA profiles



**2.A.2.** (A) PC analysis of cellular RNA-seq comparing triplicates of cells grown with or without serum, or treated with ionomycin which was used in earlier experiments to increase overall EV yield (Higginbotham et al. 2011). The color code for the different conditions is shown at the right, cell type is indicated by the indicated shapes. (B-E) Unique RNAs upregulated when (B) cells were grown in serum versus without, (C) when cells were grown serum-free versus with serum, (D) when cells were treated with ionomycin versus no treatment, and (E) when cells were untreated versus with ionomycin treatment.

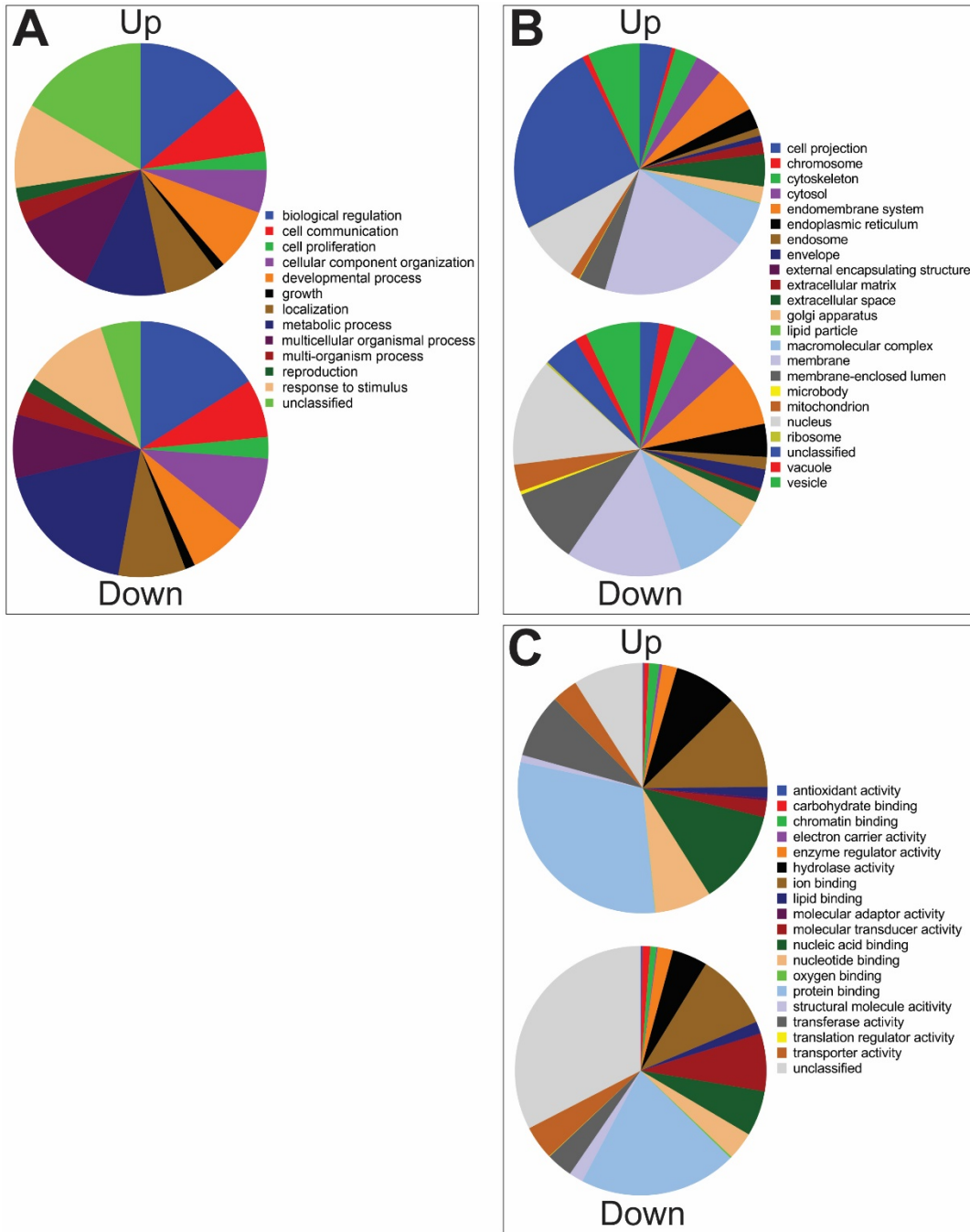
**2.A.3 Table. Top 100 KRAS-independent upregulated EV RNAs**

Gene Name	Cell Line	Log(2) Fold Change	p <sub>adj</sub>
REXO1L1P	DKs-8	9.30	4.25E-108
REXO1L1P	DLD-1	9.14	0.00E+00
REXO1L1P	DKO-1	9.05	1.40E-22
ERVH-1	DKO-1	8.47	9.60E-04
LINC01609	DLD-1	8.30	5.54E-50
LINC01609	DKO-1	8.21	7.47E-14
ESRG	DKO-1	7.98	2.69E-22
CYSLTR1	DLD-1	7.73	2.01E-29
ESRG	DLD-1	7.71	5.57E-139
LINC01609	DKs-8	7.69	0.00E+00
RP11-306O13.1	DLD-1	7.65	4.51E-24
RP11-445O16.3	DLD-1	7.64	1.48E-37
LINC00504	DLD-1	7.61	4.93E-39
TTN	DLD-1	7.59	1.38E-124
RP11-306O13.1	DKO-1	7.57	7.27E-23
HHLA1	DKO-1	7.51	9.23E-12
MAB21L3	DLD-1	7.49	2.58E-45
CYSLTR1	DKO-1	7.47	6.99E-20
LINC00504	DKO-1	7.34	1.69E-12
RP11-34D14.1	DLD-1	7.31	1.72E-51
HHLA1	DKs-8	7.30	1.17E-23
RP11-703G6.1	DKs-8	7.25	3.37E-54
MAB21L3	DKO-1	7.23	8.05E-11
Xxbac-BPG154L12.4	DLD-1	7.21	1.32E-14
HHLA1	DLD-1	7.20	2.75E-46
RP11-703G6.1	DKO-1	7.15	1.22E-10
ESRG	DKs-8	7.15	6.38E-250
TTN	DKs-8	7.14	0.00E+00
LINC00504	DKs-8	7.08	0.00E+00
RP11-34D14.1	DKO-1	7.07	1.83E-13
RP11-306O13.1	DKs-8	7.06	1.54E-110
CYSLTR1	DKs-8	7.05	0.00E+00
LACTB2-AS1	DLD-1	7.04	3.37E-18

Xxbac-BPG154L12.4	DKO-1	6.96	8.52E-13
MAB21L3	DKs-8	6.90	0.00E+00
CFAP54	DLD-1	6.88	5.92E-26
TMEM212	DLD-1	6.88	3.11E-44
C12orf50	DLD-1	6.87	6.22E-16
ADAMTSL3	DLD-1	6.86	1.11E-47
ABCC9	DLD-1	6.85	2.35E-18
TRIM22	DLD-1	6.83	7.48E-122
SPINK9	DKs-8	6.82	0.00E+00
TMEM212	DKO-1	6.74	3.03E-12
CFAP54	DKO-1	6.71	6.34E-16
RP11-703G6.1	DKs-8	6.70	0.00E+00
RP11-34D14.1	DKs-8	6.67	0.00E+00
ABCC9	DKO-1	6.66	1.64E-19
TRIM22	DKO-1	6.63	1.77E-11
C12orf50	DKO-1	6.62	3.67E-14
AC011747	DLD-1	6.59	4.32E-22
ADAMTSL3	DKO-1	6.58	1.18E-09
CTC-260E6.6	DLD-1	6.54	2.63E-45
FLJ22447	DLD-1	6.48	5.67E-22
LACTB2-AS1	DKs-8	6.47	1.37E-48
Xxbac-BPG154L12.4	DKs-8	6.44	2.25E-91
UGDH-AS1	DLD-1	6.36	3.43E-30
TMEM212	DKs-8	6.34	0.00E+00
KIAA1328	DLD-1	6.32	2.00E-55
CFAP54	DKs-8	6.32	3.39E-66
TPTEP1	DKs-8	6.28	1.47E-196
TRIM22	DKs-8	6.27	0.00E+00
ABCC9	DKs-8	6.26	5.42E-60
AC011747	DKs-8	6.22	2.09E-60
RP11-259O2.3	DLD-1	6.17	2.74E-38
AC011747	DKO-1	6.16	1.30E-15
UGDH-AS1	DKO-1	6.14	2.69E-12
RAB13	DKO-1	6.12	4.81E-04
C12orf50	DKs-8	6.11	2.80E-25
ADAMTSL3	DKs-8	6.09	0.00E+00

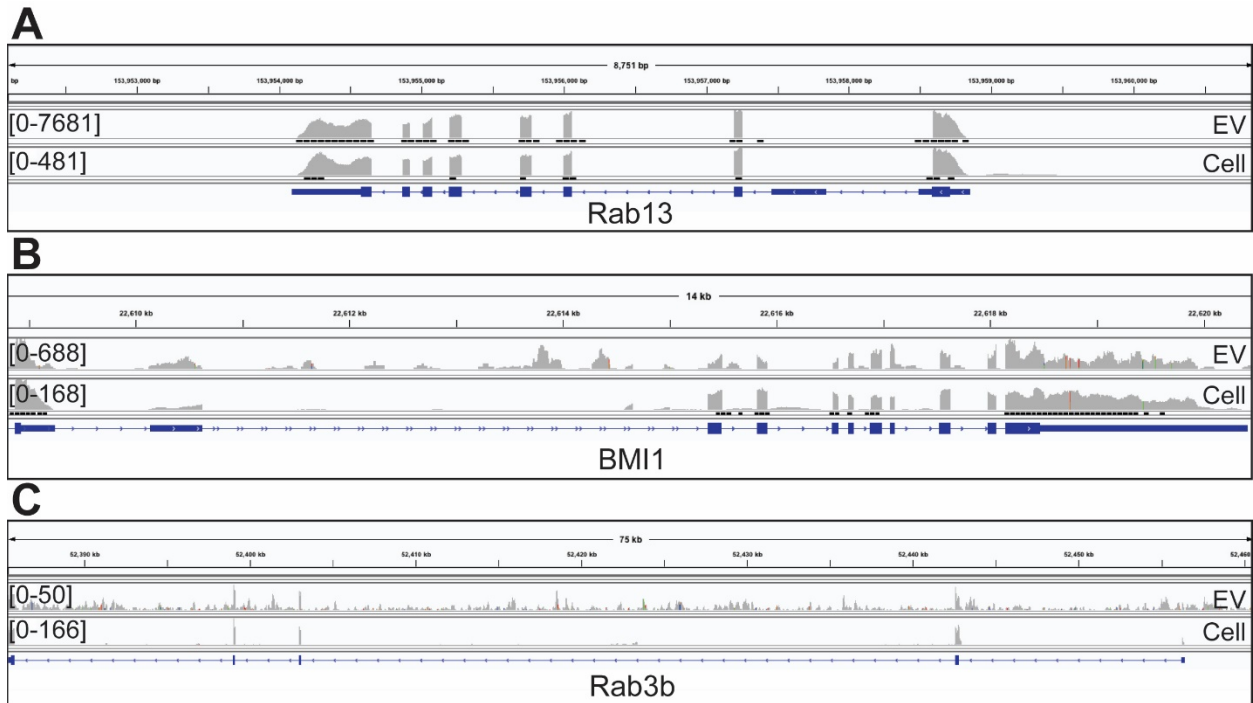
SHISA9	DLD-1	6.06	5.63E-06
RP11-259O2.3	DKO-1	5.98	1.83E-11
FLJ22447	DKO-1	5.96	3.66E-20
KIAA1328	DKO-1	5.88	4.16E-06
CTC-260E6.6	DKO-1	5.87	1.87E-06
AC007743.1	DLD-1	5.85	1.65E-06
CTC-260E6.6	DKs-8	5.83	6.45E-229
UGHD-AS1	DKs-8	5.80	0.00E+00
KIAA1328	DKs-8	5.75	0.00E+00
SHISA9	DKO-1	5.74	1.21E-21
RP11-259O2.3	DKs-8	5.71	1.16E-95
TBC1D8B	DLD-1	5.70	7.04E-30
KCNJ15	DKO-1	5.70	2.00E-06
FLJ22447	DKs-8	5.65	1.12E-17
RABGAP1L-IT1	DLD-1	5.65	1.74E-04
RP11-545I5.3	DLD-1	5.64	8.68E-17
TMEM45A	DLD-1	5.64	3.96E-06
KCNJ15	DLD-1	5.62	3.69E-20
FAM228B	DLD-1	5.62	1.65E-28
KCNQ1OT1	DLD-1	5.61	1.83E-35
AC092669.3	DLD-1	5.61	8.38E-23
SULT1B1	DLD-1	5.58	1.43E-05
CTC-340A15.2	DLD-1	5.47	7.33E-05
KCNQ1OT1	DKO-1	5.44	1.08E-09
AC007743.1	DKO-1	5.43	5.91E-08
RABGAP1L-IT1	DKO-1	5.42	8.69E-07
MIPOL1	DLD-1	5.42	2.32E-25
TBC1D8B	DKO-1	5.41	1.34E-09
TMEM45A	DKO-1	5.39	9.52E-11
C4orf32	DLD-1	5.37	3.24E-05

## 2.A.4 Gene ontology



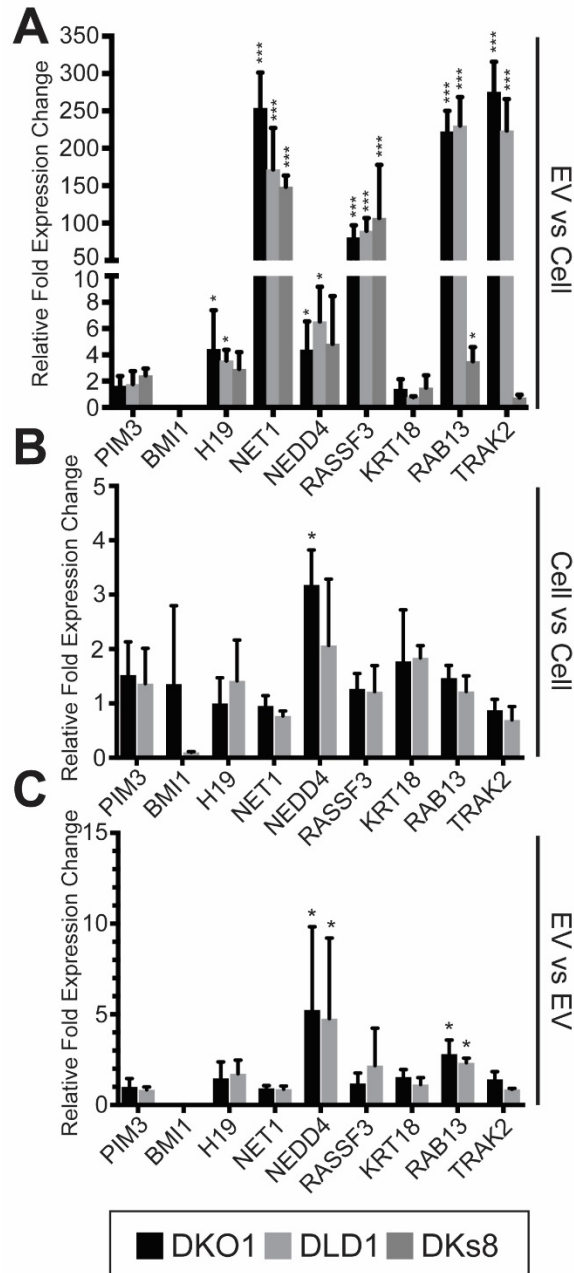
**2.A.4.** Gene ontology of RNAs globally upregulated in EV samples compared to cellular samples grouped by (A) Biological Processes, (B) Cellular Components, or (C) Molecular Function. GO categories are shown in pie charts with groups upregulated in EVs labeled 'Up' and groups downregulated in EVs labeled 'Down'.

## 2.A.5 mRNA RNA-seq read profiles



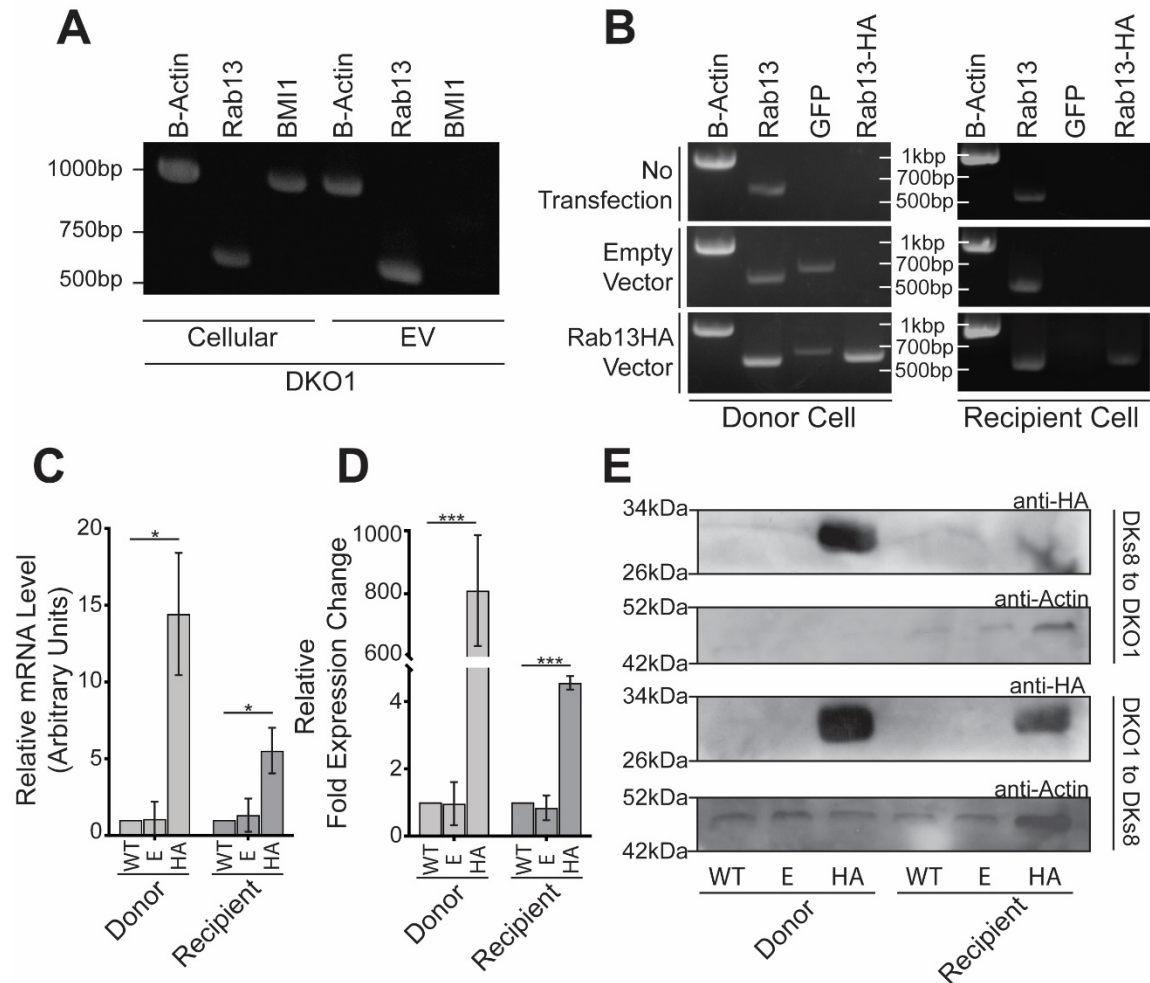
**2.A.5.** Reads were mapped across transcripts encoding Rab13, BMI1, and Rab3b. Genomic coordinates are at the top with the intron and exon boundaries shown at the bottom of each set in blue. For each mRNA, the read distribution is shown in grey with the RNA-seq pattern from EVs on top of the RNA-seq pattern from cellular RNA. Only DKO-1 RNA-seq is shown. Numbers in brackets represent read count ranges (left). (A) Read profile of *Rab13* mRNA with reads mapping almost exclusively to exons suggesting the presence of full length, spliced mRNA which was confirmed by RT-PCR. (B) Read profile of *BMI1* mRNA with reads mapping almost exclusively to exons suggesting the presence of full length, spliced mRNA. However, no full length *BMI1* mRNA could be detected in EVs, despite the read distribution pattern. (C) Read profile of *Rab3b* mRNA in EVs with reads mapping across both exons and introns suggesting that either unspliced RNA was exported to EVs or that fragmented RNA is present in the EV samples. The read distribution pattern from cellular RNA is consistent with spliced mRNA.

## 2.A.6 Validation of RNA-seq



**2.A.6.** A subset of genes (as indicated) that were upregulated by RNA-seq were subjected to RT-qPCR to validate the RNA-seq data. Validation was performed comparing (A) EV samples against cellular samples, (B) cellular samples against cellular samples, and (C) EV samples against EV samples. Samples are color-coded, where DKO-1 is black, DLD-1 is light gray, and DKs-8 is in dark gray. (\*  $p < 0.05$ , \*\*  $p < 0.01$ , \*\*\*  $p < 0.001$ , and \*\*\*\*  $p < 0.0001$ ).

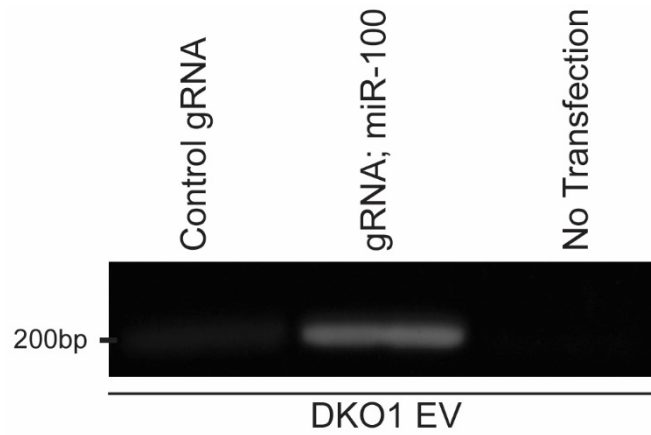
## 2.A.7 Extracellular transfer of *Rab13* mRNA



**2.A.7.** RNA-seq analysis showed upregulation of *Rab13* mRNA in EVs. (A) Detection of full length *Rab13* mRNA by RT-PCR of EV RNA using primers that span the entire coding region. Primers were also used that span the coding region of  $\beta$ -actin and BMI1. (B) Extracellular transfer of *Rab13* mRNA was tested using Transwell cultures. DKO-1 donor cells were transfected with HA-tagged *Rab13* vector and cultured with Dks-8 recipient cells in Transwell cultures for 24 hours after which RT-PCR was performed on RNA from both cells. Controls were no transfection of donor cells or transfection of donor cells with empty vector, described further in Figure 3. (C) Quantification of band intensity from triplicate Transwell experiments. (WT) No transfection, (E) Empty Vector Transfection, and (HA) *Rab13*HA Transfection. (D) RT-qPCR quantification of expression levels of *Rab13*HA from triplicate Transwell experiments. (1) No transfection, (2) Empty Vector Transfection, and (3) *Rab13*HA Transfection. (\*  $p < 0.05$ , \*\*  $p < 0.01$ , \*\*\*  $p < 0.001$ , and \*\*\*\*  $p < 0.0001$ ). (E) Western blot detecting transfer of *Rab13*-HA protein following co-culture of *Rab13*-HA expressing donor cells with untransfected recipient cells. (WT) no transfection, (E) empty vector transfection, and (HA) *Rab13*-HA transfection. DKs-8 as donor and DKO-1 as recipient (top) show no detectable levels of *Rab13*-HA in recipient cells co-cultured with transfected donor cells. DKO-1 cells as donor cells and DKs-8 cells as recipient cells (bottom) show detectable levels of *Rab13*-HA protein in recipient cells co-cultured with transfected donor cells. *Rab13*-HA size is ~28kDa. Actin size is ~42kDa.



### 2.A.8 RT-PCR of gRNAs in DKO-1 EVs



**2.A.8.** DKO-1 cells were either untransfected, transfected with vectors expressing unmodified gRNAs, or transfected with vectors expressing gRNAs containing an insertion of 1 copy of *miR-100*. EVs were isolated and RT-PCR was performed with primers detecting full length gRNA and showed that only gRNAs containing *miR-100* were detectable in exosomes.

## Chapter 3

### **Rab13 regulates sEV secretion in mutant *KRAS* colorectal cancer cells**

Scott A. Hinger<sup>1</sup>, Jessica J. Abner<sup>1</sup>, Jeffrey L. Franklin<sup>2,3,4</sup>, Dennis K. Jeppesen<sup>3</sup>,

Robert J. Coffey<sup>2,3,4</sup>, and James G. Patton<sup>1,\*</sup>

Departments of Biological Sciences<sup>1</sup>, Cell and Developmental Biology<sup>2</sup>, Medicine<sup>3</sup>, Vanderbilt University Medical Center, Nashville, TN, 37235, Veterans Affairs Medical Center<sup>4</sup>, Nashville, TN 37235, and Vanderbilt University, Nashville, TN 37235.

#### **3.1 Abstract**

Small extracellular vesicles (sEVs), 50-150nm in diameter, have been proposed to mediate cell-to-cell communication with important implications in tumor microenvironment interactions, tumor growth, and metastasis. We previously showed that mutant *KRAS* colorectal cancer (CRC) cells release sEVs containing Rab13 protein and mRNA. Previous work had shown that disruption of intracellular Rab13 trafficking inhibits epithelial cell proliferation and invasiveness. Here, we show that Rab13 additionally regulates the secretion of sEVs corresponding to both traditional exosomes and a novel subset of vesicles containing both  $\beta$ 1-integrin and Rab13. We find that exposure of recipient cells to sEVs from *KRAS* mutant donor cells increases proliferation and tumorigenesis and that knockdown of Rab13 blocks these effects. Thus, Rab13 serves as both a cargo protein and as a regulator of sEV secretion. Our data support a model whereby Rab13 can mediate its effects on cell proliferation and invasiveness via autocrine and paracrine signaling.

### 3.2 Introduction

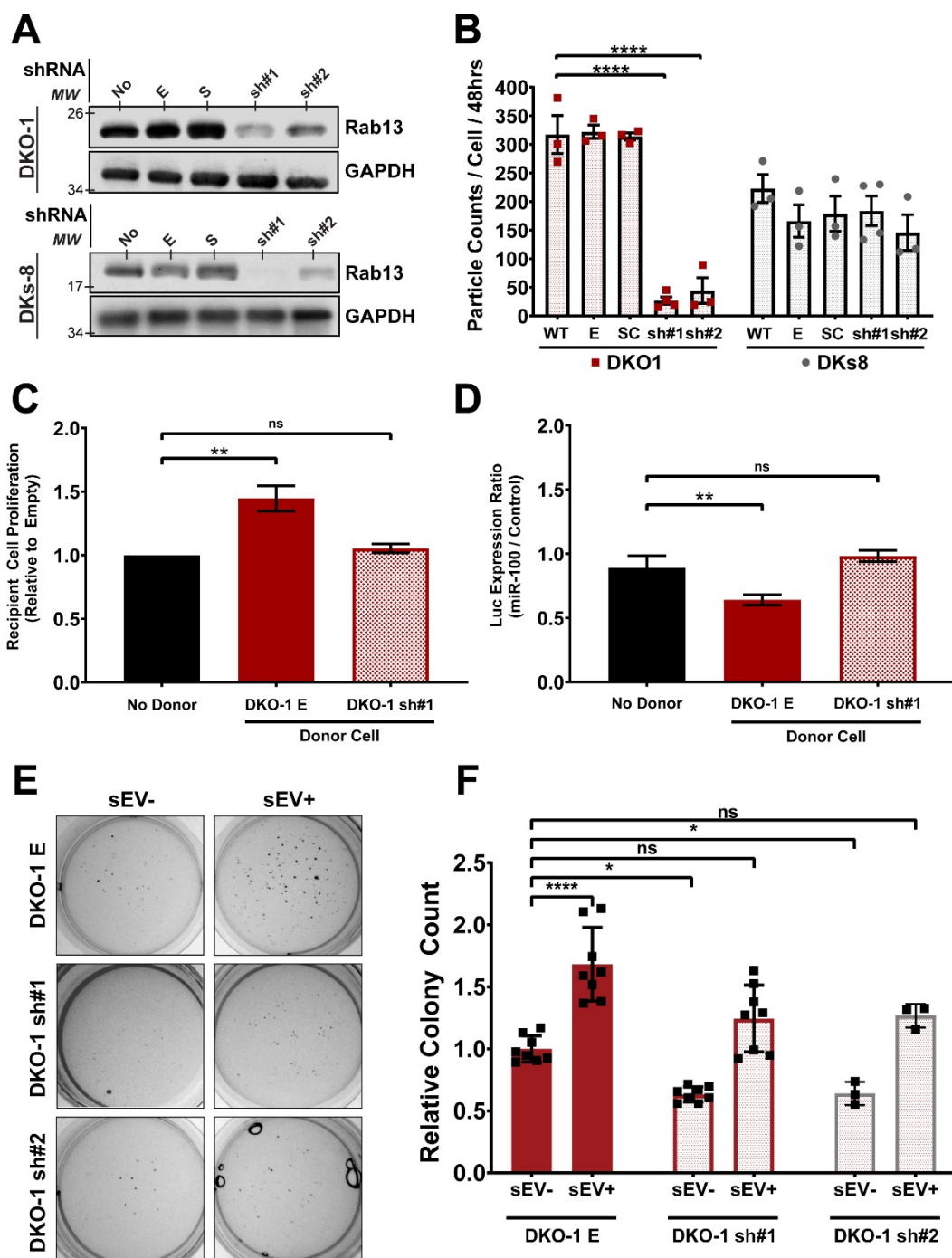
Cell-to-cell signaling via EVs has been shown to play an important role in the development and progression of various cancers, with significant effects on proliferation, invasion and metastasis. Traditionally, EVs are classified both by size and biogenesis pathway (Colombo et al., 2014b). Two major pathways have been described for EV release. In one, EVs are secreted by direct budding from the plasma membrane, including larger microvesicles (greater than 150nm) and a heterogeneous mixture of smaller vesicles (Booth et al., 2006; Kowal et al., 2016). Smaller vesicles of endosomal origin (exosomes) are secreted when multivesicular bodies fuse with the plasma membrane releasing their intraluminal contents. Functionally, these different classes of vesicles utilize distinct mechanisms controlling cargo content with cell- and disease-specific effects (Maas et al., 2016; Shifrin et al., 2013; Simons and Raposo, 2009). However, it is now becoming clear that classifying vesicles into broad classes based on size is too simplistic as it ignores differences in cargo content and biogenesis. For these reasons, the preferred nomenclature is to refer to all secreted vesicles more broadly as EVs (Thery, 2011) with differential centrifugation and density gradient centrifugation methods used to distinguish between small (sEVs), large EVs, and non-vesicular (NV) content (Jeppesen et al., 2019).

Previous work from our group using isogenic CRC cell lines has demonstrated that EV cargo content is regulated in a KRAS dependent manner, including proteins, miRNAs, circular RNAs, mRNAs, and long coding and non-coding RNAs (lncRNAs) (Cha et al., 2015a; Demory Beckler et al., 2013; Dou et al., 2016; Hinger et al., 2018). We also showed that EVs can mediate functional transfer of cargo from donor to recipient cells. However, the cellular mechanisms by which specific proteins and RNAs are selected for secretion in EVs, as well as the biogenesis of the EVs themselves, remains to be fully elucidated. We previously identified an Argonaute 2 (AGO2)-dependent, *KRAS-MEK* signaling mechanism for miRNA secretion into

EVs, but this mechanism is apparently miRNA-specific, and does not regulate global vesicle secretion (McKenzie et al., 2016). More recent work using highly refined sEV purification methods suggests that canonical exosomes (CD63+/CD81+/CD9+) from mutant KRAS cells carry very few miRNAs with undetectable levels of Argonaute proteins (Jeppesen et al., 2019). Thus, depending on the exact cell type and purification strategy, classical exosomes might make up only a small percentage of the total sEVs secreted from cells.

Rab associated G proteins (Rabs) have been known for many years to play a role in regulating endocytic trafficking in mammalian cells (Bhain and Roy, 2014). Because some EVs are secreted through similar endocytic pathways, we might expect that Rab proteins play a regulatory role in EV secretion. Indeed, Rab27a/b and Rab35 play key roles in the regulation of EV biogenesis (Hsu et al., 2010; Ostrowski et al., 2010). We previously identified another Rab family member, Rab13, in EVs from mutant KRAS cells, but its role in EV secretion remains unclear (Hinger et al., 2018). Cellular Rab13 has been shown to play a significant role in cancer progression, invasiveness, and metastasis, partly related to the regulation of tight junctions and adherens junction formation (Ioannou et al., 2015; Kanda et al., 2008; Kohler et al., 2004; Sahgal S, 2019; Yamamura et al., 2008). Rab13 also regulates  $\beta$ 1-integrin recycling in epithelial cells and  $\beta$ 1-integrin has been shown to be a marker for EVs in multiple systems (Peinado et al., 2012; Sahgal S, 2019; Tauro et al., 2013). Further,  $\beta$ 1-integrin+ sEVs promote anchorage-independent growth in a pancreatic tumor model (DeRita et al., 2019; Schooley et al., 2012). Here, we identify a novel and distinct subclass of  $\beta$ 1-integrin+/Rab13+ EVs, and furthermore, demonstrate that Rab13 regulates both the secretion of these new vesicles, as well as the secretion of classical exosomes.

Figure 9. Rab13 regulates EV secretion in a KRAS-dependent manner.



**Figure 9.** (A) Rab13 knockdowns. Stable lines expressing one of two independent shRNAs targeting Rab13 were created in wild type (DKs-8) and mutant (DKO-1) KRAS cells. Western blots were performed on cell lysates using antibodies against Rab13 or GAPDH on the parent cell lines (No) or lines expressing an empty shRNA vector (E), a scrambled shRNA vector (S), or sh#1 or sh#2 against Rab13. (B) Nanosight-tracking analysis (NTA) of sEVs isolated from the cell lines outlined in A. (C) Proliferation assays. DKs-8 recipient cells were co cultured for 48 hours in the presence of either no donor cells, DKO-1 cells expressing an empty shRNA vector (E), or DKO-1 cells stably expressing sh#1. Recipient cells were then collected and total cells were counted and plotted relative to the number of cells counted in the absence of any donor cells. (D) Luciferase reporter assays. DKs-8 recipient cells were transiently transfected with a vector expressing luciferase fused to a control 3' UTR or a 3'UTR containing three perfect binding sites for *miR-100*. Recipient cells were then co-cultured for 48 hours with either no donor cells, DKO-1 cells expressing an empty shRNA vector (E), or DKO-1 cells stably expressing sh#1. Cell lysates were prepared and luciferase expression was measured with lower luciferase expression representing more transfer of *miR-100*. (E) DKO-1 cells with or without Rab13 knockdown were grown in soft agar for 2 weeks in the presence or absence of sEVs purified from DKO-1 cells. (F) Quantification of colony counts from three biological soft agar assay replicates. Significance was determined by one-way ANOVA. \* =  $p < 0.05$ , \*\* =  $p < 0.01$ , \*\*\*\* =  $p < 0.0001$ . Data represent mean +/- SE, n=3. ns=no significance.

### 3.3 Results

#### 3.3.1 Rab13 regulates sEV secretion in a KRAS-dependent manner.

We previously showed that Rab13 mRNA and protein are enriched in sEVs from KRAS-mutant CRC cells (Hinger et al., 2018). Given proposed functional roles for Rab13, we hypothesized that Rab13 might regulate the secretion of sEVs. Independent stable KRAS-mutant and KRAS-wildtype CRC cells were generated that express shRNAs against Rab13 mRNA leading to an 70-80% reduction in Rab13 between the two distinct shRNA lines (**Fig. 9A**). Conditioned media were collected from control and knockdown cells and crude sEVs (P100; see **Fig. 11A**) were purified. Particle counts were analyzed by nanoparticle tracking analysis (**3.A.1**) and quantified relative to input cell counts. We observed a dramatic decrease in particle counts/cell when Rab13 was knocked down in two different mutant KRAS DKO-1 cell lines, but not after knockdown in wild type KRAS DKs-8 cells (**Fig. 9B**). Despite the decrease in sEVs, we did not observe any defects in cell proliferation (**3.A.2**), in contrast to previous work using breast cancer epithelial cells (Ioannou et al., 2015).

To test the functional significance of Rab13-dependent secretion of sEVs, we utilized two distinct Transwell assays (**3.A.3**). We first tested whether parent DKO-1 cells, which express normal levels of Rab13, would affect the proliferation of DKs-8 cells in a co-culture environment. When plated on opposite sides of a Transwell membrane, the presence of DKO-1 cells in the donor compartment increased the proliferation of recipient DKs-8 cells, compared to control conditions with no donor cells (**Fig. 9C**). However, Rab13 knockdown in the donor DKO-1 cells abrogated the effect on proliferation in DKs-8 recipient cells following co-culture (**Fig. 9C**). This suggests that Rab13 regulates extracellular secretion in DKO-1 cells and that decreased levels of Rab13 blocks proliferation inducing effects in recipient cells.

Previously, we showed that *miR-100* can undergo functional transfer from donor mutant KRAS cells to recipient wild type KRAS cells using luciferase reporter assays (Cha et al., 2015b). When we tested whether Rab13 knockdown might alter *miR-100* transfer, we again found that decreased levels of Rab13 reduced extracellular transfer from DKO-1 donor to DKs-8 recipient cells resulting in increased luciferase reporter expression (**Fig 9D**).

### **3.3.2 Rab13 regulates anchorage-independent growth via sEVs**

sEVs from mutant KRAS cells can promote proliferation and anchorage-independent growth in wild type cells (Demory Beckler et al., 2013; Higginbotham et al., 2011). Thus, we tested whether Rab13 knockdown in DKO-1 cells would alter colony formation in soft agar assays. First, DKO-1 cells were incubated with DKO-1 sEVs prior to embedding in soft agar. Exposure of DKO-1 cells to sEVs in this manner increased the total number of colonies in soft agar, compared to untreated DKO-1 cells, consistent with previous results (Demory Beckler et al., 2013) (**Fig. 9E-F**). We then tested the effects of Rab13 knockdown on colony growth in soft agar. Loss of Rab13 slightly reduced the number of colonies in soft agar (**Fig. 9F**). However, exposure of the knockdown lines to sEVs from normal DKO-1 cells restored the colony counts

back to control DKO-1 levels (**Fig. 9F**). Besides growth in soft agar, we also found that sEVs from DKO-1 cells caused an increase in tumor-like, migratory colonies when grown in type-1 collagen (**3.A.4**). Again, knockdown of Rab13 blocked this effect, whereas exposure to sEVs from DKO-1 cells rescued migratory colony numbers (**3.A.4**). Taken together, these results suggest that Rab13 regulates anchorage-independent and 3D growth through regulation of sEV secretion, linking sEV biogenesis and tumorigenesis in CRC.

### **3.3.3 Rab13 regulates the secretion of sEV markers**

To further investigate the role that Rab13 plays in vesicle secretion, sEVs were isolated from control and knockdown cells (**Fig. 10A**). Consistent with the overall decrease in sEVs observed after knockdown of Rab13, we observed reduced levels of the classical exosome markers CD63, CD81, and TSG101 (**Fig. 10B**). Previous work has shown that  $\beta$ 1-integrin can be detected in EVs (Hurwitz and Meckes, 2019; Paolillo and Schinelli, 2017) and that Rab13 can regulate  $\beta$ 1-integrin recycling in an epithelial cancer model (Sahgal S, 2019). Furthermore,  $\beta$ 1-integrin was detected in non-exosomal EVs (Jeppesen et al., 2019). Thus, we tested whether knockdown of Rab13 would reduce secretion of  $\beta$ 1-integrin. As shown in **Fig. 10B**, knockdown of Rab13 reduced the levels of secreted  $\beta$ 1-integrin (**Fig. 10B**).

### **3.3.4 Rab13 and $\beta$ 1-integrin co-localize at the plasma membrane**

Integrins belong to a family of cell adhesion receptors consisting of heterodimers with  $\alpha$  and  $\beta$  transmembrane subunits that interact with the extracellular matrix. Integrins have been implicated in cancer progression and metastasis (Anastasiadou and Slack, 2014; Hamidi and Ivaska, 2018; Hoshino et al., 2015; Zhang and Grizzle, 2011). Tumor cells express distinct subsets of integrins and it has been proposed that exosomal integrins can predict organ-specific metastases (Hoshino et al., 2015; Wortzel et al., 2019). In most studies examining integrins as

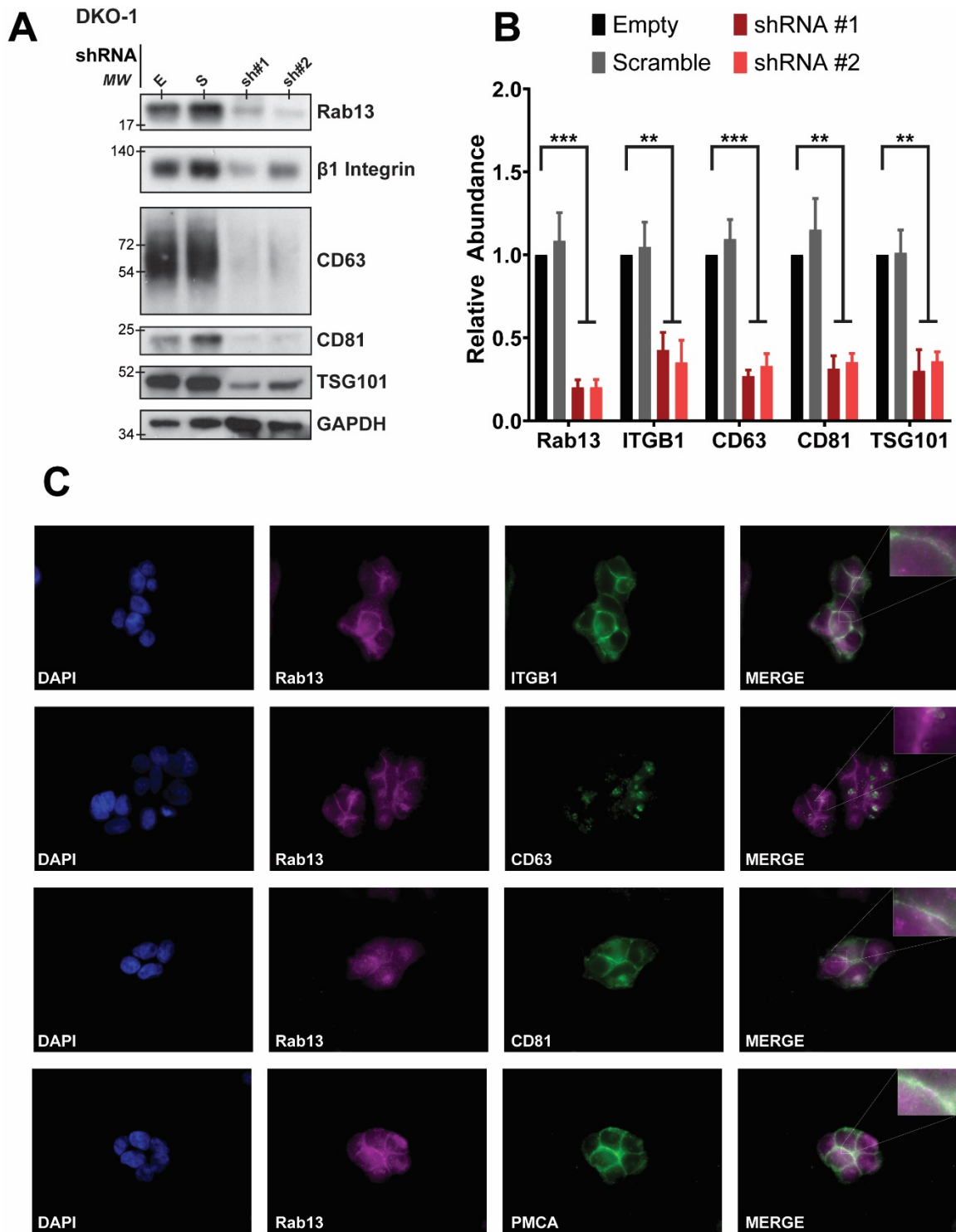


EV cargo, the distribution of integrins in EV subclasses, including classical exosomes, is complex (Jeppesen et al., 2019), depending on the exact integrin cargo interrogated. Rab13 has been implicated in  $\beta$ 1-integrin trafficking to the cell surface (Sahgal S, 2019), but its role in EV trafficking remains unknown. To gain insight into the mechanisms regulating secretion of Rab13 and  $\beta$ 1-integrin, DKO-1 cells were fixed and stained for endosomal and plasma membrane markers. Rab13 and  $\beta$ 1-integrin were found to co-localize primarily at the plasma membrane in DKO-1 cells with little to no co-localization with CD63, a marker of the MVB and of classical exosomes (**Fig. 10C**). In contrast, Rab13 and  $\beta$ 1-integrin were found to co-localize at the plasma membrane with CD81, another classical exosome maker (**Fig. 10C**).

### **3.3.5 $\beta$ 1-integrin is enriched in EVs.**

To identify which specific class of EVs contain  $\beta$ 1-integrin, media was collected from CRC cells and crude large EVs (P2), microvesicles (P10), and sEVs (P100) were purified from KRAS mutant DKO-1 cells by differential centrifugation (**Fig. 11A**). Using this method,  $\beta$ 1-integrin and Rab13 were both detected in the P10 and P100 samples, which include microvesicles and sEVs, respectively (**Fig. 11B**). This is distinct from CD63, which was detected primarily in the P100 samples (**Fig. 11B**).

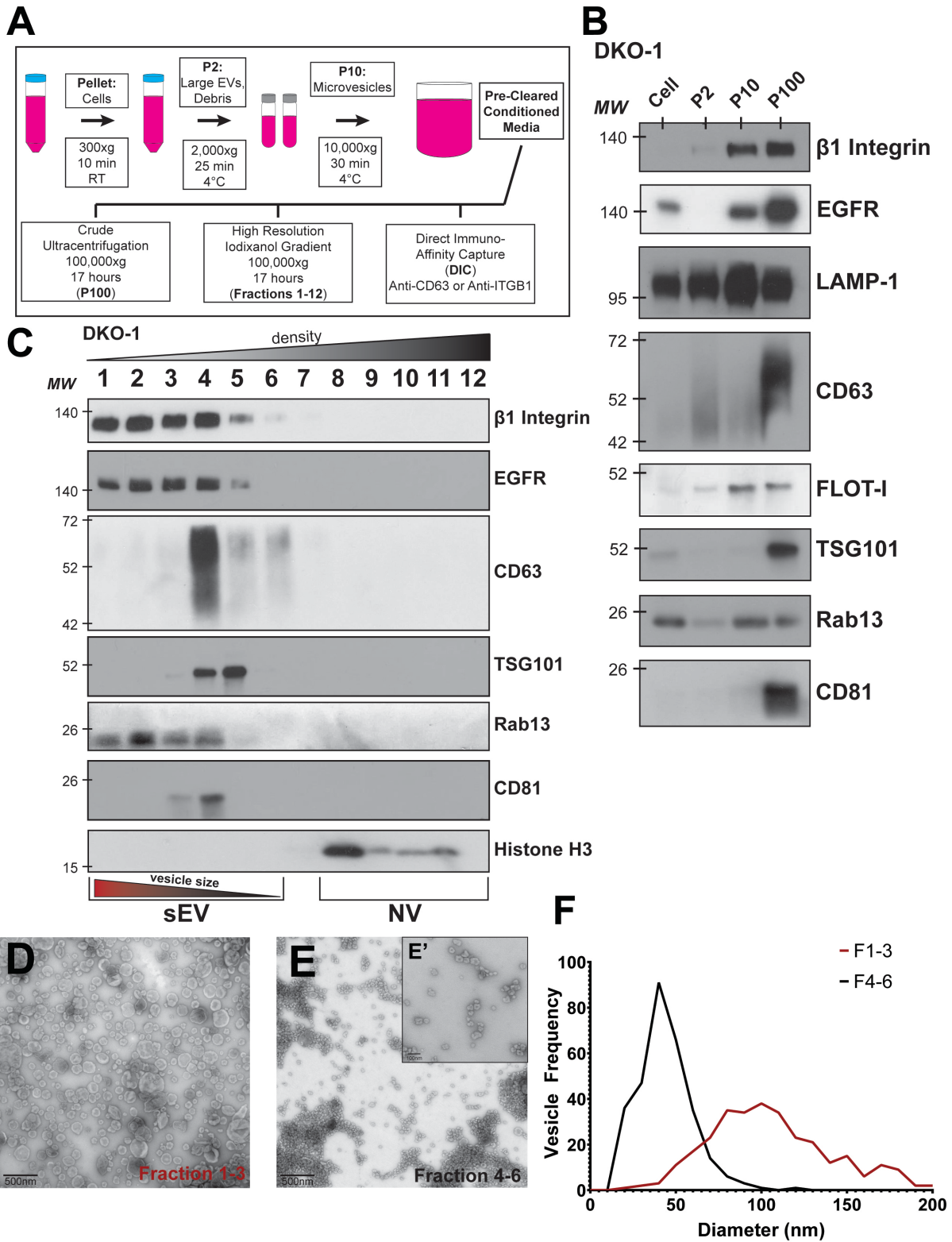
Figure 10. Rab13 regulates and co-localizes with sEV markers.



**Figure 10. (A)** Cell lysates prepared from DKO-1 cells expressing an empty shRNA vector (E), a scrambled shRNA vector (S), or shRNAs targeting Rab13. Western blots were performed with antibodies against  $\beta$ 1-integrin, CD63, CD81, and TSG101. **(B)** Quantification of immunoblots (n=3) of sEV markers under Rab13 knockdown conditions. **(C)** Immunolocalization of Rab13, sEV and plasma membrane (Plasma membrane Ca<sup>2+</sup> ATPase, PMCA) markers in DKO-1 cells. Cells were stained with DAPI (blue), Rab13 (magenta), or antibodies against  $\beta$ 1-integrin, CD63, CD81, or PMCA (green). Rab13 co-localized with the plasma membrane when contact was made between neighboring cells. Significance was analyzed by one-way ANOVA. \*\* = p < 0.01, \*\*\* = p < 0.001. Data represent mean +/- SE, n=3.

To test whether enrichment of  $\beta$ 1-integrin and Rab13 in the P100 fractions is vesicle associated or not, we utilized ultracentrifugation followed by high resolution iodixanol density gradients (Jeppesen et al., 2019). Using this method, Rab13 and  $\beta$ 1-integrin were found to co-sediment in fractions 1-3 which correspond to sEVs (**Fig. 11C**). Non-vesicular, protein aggregates localize to the higher density fractions in these gradients (Jeppesen et al., 2019). Rab13 and  $\beta$ 1-integrin were more enriched in the lighter density fractions (fractions 1-3) compared to fractions 4-6 which are enriched in the classical exosome marker CD63, and to the NV fractions (9-12) which are enriched in histone H3, an extracellular marker for protein aggregates. This suggests that Rab13 and  $\beta$ 1-integrin are associated with vesicles that are larger in size and/or more lipid rich, compared to classical exosomes. Transmission electron microscopy (TEM) images on vesicles purified from either fractions 1-3 or 4-6 showed a clear difference in vesicle size, indicating that this population of vesicles is unique from classical exosomes (**Fig. 11D-F**). The iodixanol gradients show that sEVs enriched in  $\beta$ 1-integrin are more heterogeneous in size, as they were detected not only in the P10 pellet (microvesicles), but also across a range of sEV sizes and densities (**Fig. 11B, 11C**). These data suggest that  $\beta$ 1-integrin+ EVs are distinct from classical CD63+ exosomes and are both Rab13-associated and Rab13-dependent for biogenesis.

**Figure 11. Identification of  $\beta 1$ -integrin+, Rab13+ sEVs.**

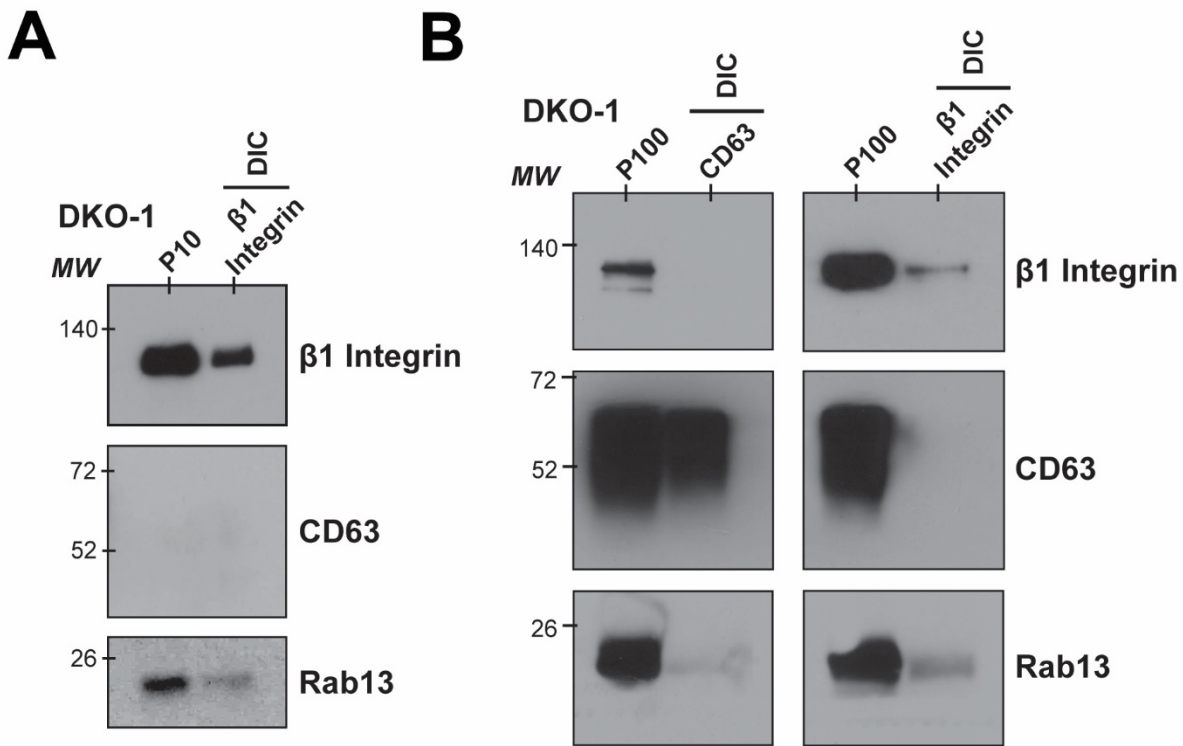


**Figure 11.** (A) sEV purification protocol. Conditioned media were collected from DKO-1 cells and subjected to differential centrifugation to pellet cells, large EVs, cell debris, and microvesicles, as indicated. Pre-cleared conditioned media was then subjected to one of three different isolation techniques: overnight ultracentrifugation at 100,000g (crude sEVs), high resolution iodixanol gradient purification, or direct immuno-affinity capture. (B) Fractions described in A were subjected to western blot analysis using antibodies against the indicated proteins. LAMP-1 is a marker of the lysosome. CD63, TSG101, and CD81 are classical markers of exosomes. (C) Immunoblots of sEVs and non-vesicular (NV) fractions purified from DKO-1 cells following high resolution 12-36% iodixanol gradient purification. (D) Transmission electron microscopy (TEM) of vesicles isolated by high resolution iodixanol gradients, fractions 1-3. Scale bar=500nm. (E) Transmission electron microscopy (TEM) of vesicles isolated by high resolution iodixanol gradient purification, fractions 4-6. Scale bar=500nm. (E') Higher resolution TEM image from E. Scale bar=100nm. (F) Vesicle sizes from the high resolution iodixanol gradients were determined and plotted. Black line corresponds to fractions 4-6 and red line corresponds to fractions 1-3. The mean diameter of the vesicles in fractions 1-3 was significantly different ( $p$ -value =  $2.4 \times 10^{-79}$ ) from the mean diameter in fractions 4-6 by Student's t-test.

### 3.3.6 $\beta$ 1-integrin+ EVs are distinct from CD63+ exosomes

To further test if  $\beta$ 1-integrin+ EVs are distinct from CD63+ classical exosomes, we used direct immuno-affinity capture (DIC) to isolate distinct EVs enriched in both the P10 microvesicle and P100 sEV samples (Jeppesen et al., 2019). P10 (**Fig. 12A**) or P100 (**Fig. 12B**) samples were incubated with beads coated with antibodies against either  $\beta$ 1-integrin or CD63. After incubation, the beads were extensively washed, the bound material was released in lysis buffer, and western blots were performed. When beads coupled to  $\beta$ 1-integrin were incubated with P10 fractions, the bound material was enriched for both  $\beta$ 1-integrin (as expected) and Rab13, supporting the hypothesis that these proteins are in the same vesicle (**Fig. 12A**). Due to low abundance of CD63 in the P10 microvesicle population, DIC against CD63 was unsuccessful. Instead, DIC was carried out on P100 samples using beads coated with antibodies against CD63+ (classical exosomes) or  $\beta$ 1-integrin. With this method, no association was detected between CD63 and  $\beta$ 1-integrin (**Fig. 12B**). Analysis of the P100 fractions showed enrichment of Rab13 in  $\beta$ 1-integrin+ sEVs, further confirming the link between Rab13 and  $\beta$ 1-integrin+ EVs (**Fig. 12B**).

**Figure 12.  $\beta$ 1-integrin<sup>+</sup>/Rab13<sup>+</sup> EVs are distinct from CD63<sup>+</sup> exosomes**



**Figure 12.** Direct immunoaffinity capture (DIC) was used to purify vesicles associated with either  $\beta$ 1-integrin or CD63 (Jeppesen et al., 2019). **(A)** Vesicles from the P10 centrifugation step were immunoaffinity captured with antibodies against  $\beta$ 1-integrin and then western blots were performed on the captured material using antibodies against  $\beta$ 1-integrin, CD63 or Rab13. **(B)** Vesicles from the P100 centrifugation step were immunoaffinity captured with antibodies against either CD63 or  $\beta$ 1-integrin and then western blots were performed as in A. DIC shows a distinction between  $\beta$ 1-integrin<sup>+</sup> sEVs and the CD63<sup>+</sup> classical exosomes, with an enrichment of Rab13 in the  $\beta$ 1-integrin<sup>+</sup> sEVs.

Rab13 was also detected in fractions overlapping with CD63<sup>+</sup> (classical exosomes), which could explain why knockdown of Rab13 also reduced the secretion of classical exosome markers (**Fig. 10**) although Rab13 might also affect biogenesis of EVs without itself being a cargo protein. Together, the data support a novel population of  $\beta$ 1-integrin<sup>+</sup> EVs distinct from classical exosomes that are enriched in both the P10 microvesicle population and the P100 sEV population. The data also demonstrate a link between Rab13 and  $\beta$ 1-integrin<sup>+</sup> EVs, supporting a new population of EVs whose biogenesis is Rab13-dependent.

## **3.4 Discussion**

### **3.4.1 Rab13 regulates EV secretion in mutant KRAS cells.**

In this study, we demonstrate that Rab13 can regulate the secretion of sEVs in a KRAS-dependent mechanism. Previous work has shown that Rab27a/b and Rab35 regulate EV secretion (Hsu et al., 2010; Ostrowski et al., 2010). Our work expands the number of Rab family members that can regulate EV biogenesis and also uncovers a potential new mechanism of secretion distinct from fusion of MVBs with the plasma membrane. Rab proteins as a family may play a significant role in the secretion of multiple subclasses of EVs, with the caveat that the specific role played by individual Rab proteins may be both cell-type and disease-state specific.

Rab13-dependent trafficking of  $\beta$ 1-integrin has been shown in breast cancer epithelial cells (Sahgal S, 2019) and  $\beta$ 1-integrins have been identified in sEVs released from a number of cells, notably breast and pancreatic cancer cells (Hoshino et al., 2015; Paolillo and Schinelli, 2017; Wortzel et al., 2019). We show that Rab13-dependent sEVs promote cell growth, miRNA transfer, and anchorage-independent growth in a KRAS-dependent manner in CRC cells. Decreased levels of Rab13 reduced secreted  $\beta$ 1-integrin levels and inhibited cell growth, miRNA transfer, and anchorage-independent growth. Previously, classical exosomes containing  $\beta$ 1-integrin were proposed to promote anchorage-independent growth in a pancreatic tumor model (DeRita et al., 2019). By immunocapture, we observed few, if any,  $\beta$ 1-integrin-containing vesicles associated with the classical exosome marker CD63, suggesting that  $\beta$ 1-integrin+, Rab13-dependent sEVs might be responsible for promoting anchorage-independent growth.

### 3.4.2 Heterogeneity in sEV populations.

There is growing evidence that there is significant EV heterogeneity, even among traditional subclasses such as exosomes. Although exosomes have traditionally been described as the primary form of sEVs, not all vesicles ~40-150nm are classical exosomes (Jeppesen et al., 2019). Classifying EV populations by size is not sufficient to characterize or identify one subclass over another. Full understanding of overall EV heterogeneity requires standardized purification methods (They et al., 2018), as well as an appreciation that EV cargo can differ in a cell-context manner. The recent use of high resolution density gradient fractionation methods further demonstrates that the exact purification strategies adopted can also affect the presence of protein and RNA cargo (Jeppesen et al., 2019). When we employed high resolution gradients, we discovered that Rab13 is associated with  $\beta$ 1-integrins in a population of sEVs that are distinct from classical CD63+ exosomes. Furthermore, we found that Rab13 is required for the efficient release of EVs in mutant KRAS cells but not in isogenic wild type KRAS cells.  $\beta$ 1-integrin+ EVs are found in both P100 sEV and P10 microvesicle fractions, unlike classical CD63+ exosomes which are enriched in P100 sEV populations. This suggests that there may be overlap between what are currently considered classical sEVs and classical microvesicles. The cellular localization and size of  $\beta$ 1-integrin+/Rab13+ sEVs suggest that these EVs are more likely secreted from the plasma membrane than via fusion of MVBs with the plasma membrane.

The high-resolution density gradients that we utilized followed a different protocol from Jeppesen et al. (2019) with differences in ultracentrifugation times and we did not subject supernatants from conditioned media (see Fig. 4) to filtration through a 0.2 micron filter before they were used as input for the density gradients. Had we followed the exact protocol described by Jeppesen et al (2019) (Jeppesen et al., 2019), the larger  $\beta$ 1-integrin+, Rab13+ vesicles would not have been present in the gradients and therefore would not have been detected. This



further emphasizes the point that the extent of vesicle heterogeneity is dependent on the choice of purification protocol.

### **3.4.3 Rab13 localization and cell confluency**

Our immunostaining data (Fig. 9) shows that Rab13 localizes to the plasma membrane and co-localizes with  $\beta$ 1-integrin in mutant KRAS cells. For those experiments, we performed the localization experiments at the same culture times and conditions as when we isolated EVs. However, in the course of those experiments, we noticed that when cells are plated at low density, Rab13 localizes more broadly to the cytoplasm and then re-localizes to the plasma membrane when cell-to-cell contact occurs. It is possible that the role that we observe for Rab13 in regulating EV secretion, especially secretion of  $\beta$ 1-integrin+, Rab13+ sEVs, is dependent on culture density or confluency. Interestingly, we previously observed differences in miRNA secretion between mutant (DKO-1) and wild type (Dks-8) KRAS cells (Cha et al., 2015a; McKenzie et al., 2016). Even when cultured at low density, mutant KRAS cells tend to clump together and make contact with one another, whereas individual wild-type KRAS cells spread out and only come into contact as the confluency increases. The secretion of  $\beta$ 1-integrin+, Rab13+ vesicles (and possibly other EVs) might be confluency-dependent, which could also account for differences in miRNA export.

### **3.4.4 EV heterogeneity and extracellular RNA**

In the study of extracellular RNA, miRNAs have dominated, due to their small size and the ability to demonstrate functional transfer of miRNA from donor to recipient cells (Aucher et al., 2013; Cha et al., 2015b; Chen et al., 2012; Fabbri et al., 2012; Melo et al., 2014; Ono et al., 2014; Zhang et al., 2015; Zomer et al., 2010). Previous work from our group has demonstrated KRAS-dependent sorting of Argonaute 2 protein (AGO2) into exosomes, presumably with

associated miRNAs (McKenzie et al., 2016). However, depending on the cell type and purification protocol, CD63+ exosomes have been isolated that lack detectable levels of AGO2 proteins (Jeppesen et al., 2019; Temoche-Diaz et al., 2019). One possible explanation is cell-type specific secretion of miRNAs associated with AGO2 from the plasma membrane like the novel population of  $\beta$ 1-integrin+/Rab13-dependent sEVs that we have identified here. Another possibility is secretion of naked miRNAs in  $\beta$ 1-integrin+, Rab13-dependent sEVs that activate Toll-Like Receptor 8 within the endosomal system (Fabbri et al., 2013). Nonetheless, our results expand what is known about EV heterogeneity and biogenesis, adding a new wrinkle that EV cargo composition across different EV subclasses can depend on Rab13 and KRAS status.

### **3.5 Methods**

#### **3.5.1 Cell culture**

DKO-1 and DKs-8 CRC cells are isogenic cell lines derived from the parental DLD-1 line (Shirasawa et al., 1993). DLD-1 cells are heterozygous for KRAS, Dks-8 cells contain a single wild type allele of KRAS, and DKO-1 cells contain a single mutant KRAS allele. Cells were cultured in standard DMEM (Gibco) with 10% FBS, 1% non-essential amino acids, 1% L-glutamine, and 1% penicillin/streptomycin (Gibco). Cells were grown at 37°C in 5% CO<sub>2</sub>. Cells were passaged a maximum of 10 times before being discarded.

#### **3.5.2 Isolation of EVs**

EVs were isolated through three varying levels of purity. Cells were seeded into 3-20 T175 flasks (Corning) at a density of  $6.5 \times 10^6$  (DKO-1) or  $7.5 \times 10^6$  (DKs-8) cells per flask. Cells were grown in the presence of serum to 80% confluency (~48 hours), washed three times with 1x Dulbecco's PBS (DPBS; Gibco), and then grown for 48 hours in serum free media. Cell-

conditioned media (CM) was collected and subjected to differential centrifugation in three steps: 1000rpm for 10 minutes (room temperature), 2000xg for 25 minutes (4°C), and then 10,000xg for 30 minutes (4°C). These steps produce cell pellets, cell debris and large EVs, and microvesicles, respectively. P100 pellets (crude sEVs) were obtained by centrifuging CM that had been subject to the three steps above for additional 17 hours at 100,000xg (4°C). Pellets were suspended in 1xDPBS and washed by centrifugation at 100,000xg twice for 70 minutes each time (4°C). Pellets were then resuspended in 20µL 1xPBS. For gradient preparations, CM subject to the three steps above was concentrated using a 100K concentrator (MilliPore) down to ~5mL. The concentrated media was then layered onto a 1mL 60% iodixanol cushions (Optiprep), and centrifuged at 100,000xg for 17 hours (4°C). The bottom 3mL was collected and then layered on top of an iodixanol discontinuous gradient consisting of 3 ml layers of 40%, 20% (CM layer), 10%, and 5% iodixanol. After centrifugation at 100,000xg for 17 hours (4°C), 1mL fractions (12) were collected (top to bottom). Each fraction was diluted in 12mL 1xDPBS and then centrifuged at 100,000xg for 3 hours (4°C). Final pellets were resuspended in 10-30µL 1xPBS.

### **3.5.3 Nanoparticle tracking analysis (NTA)**

Particle sizes and numbers were analyzed using the Zetaview® Nanoparticle Tracking Video Microscope PMX-120 (Particle Matrix) and associated software. After optimization of the software, settings were held constant across all four samples for each replicate. Typical concentration of vesicles ranged from  $10^8$  to  $10^{11}$  particles/mL.

### **3.5.4 Direct immunoaffinity capture of sEVs**

DIC was carried out as previously published (Jeppesen et al., 2019). In short, antibodies against either CD63+ (BD bioscience) or  $\beta$ 1-integrin+ (BD bioscience) were bound to

Dynabeads (ThermoFisher) at 5µg of antibody per 1mg beads. Conjugated beads were then washed, and incubated with DKO-1 pre-cleared conditioned media overnight, agitating at 4°C. Following incubation, beads were washed three times in DIC wash buffer, then re-suspended in 1x RIPA buffer (ThermoFisher). Samples were then loaded onto PAGE gels (Biorad) for western blot analyses.

DIC against the P10 pellet (microvesicles) was carried out in the same fashion but the P10 pellet was resuspended in DIC wash buffer, and then incubated with conjugated beads.

### **3.5.5 Plasmid construction**

Human Rab13 cDNA was synthesized using Accuscript RT (Agilent Technologies) from RNA purified from DKO-1 CRC cells. Rab13HA cDNAs were inserted into the pcDNA3.1+(Zeocin) plasmid using BamHI and NotI (New England Biolabs). shRNA plasmids were a gift from the Vanderbilt shRNA Core (Vanderbilt University). Rab13 shRNA #1 targeted the 3'UTR while shRNA #2 targeted the 3' end of the Rab13 ORF. All plasmids were confirmed by sequencing (Genewiz, South Plainfield, NJ, USA).

### **Primers**

Rab13HA\_F: 5'-ATACGGATCCATGCCAAAGCCTACGAC

Rab13HA\_R: 5'-ATACGCGGCCGCTCAAGCGTAATCTGGAACATC

### **3.5.6 Protein collection and western blotting**

Protein concentrations were quantified by BCA assays (BIO-RAD). For western blots, proteins were denatured in 1x RIPA buffer (Life Technologies). 2-5µg of total protein were loaded onto pre-cast gels (10 or 12% MINI-PROTEAN TGX® 12 by 15 or 50µL well pre-casted gel, respectively; BIO-RAD). Separated proteins were transferred to nitrocellulose using the

Trans-Blot® Turbo Transfer System (BIO-RAD). Membranes were blocked in 5% milk in TBS-T for 1 hour at room temperature. Primary antibodies were incubated overnight in 5% milk in TBS-T at 4°C. Secondary antibodies were incubated in 5% milk in TBS-T for 1 hour at room temperature. Blots were then washed in 1x TBS-T three times. For visualization, membranes were treated with SuperSignal™ West Femto Maximum Sensitivity Substrate for 60 seconds (Thermo Scientific). Blots were then exposed to film and developed for ~1 second to ~5 minutes depending on band intensity.

### **3.5.7 Transfection of shRNA plasmids and Rab13HA expression plasmids**

Plasmids were transfected using the Lipofectamine 2000 protocol (ThermoFisher). Cells were seeded at  $0.1 \times 10^6$  cells per well in 12 well dishes (Corning) and incubated for 24 hours at 37°C. 500-1000ng of DNA were incubated with 5µL Lipofectamine 2000 per well for 20 minutes at room temperature, and then added to individual wells. Cells were then incubated at 37°C for 24 hours before antibiotic selection for 1-2 weeks. shRNA vectors were selected using 1ug/mL Puromycin while Rab13HA expression vectors were selected using 50-100mg/mL Zeocin (ThermoFisher). shRNA transfections were confirmed via GFP visualization and Rab13HA expression was confirmed by western blot detection via an α-HA antibody. Rescue experiments transfected Rab13HA cDNA into shRNA vector expressing cells followed by selection with both Puromycin and Zeocin.

### **3.5.8 Three-dimensional culturing of DKO-1 cells in type-1 collagen**

Cells were cultured in type-1 collagen as previously published (Li et al., 2014). In short, 500 DKO-1 cells were embedded in a 2.5mg/mL type-1 collagen solution with 1x DMEM and 10% FBS in a single wells (Advanced BioMatrix). Each well contained three separate 450µL layers of collagen solution, with the cells embedded in the center layer. Each layer was solidified

separately at 37°C for 20-40 minutes. The collagen layers were covered with 500µL DMEM media. When supplementing DKO-1 sEVs, each well was given ~10µg of DKO-1 P100 sEVs every 4 days when the media was changed. Colonies were allowed to develop for 3 weeks at 37°C, and then counted. A total of 9 different wells were counted per experiment and experimental condition.

### **3.5.9 Transwell proliferation assays**

Donor cells were seeded at a density of  $0.05 \times 10^6$  cells per Transwell. Recipient cells were seeded at a density of  $0.1 \times 10^6$  cells per well. Donor and recipient cells were seeded separately, washed three times in 1xDPBS, and then co-cultured in serum free medium. Following 48 hours of co-culture at 37°C, recipient cells were collected and then counted using a BioRad cell counter. Each experiment was carried out with three technical (individual wells) and three biological (distinct Transwell plates) replicates.

### **3.5.10 Transwell luciferase reporter assays**

Recipient cells were plated in 6-well plates at a density of  $\sim 2.5 \times 10^5$  cells and cultured in DMEM supplemented with 10% bovine growth serum for 24 hours. Media were replaced and cells were co-transfected (Promega, E2311, Madison, WI, USA) with 1.5 µg of Luc-reporter plasmid and 1.5 µg β-gal plasmid DNA/well. Donor cells were plated on top of 0.4 µm polyester membrane Transwell filters (Corning, 3450, Corning, NY, USA) at  $\sim 2.5 \times 10^5$  cells/well for 24 hours. Media from donor Transwells and recipient 6-well plates were removed and replaced with DMEM without FBS. Co-culture of donor and recipient cells was conducted for either 48 hours before recipient cells were harvested. Lysates were prepared in 1X Reporter lysis buffer (Promega, E2510) and luciferase assays were performed according to the manufacturers protocol (Promega, E2510). β-gal expression was simultaneously determined from the lysates (Promega). Differences in transfection efficiency were accounted for by normalizing Luc

expression to  $\beta$ -Gal expression (Luc/ $\beta$ -Gal). All assays were performed on 3 biological replicates, each with 3 technical replicates.

### **3.5.11 Proliferation assays**

Cells were plated at  $0.1 \times 10^6$  cells per well in 12 well dishes (Corning). Individual wells were collected every 24 hours following adherence, and cell counts were calculated using the BioRad Cell Counting System (BioRad). Each time point was collected three different times, and the mean was plotted to calculate a relative exponential growth curve (Prism 9).

### **3.5.12 Soft agar assays**

Soft Agar assays were carried out as described (Demory Beckler et al., 2013). In short, 1% Noble Agar (Sigma-Aldrich) was warmed and then mixed with 2xDMEM media and 500 $\mu$ L of the mixture was plated in each well and allowed to solidify at room temperature. 500 cells (1500 cells per triplicate) were resuspended in 500 $\mu$ L standard DMEM media and incubated with or without 10 $\mu$ g DKO-1 P100 sEVs for 2 hours at 37°C. Following incubation, cells were centrifuged at 1000rpm for 5 minutes (room temperature), and resuspended in 1.5mL, 0.3% Noble Agar, 1x DMEM solution followed by plating of 500 $\mu$ L of the solution on top of the previous layer and allowed to solidify at room temperature until each layer solidified. 500 $\mu$ L of fresh standard DMEM culture media was then added over the solidified cultures, supplemented with or without 10 $\mu$ g of DKO-1 P100 sEVs. Cell media was then replaced every 4 days. Cultures were incubated at 37 °C for 2 weeks to allow colony formation. Colonies were stained with nitroblue tetrazolium chloride solution (Sigma) overnight at 37°C, and then counted the following day.

### **3.5.13 Immunocytochemistry**

DKO-1 cells were seeded at  $1 \times 10^5$  cells per well in 12 well dishes (Corning) containing a

single glass coverslip (Fisherbrand). Cells were given ~24 hours to adhere and grow at 37°C after which cells were washed twice in 1xPBS and fixed in 4% paraformaldehyde for 20 minutes at room temperature. Cells were permeabilized using 0.1% Triton X-100 for 15 minutes at room temperature and then incubated with 5% BSA and 5% donkey serum for 1 hour at room temperature. Incubation with primary antibodies in 10% donkey serum at 1:100 dilution was overnight at 4°C. Cells were then washed three times in 1% donkey serum for 10 minutes at room temperature, followed by incubation with secondary antibodies in 10% donkey serum at 1:100 dilution for 1 hour at room temperature in the dark. Cells were then washed with 1% donkey serum in PBS three times for 10 minutes at room temperature before being mounted (VectaShield), sealed, and imaged on a Zeiss Observer Z.1.

#### **3.5.14 Transmission electron microscopy of EVs**

TEM was carried out using a modified form of the protocol described previously (Jeppesen et al., 2019). EVs were purified by the above outlined high resolution iodixanol gradient and pooled into two populations: Fractions 1-3 and fractions 4-6. These two pools were then absorbed onto carbon-coated formvar grids (Electron microscopy sciences) for 5 minutes at room temperature by floating the grids on 5uL of the sample. After absorption of the vesicles, the grids were quickly washed in ddH<sub>2</sub>O, blotted, stained in 2% uranyl acetate for 30 seconds then dried on filter paper. Transmission electron microscopy was performed on a Tecnai T12 using a AMT CCD camera. Negative staining was performed in part through the use of the Vanderbilt Cell Imaging Shared Resource (supported by NIH grants CA68485, DK20593, DK58404, DK59637 and EY08126).

#### **3.6 Acknowledgements**

We would like to thank Dr. Evan Krystofiak of CISR for help with processing TEM images. This work was supported by the NIH Common Fund Extracellular RNA Communication



Program, grant U19 CA179514, with additional support from the Stevenson and Gisela Mosig endowments to Vanderbilt University.

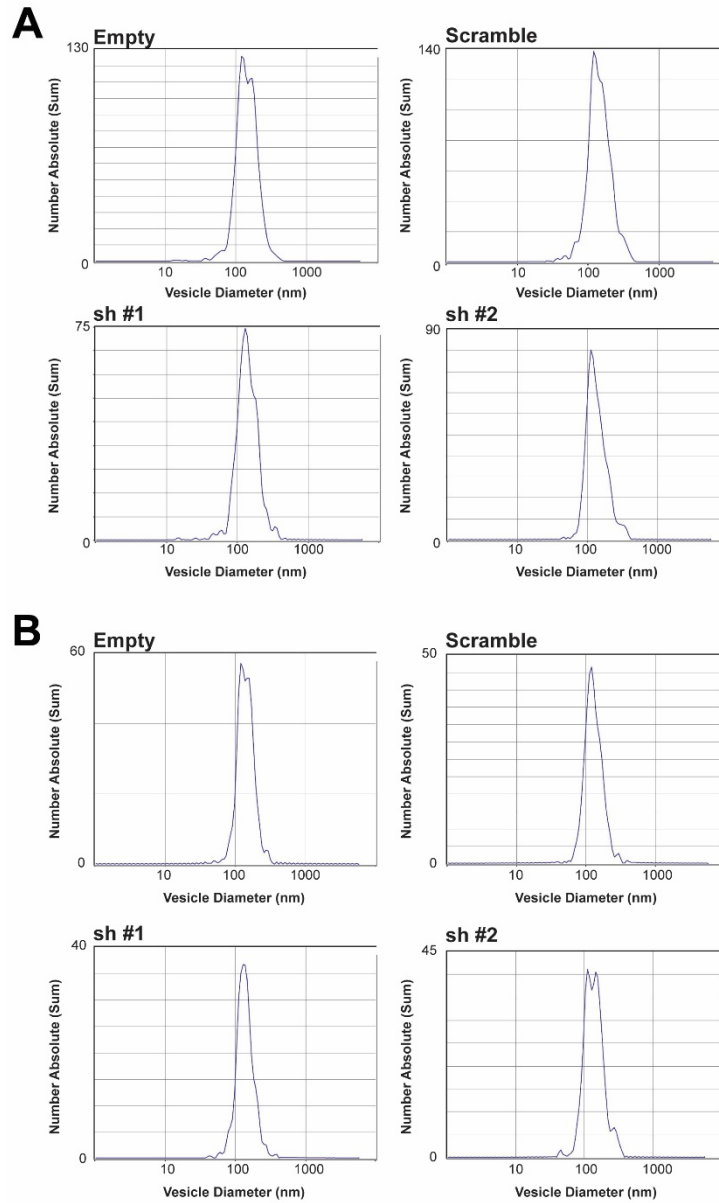
### **3.7 Author contributions**

SAH designed and performed most of the experimental work with help from JA. JGP directed the project and SAH, JLF, DKJ, RJC, and JGP wrote the manuscript.

### 3.A Appendix

#### 3.A.1 NTA analysis of sEVs collected from DKO-1 and DKs-8 cells under Rab13 knockdown conditions

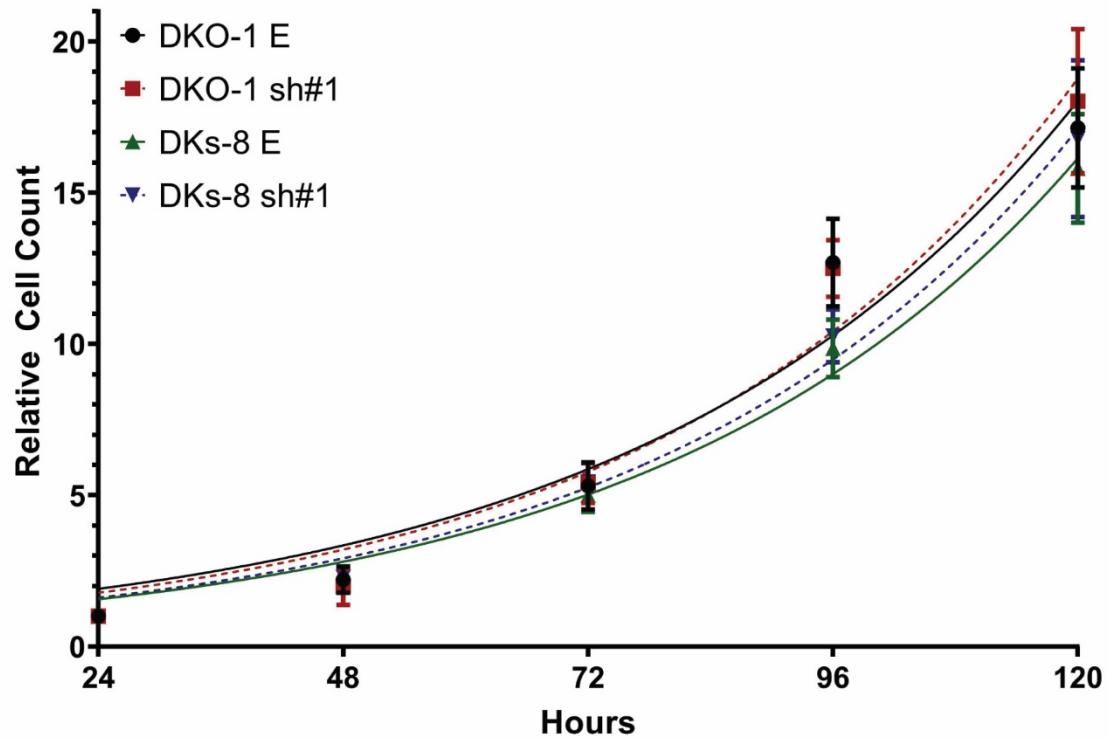
##### knockdown conditions



**3.A.1.** NTA analysis of sEVs collected from DKO-1 cells under Rab13 knockdown conditions. (A) Representative plot of vesicle size analyzed by NTA analysis of DKO-1 cells expressing an empty, scramble, sh#1, and sh#2 shRNA vectors. (B) Representative plot of vesicle size analyzed by NTA analysis of DKs-8 cells expressing an empty, scramble, sh#1, and sh#2 shRNA vectors.

### 3.A.2 Proliferation of cells under Rab13 knockdown conditions

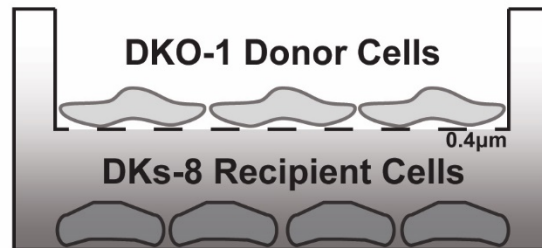
# A



**3.A.2.** (A) DKO-1 and DKs-8 cells under Rab13 knockdown conditions were seeded in 12 well plates and cultured for 120 hours. Cells were collected every 24 hours and counted. Data are from three biological replicates. Student's t-test found no significant difference between empty or shRNA-transfected cells.

### 3.A.3 Transwell assay schematic

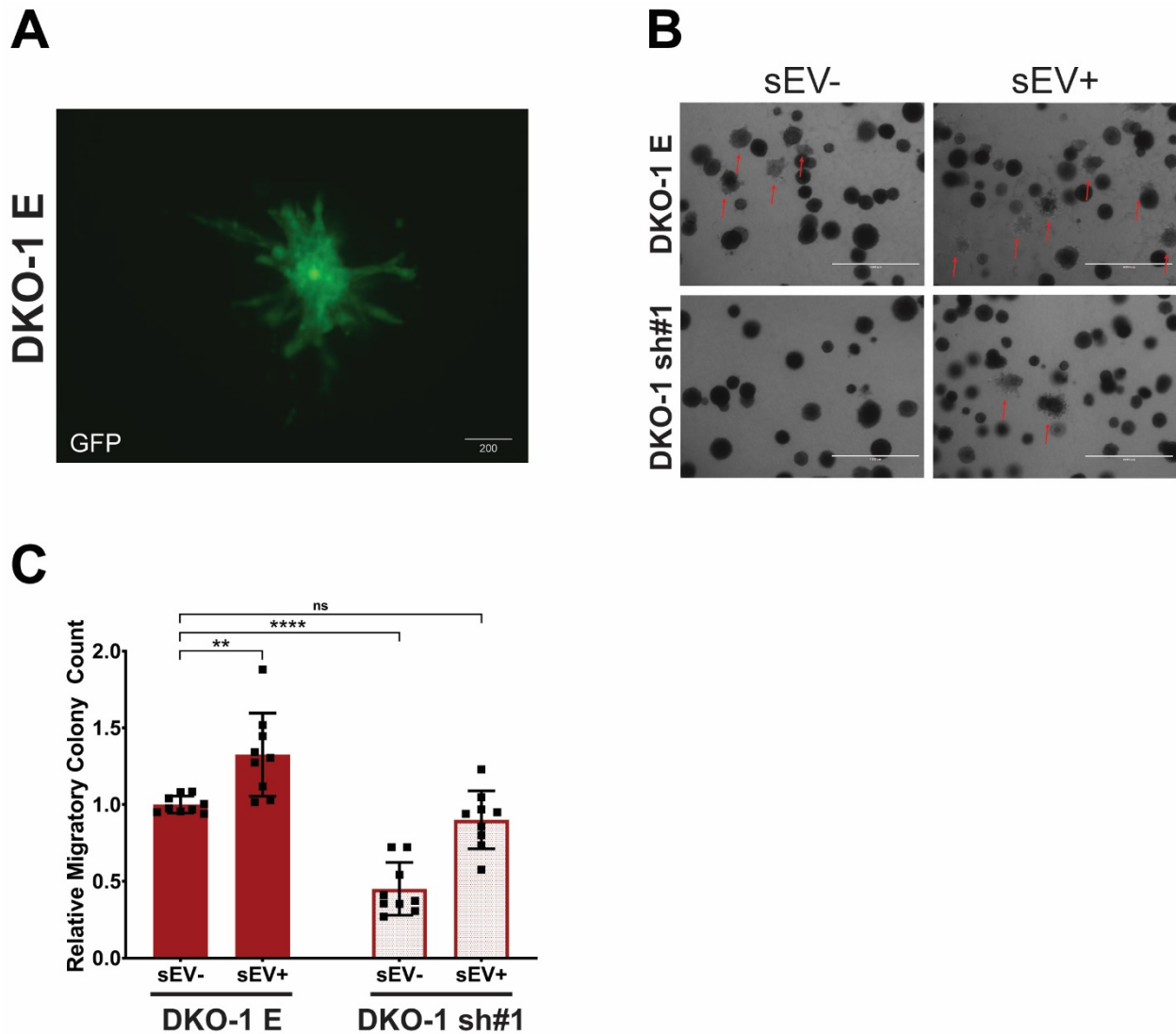
**A**



**(C) Proliferation (D) Luciferase Assay**

**3.A.3. (A)** Transwell assays. Donor and recipient cells were seeded and grown separately for 24-48 hours before co-culture opposite a 0.4μm polyester membrane.

### 3.A.4 Rab13 regulates growth in type-1 collagen via sEV secretion



**3.A.4.** (A) Image of DKO-1 migratory colony morphology grown in type-1 collagen. (B) DKO-1 cells under Rab13 knockdown conditions were embedded in type-1 collagen with or without exposure to sEVs purified from DKO-1 cells. Migratory colonies were then counted under each condition. (C) Quantitation of migratory colony counts under Rab13 knockdown conditions. Each data point represents a technical replicate from one of three biological replicates. Statistics were analyzed by one-way ANOVA. \*\* =  $p < 0.01$ , \*\*\*\* =  $p < 0.0001$ . ns=no significance.

## Chapter 4

### exRNA and cetuximab resistance

Scott A. Hinger<sup>1</sup>, Ramona Graves-Deal<sup>3</sup>, Jeffrey L. Franklin<sup>2,3,4</sup>, Qin Zhang<sup>3</sup>, James N. Higginbotham<sup>1</sup>, Robert J. Coffey<sup>2,3,4</sup>, and James G. Patton<sup>1,\*</sup>

Departments of Biological Sciences<sup>1</sup>, Cell and Developmental Biology<sup>2</sup>, Medicine<sup>3</sup>, Vanderbilt University Medical Center, Nashville, TN, 37235, Veterans Affairs Medical Center<sup>4</sup>, Nashville, TN 37235, and Vanderbilt University, Nashville, TN 37235.

#### 4.1 Abstract

Recently, Lu et al identified a novel non-mutational mechanism of cetuximab (CTX) resistance in colorectal cancer (CRC). CTX is a monoclonal antibody (mAb) against the Epidermal Growth Factor Receptor (EGFR) and the most common form of CTX resistance is due to activating mutations in *KRAS*. To identify non-mutational mechanisms of anti-EGFR resistance, single cells from human CRC cell line, HCA-7, were placed in type-1 collagen. Colonies with a single layer of polarized cells with a central lumen were identified and designated cystic colonies (CC). Individual colonies were manually isolated, passaged over 20 times on plastic and retained their cystic morphology when placed again in 3D type 1 collagen. CC cells were markedly growth inhibited by addition of cetuximab in 3D but not 2D culture. Prolonged low dose exposure of CC to CTX resulted in emergence of colonies resistant to cetuximab, designated CC-CTX resistant (CC-CR). By RNA-seq analysis of CC and CC-CR colonies isolated from 3D culture, MIR100HG was identified as the most highly expressed

transcript in CC-CR and the two most highly expressed miRs were two miRs embedded in the 3d intron of MIR100HG, *miR-100* and *miR-125b*. *miR-100* and *miR-125b* cooperatively targeted five WNT negative regulators, resulting in increased WNT signaling. Blockade of WNT signaling and antagomirs to these miRNAs restored CTX sensitivity both *in vitro* and *in vivo*. In this chapter, I describe our efforts to test whether CTX resistance could be spread via extracellular vesicles (EVs) since we previously showed that *miR-100* and *miR-125b* are enriched in small (s)EVs from CRC cells and that *miR-100* can be functionally transferred by CRC EVs.

## 4.2 Introduction

Cetuximab (CTX) is a monoclonal antibody (mAb) directed at the extracellular domain EGFR. CTX is used as a treatment for wild-type *KRAS* metastatic CRC, and as a monotherapy, increases the median survival from 4.6 months to 6.1 months in CRC patients . However, resistance to CTX occurs in ~80% of all patients treated due to acquired mutations in *KRAS*, *NRAS*, *BRAF*, and *EGFR* (Bertotti et al., 2015). Whether or not CTX resistance can be developed through non-genetic mechanisms but the mechanisms remain to be elucidated.

Recently published work from the Coffey laboratory (Lu et al., 2017) identified a non-genetic mechanism of CTX resistance in CRC. CTX susceptible cells (referred to as CC cells, described here (Li et al., 2014)) that are wildtype for *KRAS*, *BRAF*, *NRAS*, and *EGFR* were grown in three dimensional type-1 collagen and were exposed to low levels of CTX. Following two weeks of CTX treatment in 3D, living CC cells were collected and expanded in 2D. These cells were then embedded in new 3D matrix, and selected again with CTX. After multiple rounds of three-dimensional selection (~4 months), a resistant line that was capable of growing in 3D in the presence of CTX was identified, termed CC-CR (CC-CTX resistant). Whole exome sequencing revealed no mutations in known genetic mechanisms underlying CTX resistance

(Lu et al., 2017). RNA-sequencing analysis revealed that CC-CR cells have extremely elevated levels of non-coding RNAs transcribed from the MIR100HG locus, including *MIR100HG* (the spliced lncRNA), *miR-100*, and *miR-125b*. RT-qPCR data revealed a strong correlation between CTX resistance and *MIR100HG/miR-100/miR-125b* levels across many CRC cell models, suggesting these ncRNAs play a significant role in the development of CTX resistance. The MIR100HG locus has also been linked to the progression of acute megakaryoblastic leukemia, furthering the importance of this locus in cancer development (Emmrich et al., 2014).

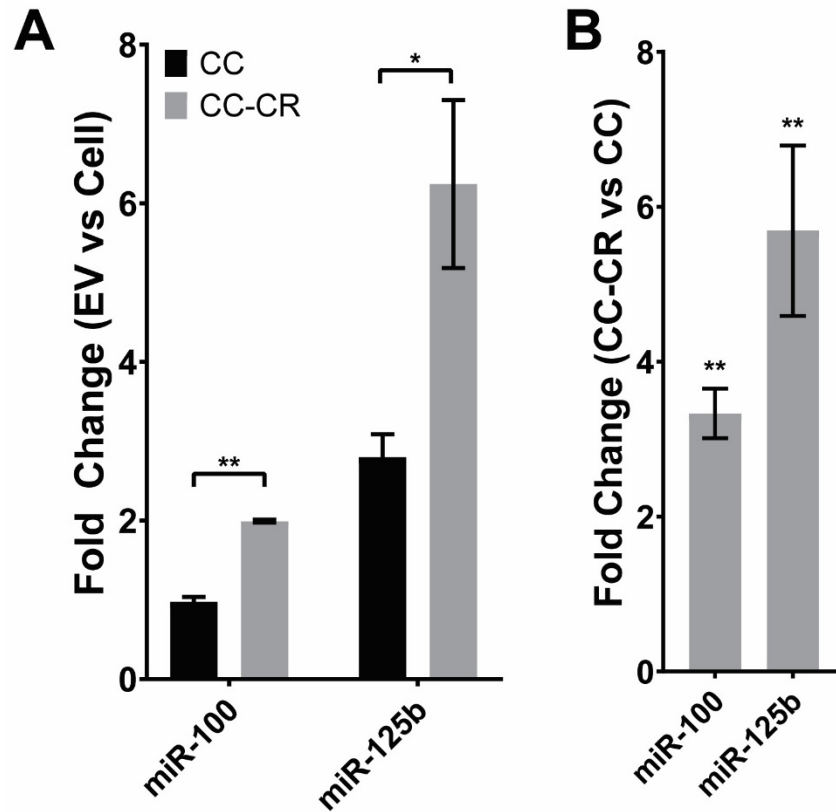
After demonstrating that cellular levels of RNAs from the MIR100HG locus were upregulated, Lu et al (2017) showed that the inhibition of *miR-100* and *miR-125b* was sufficient to restore CTX susceptibility in CC-CR cells both in 3D culture and in mouse tumor xenografts. In contrast, over expression of *miR-100* and *miR-125b* in CC cells promoted CTX resistance (Lu et al., 2017). To understand how these miRNAs were promoting resistance in CC cells, prediction algorithms were used to detect target mRNAs for these miRNAs resulting in the identification of 3' UTR five different Wnt negative regulators: DKK1, DKK3, ZNRF3, RNF43, and APC2 (Lu et al., 2017). Further analysis showed that CC-CR cells had significantly lower mRNA and protein levels for these Wnt negative regulators when compared to CC cells, suggesting that CTX resistance may be developed through the increased activation of the Wnt signaling cascade. In support of that model, co-treatment of CC-CR cells with both CTX and a Wnt inhibitor significantly reduced tumor growth in a mouse xenograft model, confirming a novel link between CTX resistance, EGFR, and Wnt signaling in CRC (Lu et al., 2017). Analysis of human tumors supported this novel epigenetic mechanism of CTX resistance (Lu et al., 2017).

Previous work from our laboratory has shown an enrichment of *miR-100* and *miR-125b* in CRC EVs, raising the possibility that CTX resistance might also be mediated by functional transfer of miRNAs between resistant and non-resistant tumor cells (Cha et al., 2015b). In



support of this, recently published work has linked EVs to the development of CTX resistance in various CRC models (Hon et al., 2019; Zhang et al., 2017).

**Figure 13. *miR-100* and *miR-125b* are enriched in CC-CR EVs**



**Figure 13.** RT-qPCR against *miR-100* and *miR-125b* from CC and CC-CR cell-derived EVs grown in 2D. (A) RT-qPCR analysis comparing CC and CC-CR EVs to their matched cells. (B) RT-qPCR analysis comparing CC-CR EVs to CC EVs. \* = p-value < 0.05, \*\* = p-value < 0.01. Statistics (paired t-test) were against  $\Delta\Delta Ct$  values and plotted as fold change.

## 4.3 Results

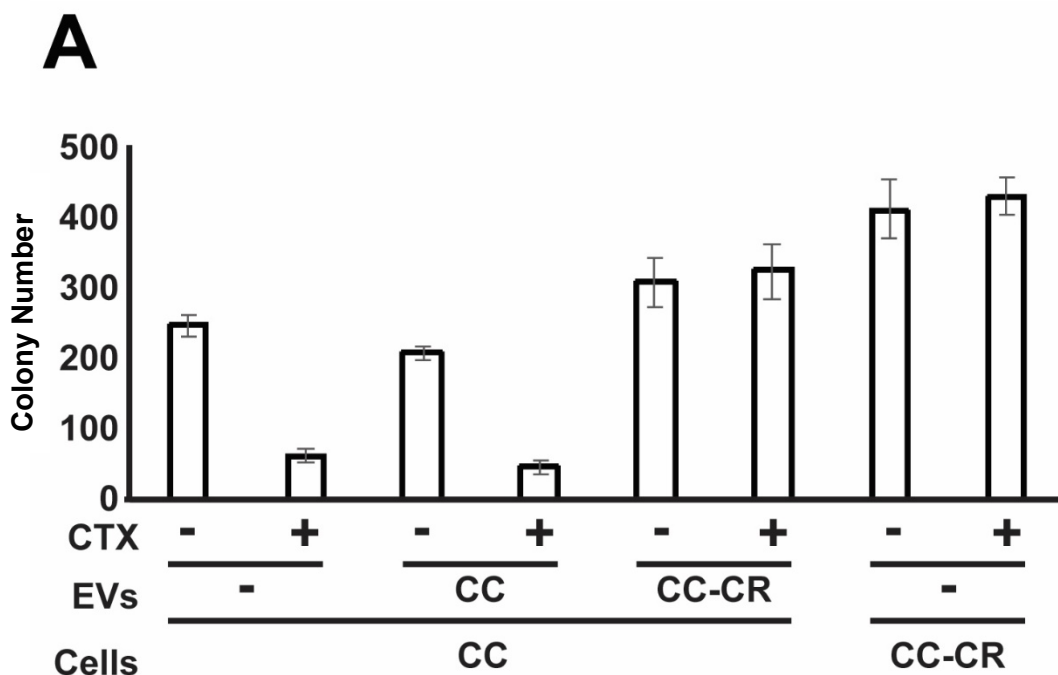
### 4.3.1 *miR-100* and *miR-125b* are highly expressed in EVs derived from CTX-resistant CRC Cells

To determine if EVs can promote CTX resistance in the CC-CR/CC cell model, and if this resistance is mediated by transfer of *miR-100* and *miR-125b* sEVs were collected from both CC and CC-CR cells. The levels of *miR-100* and *miR-125b* were found to be significantly elevated in CC-CR EVs compared to cells (**Fig. 13A**). Further, the levels of *miR-100* and *miR-125b* were significantly enriched in CC-CR EVs compared to CC EVs, mirroring their cellular enrichments, and indicating that CC-CR selectively secrete *miR-100* and *miR-125b* (**Fig. 13B**).

### 4.3.2 CC-CR EVs can promote CTX resistance in CC cells

CRC-derived EVs have been previously linked to the development of CTX resistance (Hon et al., 2019). To test whether or not a similar transfer occurs in our system, CC cells were grown with or without CC-CR EVs in 3D type-1 collagen in the presence of CTX. CC cells grown with CC-CR EVs showed higher levels of colony formation in the presence of CTX compared to CC cells grown without EVs, indicating that CC-CR EVs can promote CTX resistance via cell-cell communication (**Fig. 13**).

**Figure 14. EVs from CC-CR cells confer CTX resistance to CC cells**



**Figure 14.** (A) CC or CC-CR cells were plated in type-1 collagen with CC or CC-CR EVs as indicated and then treated with or without CTX (0.3 ug/ml). EVs and drugs were added every 3-5 days and colonies were counted at day 14. Y axis indicates number of colonies counted per replicate.

#### 4.4 Discussion

The data here suggest that CTX-resistant CRC cells are capable of transferring resistance via EV transfer. Previously published work has shown EVs can mediate CTX resistance in CRC, but the exact mechanism of resistance remains to be determined (Hon et al., 2019; Zhang et al., 2017). One potential mechanism of resistance could be through transfer and uptake of EV-associated miRNAs. Whether *miR-100* and *miR-125b* are the key players in this transfer phenotype remains to be determined, but previous work in Transwell cultures has shown that *miR-100* can be functionally transferred through the extracellular space (Cha et al., 2015a). Interestingly, *miR-125b* was also enriched in CC EVs compared to cells, suggesting there may be a CRC-driven mechanism for *miR-125b* secretion that may also promote CTX

resistance. This finding is supported by the fact that *miR-125b* is enriched in EVs from a number of CRC cell lines, along with *miR-100*, and could explain why CTX treatment is only effective in a small percentage of CRC patients (4.A.1). This may also help to explain the mechanism by which CC-CR cells developed resistance through a non-genetic mechanism, and may function as a successful plasma-derived, non-invasive biomarker when determining if CRC patients are good candidates for CTX treatment.

The data presented here was carried out using EVs isolated by differential ultracentrifugation. It is now clear that such purification methods result in a heterogenous mix of EVs. Thus, future work is needed to determine the exact mechanism of miRNA transfer, whether via EVs or by transfer of non-vesicular components including Argonaute-containing protein complexes (Arroyo et al., 2011), HDL particles (Vickers et al., 2011), or other nanoparticles such as exomeres (Zhang et al., 2018; Zhang et al., 2019). Also, the EVs used here were isolated from cells grown in 2D. Lu et al (2017) found that both CC and CC-CR cells are resistant to CTX in 2D, suggesting that the mechanism of resistance is dependent on the exact growth conditions, particularly the presence of type-1 collagen (Lu et al., 2017). Whether or not EVs secreted from the cells varies depending on culture conditions remains unknown, but will be important to shed light on how and why EVs function in different capacities under differing conditions.

## **4.5 Methods**

### **4.5.1 Cell culture**

CC and CC-CR CRC cells are cell lines derived from the parental HCA-7 (Li et al., 2014). HCA-7 cells are a human microsatellite-unstable CRC-derived cell line (Kirkland, 1985).

Cells were cultured in standard DMEM (Gibco) with 10% FBS, 1% non-essential amino acids, 1% L-glutamine, and 1% penicillin/streptomycin (Gibco). Cells were grown at 37°C in 5% CO<sub>2</sub>. Cells were passaged a maximum of 10 times before being discarded.

#### **4.5.2 EV isolation**

Cells were seeded into 3-20 T175 flasks (Corning) at a density of  $7.0 \times 10^6$  (CC or CC-CR) cells per flask. Cells were grown in the presence of serum to 80% confluency (~48 hours), washed three times with 1x Dulbecco's PBS (DPBS; Gibco), and then grown for 48 hours in serum-free medium. Cell-conditioned medium (CM) was collected and subjected to differential centrifugation in three steps: 1000rpm for 10 minutes (room temperature), 2000xg for 25 minutes (4°C), and then 10,000xg for 30 minutes (4°C). These steps produce cell pellets, cell debris and large EVs, and microvesicles, respectively. CM was then filtered through a 0.2µM filter (FisherScientific) to obtain pre-cleared CM. P100 pellets (crude sEVs) were obtained by centrifuging pre-cleared CM for additional 17 hours at 100,000xg (4°C). Pellets were suspended in 1xDPBS and washed by centrifugation at 100,000xg twice for 70 minutes each time (4°C). Pellets were then resuspended in 20µL 1xPBS.

#### **4.5.3 RT-qPCR**

Taqman small RNA assays (Life Technologies) were performed for indicated miRNAs on cellular and exosomal RNA samples. Briefly, 10 ng of total RNA was used per individual RT reactions; 0.67 µl of the resultant cDNA was used in 10 µl qPCR reactions. qPCR reactions were conducted in 386-well plates on a Bio-Rad CFX96 instrument. All C(t) values were ≤40. Triplicate C(t) values were averaged and normalized to U6 snRNA. Fold-changes were

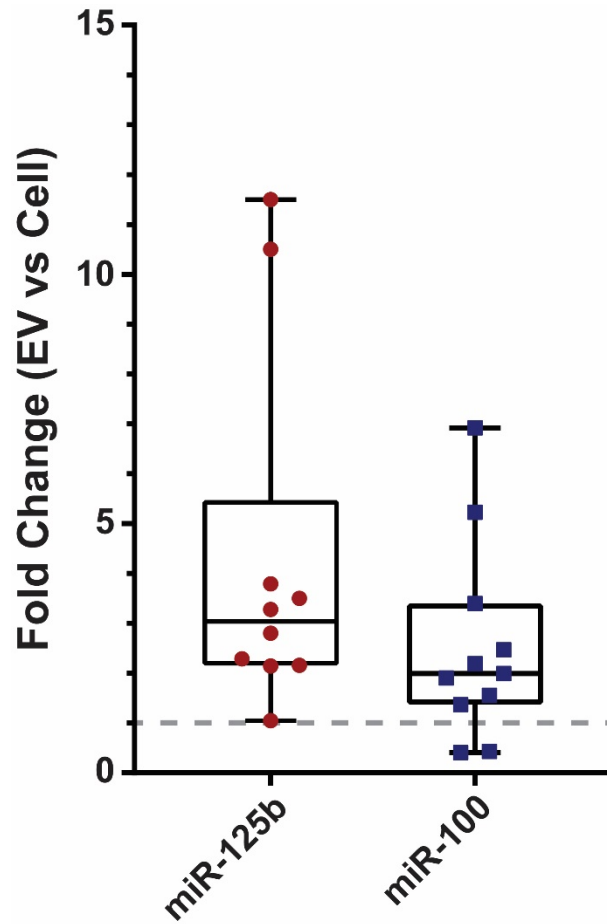
calculated using the  $\Delta\Delta C(t)$  method,  $FC = 2^{-\Delta\Delta C(t)}$ . Analysis was performed on three independent cell and exosomal RNA samples.

#### **4.5.1 Three-dimensional culturing of CC and CC-CR cells in type-1 collagen**

Cells were cultured in type-1 collagen as previously published (Li et al., 2014). In short, 2000 CC or CC-CR cells were embedded in a 2.5mg/mL type-1 collagen solution with 1x DMEM and 10% FBS in a single wells (Advanced BioMatrix). Each well contained three separate 450 $\mu$ L layers of collagen solution, with the cells embedded in the center layer. Each layer was solidified separately at 37°C for 20-40 minutes. The collagen layers were covered with 500 $\mu$ L DMEM media. When supplementing sEVs, each well was given ~10 $\mu$ g of P100 sEVs every 4 days when the media was changed, along with CTX at 0.3 $\mu$ g/mL. Colonies were allowed to develop for 2 weeks at 37°C, and then counted.

## 4.A Appendix

### 4.A.1 miR-125b and miR-100 levels in CRC cell-derived EVs



**4.A.1** RT-qPCR analysis of *miR-125b* (red, n=10) and *miR-100* (blue, n=11) from various CRC cell models, comparing EV levels to their matched cell level. Cell lines included: HCT-116, DKO-1, LOVO, HCT-15, LS174T, HKE-3, DKs-8, HuTu-80, CC, CC-CR, and SC. *miR-125b* and *miR-100* are enriched, on average, across multiple CRC models. Fold change is calculated by taking  $2^{(-\Delta\Delta\text{Ct}^{\text{EV}} - \Delta\text{Ct}^{\text{cell}})}$ .

## Discussion

The findings in the previous chapters demonstrate various functions CRC cell-derived EVs have in both the transfer of long RNAs, as well as their role in cancer development and progression. Although few RNAs were detected at full length in EVs, our findings suggest that small mRNAs and lncRNAs have the ability to be loaded as full-length transcripts into sEVs, and that these transcripts can be transferred through the extracellular space between KRAS-mutant and KRAS-wildtype CRC cells. Of the highly enriched mRNAs in KRAS-mutant EVs, Rab13 stood out, as its associated protein was also enriched in DKO-1 EVs (Demory Beckler et al., 2013), and because previous studies have found it to play a significant role in tumorigenesis and cancer progression (Ioannou et al., 2015). Thus, Rab13 is not only a cargo, both as mRNA and protein, but is also a regulator of EV secretion in KRAS-mutant CRC cells. Through its regulation of EV secretion, Rab13 knockdown inhibited the functional transfer of miRNAs, the proliferative capacity of EVs, and EV-dependent anchorage-independent growth in 3D. Rab13 is enriched in  $\beta$ 1-integrin+ small EVs, which are distinct from classical CD63+ exosomes and that finding, along with data from Jeppesen et al (2019), suggest a highly heterogeneous mixture of small EVs are secreted from KRAS-mutant CRC cells. The detection of various subtypes of small EVs is heavily tied to the isolation protocol to which the conditioned media is subjected (Jeppesen et al., 2019).

My preliminary work suggests that small EVs from CRC cells can also promote resistance to cetuximab, a therapeutic agent used in the treatment of CRC, through the delivery of *miR-100* and *miR-125b*. The enrichment of *miR-100* and *miR-125b* in multiple CRC cell line-derived EVs suggests a common mechanism for the transfer of resistance through



the extracellular space, and may suggest, at least partially, why cetuximab has limited efficacy in CRC patients (Misale et al., 2014).

Although the findings described here have helped drive the exRNA and EV field forward in better understanding the molecular make-up and biogenesis pathways, there are still many unanswered questions remaining. Below, I will describe potential discrepancies, current limitations, and potential new directions involved in (1) the limitations of long RNAs in EVs, (2) how the intracellular roles of Rab13 in cancer could be ascribed to regulation of EV biogenesis, and finally, (3) how CC-CR EVs may drive CTX resistance via a *miR-100/miR-125b*-independent mechanism.

### **5.1 Limitations of long RNAs in EVs**

The first evidence that EVs contain functional mRNAs was reported in human mast cells, where EV-associated RNA could be used to encode intact proteins in an *in vitro* translation assay (Valadi et al., 2007). Unfortunately, the experimental design in that study, along with many follow-up studies (Freedman et al., 2016; Ji et al., 2014; Kogure et al., 2013; Qu et al., 2016; Wei et al., 2017; Yuan et al., 2016), failed to demonstrate that full-length mRNAs are detectable in small EVs, and that these mRNAs can be transferred through the extracellular space to function in recipient cells (Zomer et al., 2015). Our findings, for the first time, show that mRNAs can be transferred with an apparent size limitation of ~1kB (Hinger et al., 2018) (**Chapter 2**). This raises an interesting question: is there a physical size limitation for long RNAs in small EVs?

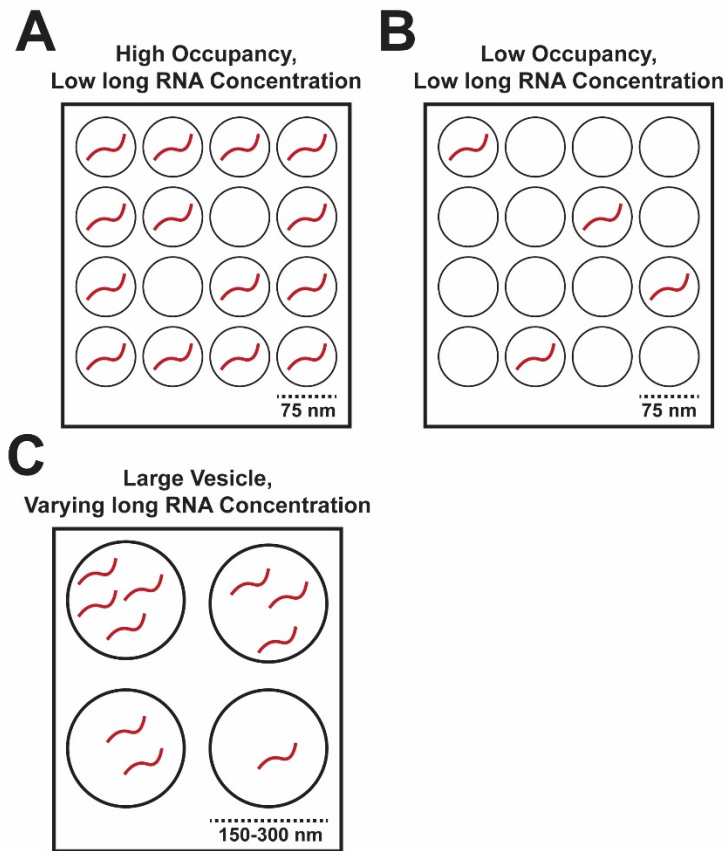
Advancements in cryogenic electron microscopy (cryo-EM) and associated computational analyses of large single-stranded RNAs (ssRNAs) may aid in understanding the potential size limitations for long RNAs in small EVs. Gopal et al (2012) analyzed viral ssRNAs

ranging from 900-2700 nucleotides in length and found in solution, the average diameter of these ssRNAs range from 50-75nm (Gopal et al., 2012). This suggests two important hurdles for the loading and functional transfer of long RNAs. First, the average size of a typical full-length mRNA in mammals (~2,200 base pairs) would not be able to fit in vesicles under ~75nm in diameter. This would prevent most full-length mRNAs from being loaded into the vast majority of small EVs (50-100nm in diameter). Second, this suggests that sEVs would, at most, contain only a single full-length mRNA. Quantitative analysis of miRNA content in small EVs suggested two models for occurrence and quantity of miRNAs per sEV: low EV occupancy, low miRNA concentration, or low EV occupancy, high miRNA concentration (Chevillet et al., 2014). The analysis of ssRNA tertiary structure suggests that longer RNAs cannot follow high concentration models predicted for extracellular miRNAs. Instead, long RNAs would have to be secreted in low concentration models and in either high or low occupancy (**Fig. 15**). Both models suggest the need for high levels of small EV transfer to induce a noticeable impact on recipient cells.

While the size estimates above were performed on ssRNA, it is known that many RNA binding proteins (RBPs) are present in small EVs (Statello et al., 2018). RBPs may alter the secondary and tertiary structure of their associated RNAs, although this mechanism is not well understood. RNA-RBP interactions may potentially increase or decrease the volume of secreted long RNAs and thereby regulate which RNAs are capable of being exported. Further work is necessary to understand whether RBPs can regulate RNA tertiary structure, and whether or not this plays a significant role in loading long RNAs into EVs.

If long RNAs are indeed secreted as full-length transcripts, the computational findings above would suggest that larger EVs, like plasma membrane-derived vesicles (for example, microvesicles), would be more capable of functional transfer. Another possibility is that full-length mRNAs (or lncRNAs) are not associated with vesicles at all and are transferred as part of

**Figure 15. Potential Stoichiometric Models for long RNAs in EVs**



**Figure 15.** (A) High occupancy, low long RNA concentration, where a single long RNA is loaded into a single small EV, but the majority of secreted small EVs contain a single copy. (B) Low occupancy, low long RNA concentration, where a single long RNA is loaded into a single small EV, and only a small minority of EVs get a single copy. (C) The use of larger vesicles could allow for multiple copies of a single long RNA, increasing the efficiency of transfer.

protein-RNA complexes. Another possibility is that full-length mRNAs (or lncRNAs) are not associated with vesicles at all and are transferred as part of protein-RNA complexes. The Transwell assays used here to assay functional transfer of Rab 13 mRNA cannot exclude the transfer by larger EVs or protein aggregates. Further, the isolation techniques include vesicles up to ~200nm in diameter and protein aggregates large enough to sediment at 100,000xg (Hinger et al., 2018), (EM from **Fig. 11**). Experiments subjecting sEV samples to RNase may help to better understand with which secreted particle(s) functional long RNAs are associated. Interestingly, many of the long RNAs enriched in our EVs were also found to be enriched in breast cancer cell protrusions, including Rab13 mRNA (Jakobsen et al., 2013). One possibility is that CRC cells develop protrusions enriched in Rab13 mRNA and protein, and that rapid blebbing or budding of the plasma membrane leads to the enrichment of these molecules in secreted particles. In fact, the interaction between DENND2B and Rab13 has been linked to the formation of cell protrusions in a breast cancer cell model (Ioannou et al., 2015). Taken together, Rab13 may control PM-derived EVs secretions through its regulation of cell protrusion formation and thus regulate its own mRNA and protein secretion. Repeating the Boyden chamber experiment carried out by Jakobsen et al (2013) with our KRAS-mutant CRC cells (DKO-1) could aid in confirming if long RNA-containing EVs are secreted via membrane protrusions (Jakobsen et al., 2013). Proteomic and RNA-seq analysis on DKO-1 protrusions, followed by differential comparison against our current small EV RNA-seq and proteomic libraries (Demory Beckler et al., 2013; Hinger et al., 2018), would allow determination of the overlap of macromolecules enriched in the two populations compared to cellular levels. If overlap is detected, it would suggest that cancer cells use cell membrane protrusions to facilitate the secretion of RNA-laden vesicles into the extracellular space.

Even if the majority of detectable long RNAs in EVs are not full length, it remains possible that fragmented RNAs function in unknown mechanisms via EV secretion. One

possibility is that fragmented RNAs induce the innate immune system, leading to significant downstream effects (van der Grein and Nolte-'t Hoen, 2014). This mechanism, which has been shown to occur via EV-associated miRNA transfer, may explain how long RNAs induce large scale changes in the tumor microenvironment, albeit through a non-canonical RNA mechanism (Fabbri et al., 2012). Foreign RNA sensing Toll-Like receptors, specifically TLR3, TLR7, TLR8, and TLR9, may detect fragmented exRNAs (Miyake et al., 2018). TLR3 and TLR9 have also been shown to be expressed not only by immune cells, but also cancer cells, particularly CRC cells, raising the possibility that TLR activation can play a role in both immune activation and tumor microenvironment interactions (Sato et al., 2009). Cancer cell associated TLRs have been shown to promote carcinogenesis through activating NF- $\kappa$ B and other anti-apoptotic factors in CRC models (Schmausser et al., 2005). It will be interesting to determine whether upregulation of various anti-apoptotic factors occurs in cells treated with DKO-1 EVs. This would indicate TLR activation and provide a mechanistic explanation for the effects of exRNA in the absence of full-length transfer.

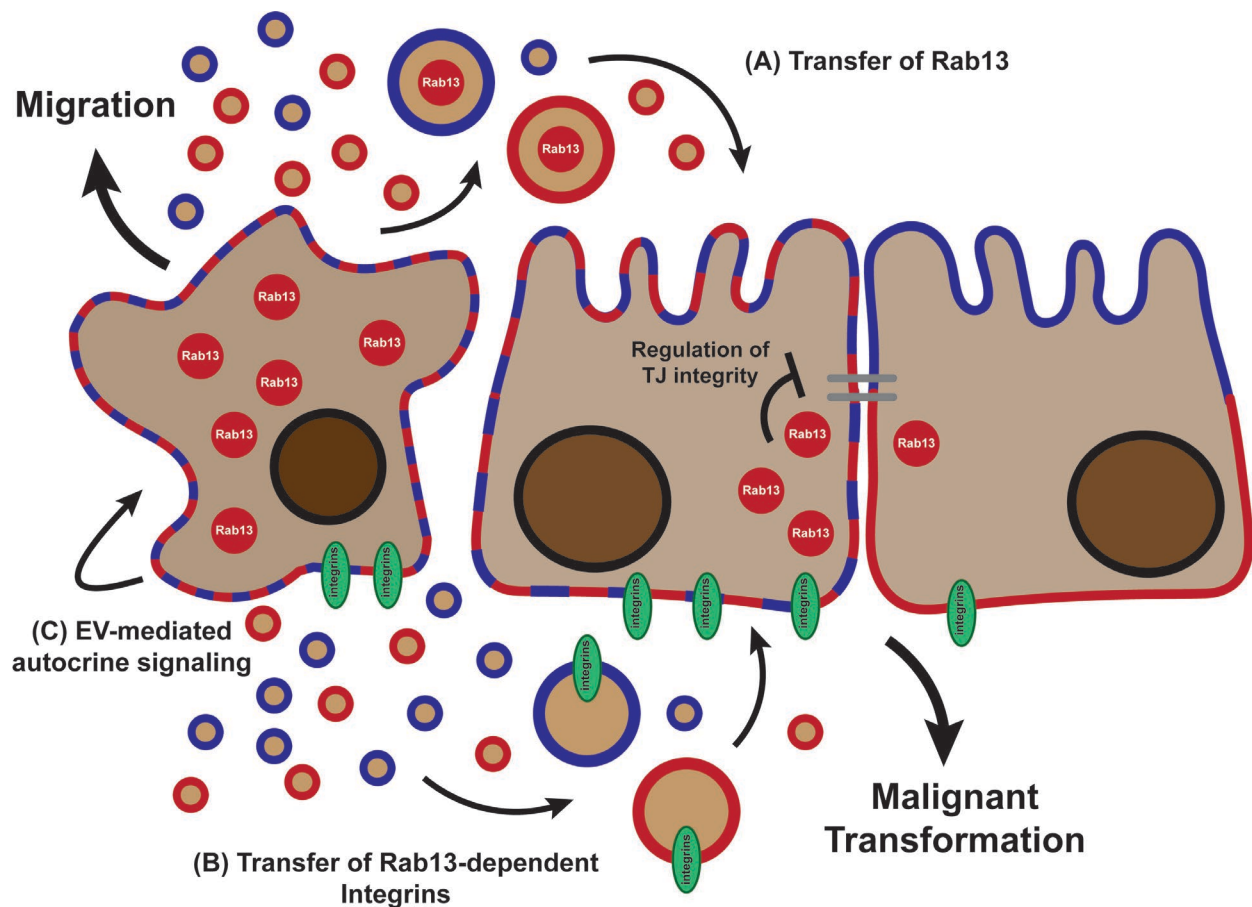
## **5.2 Intracellular vs extracellular roles of Rab13**

Intracellular Rab13 has been implicated in cancer progression, metastasis, and invasiveness (review, (McPherson, 2016)). I have shown that Rab13 is an important player in EV biogenesis, and that Rab13-dependent EV secretion and Rab13 sEVs can mediate the same phenotypes reported for intracellular Rab13 (**Chapter 3**). One of the primary functions of Rab13 in epithelial cells is its regulation of tight junction (TJ) formation (Kohler et al., 2004; Marzesco et al., 2002). Rab13 does this, in part, by trafficking vesicle-associated proteins to TJs, and by regulating the trafficking of material between apical and basolateral surfaces (Nokes et al., 2008). Interestingly, TJ disorganization is heavily tied to cancer tumorigenesis and

metastasis (Martin and Jiang, 2009). In fact, over-active Rab13 has also been shown to inhibit TJ integrity by negatively regulating PKA signaling (Kohler et al., 2004). Further, it has been shown that cancer cells secrete higher levels of small EVs when compared to non-cancerous cells (Szczepanski et al., 2011). Even in our model, DKO-1 cells secrete more EVs than their matched KRAS-wildtype DKs-8 sister cells (**Chapter 3**). One possible explanation for this difference could be through inhibition of TJ integrity, and therefore, the loss of epithelial cell polarity. In fact, breast cancer cells have been shown to secrete distinct EVs at higher concentrations when compared to polarized normal mammary epithelial cells (Chin et al., 2018). Activation and overexpression of Rab13 promotes the misregulation of TJ formation, which could then lead to increased secretion of small EVs (**Fig. 16**). This hypothesis is supported in our model, as KRAS-mutant cells have both higher levels of cellular Rab13 and secrete more EVs than their matched KRAS-wildtype cells, and could be further tested through the overexpression of dominant-active Rab13 mutants in both DKO-1 and DKs-8 cells. These findings could also help to explain why knockdown of Rab13 reduced anchorage-independent growth, since overcoming cell-to-cell adhesion stability is a primary driver to escape anoikis and promote tumorigenesis (Guadamillas et al., 2011). Restoration of anchorage-independent growth by exposure of Rab13 knockdown cells to small EVs from Rab13-expressing cells suggests that Rab13 functions via an EV-mediated mechanism (**Chapter 3**). Interestingly, DKO-1 small EVs can promote anchorage-independent growth of DKs-8 cells, but the mechanism by which this happens is not precisely known (Demory Beckler et al., 2013). My work offers the possibility that transfer of Rab13-laden small EVs can promote growth via negatively regulating the integrity of recipient cell TJs. Because of this possibility, it will be important to test the functional differences between sEVs secreted from DKO-1 cells with or without Rab13 knockdown to distinguish if the derived phenotypes are driven by the transfer of Rab13 protein or cargo regulated by Rab13-dependent EV biogenesis. It may be that Rab13 regulates the

secretion of integrins, including  $\beta 1$ -integrin, which have been linked to EV-mediated anchorage independent growth (DeRita et al., 2019) and EV-mediated organ-specific metastasis (Hoshino et al., 2015). A predicted outcome of the proposed model is that overexpression of Rab13 in DKs-8 cells should promote anchorage-independent growth.

**Figure 16. Potential functions of Rab13 in Epithelial Cancer Cell Progression**



**Figure 16.** Epithelial cell-derived cancer cells with high levels of Rab13 expression (left) negatively regulate tight junction formation leading to increased secretion of small EVs with misregulated EV cargo when compared to normal epithelial cells. These cancer cells can then promote transformation via the transfer of (A) Rab13 protein (red circle) and mRNA (not pictured), leading to decreased integrity of recipient cell TJs and/or (B) Rab13-dependent integrins, like  $\beta 1$ -integrin, which have been linked to anchorage-independent growth. (C) Cancer cells may also regulate cell migration via EV-mediated autocrine signaling, which may be driven, in part, by overexpression or activation of Rab13.

Further, it will be important to test whether Rab13 is regulating EV markers like  $\beta$ 1-integrin intracellularly, or if its role is strictly tied to secretion. Measuring PKA and VASP phosphorylation in DKs-8 recipient cells would also provide insight into whether or not transfer of Rab13 by small EVs is inhibiting TJ integrity, which has been described as an intracellular function of Rab13 in MDCK cells (Kohler et al., 2004).

Rab13 has also been shown to be required for epithelial cell scattering and migration, drivers of cancer cell invasion (Kanda et al., 2008). Primarily, Rab13 has been linked to the trafficking of integrins to the leading edge of cells, promoting migration (Ioannou et al., 2015). Interestingly, small EVs are secreted at the leading edge of cells to drive invasive behavior (Hoshino et al., 2013). Rab13 could, then, promote cell migration through two mechanisms. First, via the trafficking of integrins to the leading edge of cells (Ioannou et al., 2015). Second, via the trafficking of endosomes to the plasma membrane, facilitating the secretion of small EVs into the extracellular space, promoting cell migration by EV-mediated autocrine signaling events. A simple way to test this hypothesis is to repeat similar chemotaxis and/or migration assays carried out in a highly motile cancer cell model, as shown in Sung et al (2017) and Hoshino et al (2013), respectively (Hoshino et al., 2013; Sung and Weaver, 2017). If Rab13 is driving cell motility via EV secretion, knockdown of Rab13 should inhibit directional cell movement in a cancer cell model, and the addition of small EVs should rescue the phenotype. This has already been shown to be the case for Rab27a, a Rab protein that has been linked to small EV secretion at the leading edge of migratory cells (Hoshino et al., 2013). If Rab13 were to show a similar phenotype, it would suggest redundancy in regard to Rab proteins facilitating the secretion of small EVs and further explain why knockdown of Rab proteins involved in EV secretion seem to be heavily tied to cell- and disease-dependent mechanisms. The other possibility is that Rab13 can successfully regulate multiple subtypes of EVs. To test between these two hypotheses, epistasis experiments could be carried out to test the differences



between knockdown of Rab13 and other Rab proteins, like Rab27, which has been shown to also regulate EV secretion in our DKO-1 cell model.

It has been suggested that Rab proteins may play redundant roles in EV secretion, which would explain the cell- and disease-state specific roles Rab proteins have been shown to play. Because of this possibility, it will be important to measure the functional differences between the knockdown and expression of Rab13, Rab27, or Rab35 in DKO-1 or DKs-8 cells, both by total EV quantification and the detection of specific EV subtype markers. These studies could help to better understand the various mechanisms involved in the secretion of sEVs, particularly in CRC cells. Another reason for Rab-dependent EV redundancy may be due to Rab effector proteins or guanine exchange factors that have been shown to interact with multiple Rab partners (Yoshimura et al., 2010). Because of this overlap, it will be important to determine what proteins upstream or downstream of Rab13 also regulate EV secretion in CRC cells. An interesting target to focus on could be the Rab13 effector protein MICAL-L2, which has been previously linked to cancer progression (Ioannou et al., 2015; Kanda et al., 2008). MICAL-L2 may interact with other Rab proteins, like Rab27 or Rab35, at the plasma membrane, and may be the primary facilitator of sEV secretion. The finding that Rab effector proteins drive EV secretion, and not the Rab proteins themselves, would help to explain why Rab proteins have inconsistent functional significance across various cell and tissue models.

### **5.3 Alternative mechanisms for EV-mediated CTX resistance in the CC/CC-CR model**

Our preliminary findings suggest that cetuximab (CTX) resistant cells can promote resistance via the transfer of miRNA-laden small EVs (**Chapter 4**). However, the data is not conclusive, and further work is required to determine whether or not the transfer of *miR-100* and *miR-125b*, or sEVs in general, are capable of driving CTX resistance in recipient cells. When

describing the original resistant line (CC-CR), Lu et al (2017) showed an enrichment of phosphorylated EGFR, as well as a slight enrichment of overall EGFR (Lu et al., 2017). EGFR has been shown to be present on small EVs, and has been detected in CRC cell-derived EVs (Demory Beckler et al., 2013). Enrichment of EGFR on small EVs produced by CC-CR cells could provide an additional explanation for the reduced efficacy of CTX on CC cells when treated with CC-CR EVs. Previous groups have already shown that EVs have the potential to sequester chemotherapeutics by expressing targeted receptors on the membrane surface (Ciravolo et al., 2012). From a stoichiometric standpoint, increasing the total amount of EGFR in the tumor microenvironment would reduce the functional capacity of CTX, allowing susceptible cells, like CC cells, to continue to grow even under therapeutic treatment. Because of this, it will be important to compare the relative levels of EGFR on CC and CC-CR cell derived EVs, as CC EVs do not promote resistance to CTX. Therapeutic sequestering by EVs could help to explain how CRC tumors develop resistance to CTX, and could help to explain why CTX has limited efficacy in human patients. To better understand this possibility, it will be important to calculate the effectiveness of circulating sEVs in sequestering CTX, and whether this mechanism can impact the efficacy of CTX at therapeutic concentrations.

Lu et al (2007) found that resistance to CTX in CC-CR cells was through the activation of Wnt signaling through *miR-100* and *miR-125b* mediated negative regulation of Wnt cascade negative regulators (Lu et al., 2017). EV-mediated paracrine activation of Wnt in CC cells could also drive resistance to CTX. In fact CRC cell-derived EVs can activate Wnt signaling in a paracrine manner, transferring functional Wnt3a and Wnt5b through the extracellular space (Harada et al., 2017; Huang and Feng, 2017). Thus, it may be that CC-CR EVs induce CTX resistance in CC cells through both the transfer of *miR-100* and *miR-125b*, thereby downregulating Wnt negative regulators, and by direct activation of Wnt signaling. Currently, there is no evidence to suggest that CC-CR derived EVs can activate Wnt signaling. This could

be tested by comparing levels of Wnt ligands associated with CC and CC-CR EVs, again, because CC EVs are unable to induce resistance. Another method to test EV-mediated Wnt activation is by measuring the total level and/or the nuclear enrichment of  $\beta$ -catenin in the EV treated CC cells, which could be measured by a TopFlash luciferase reporter assay. It may be that CC-CR EVs mediate resistance through multiple mechanisms, including the two described here, as well as through the transfer of *miR-100* and *miR-125b*. Further work will be required to fully understand the mechanism by which CC-CR cells can transfer CTX resistance through the extracellular space.

## References

- Abdouh, M., Floris, M., Gao, Z.H., Arena, V., Arena, M., and Arena, G.O. (2019). Colorectal cancer-derived extracellular vesicles induce transformation of fibroblasts into colon carcinoma cells. *J Exp Clin Cancer Res* 38, 257.
- Abels, E.R., and Breakefield, X.O. (2016). Introduction to Extracellular Vesicles: Biogenesis, RNA Cargo Selection, Content, Release, and Uptake. *Cell Mol Neurobiol* 36, 301-312.
- Abou-Zeid, N., Pandjaitan, R., Sengmanivong, L., David, V., Le Pavec, G., Salamero, J., and Zahraoui, A. (2011). MICAL-like1 mediates epidermal growth factor receptor endocytosis. *Mol Biol Cell* 22, 3431-3441.
- Abrami, L., Brandi, L., Moayeri, M., Brown, M.J., Krantz, B.A., Leppla, S.H., and van der Goot, F.G. (2013). Hijacking multivesicular bodies enables long-term and exosome-mediated long-distance action of anthrax toxin. *Cell Rep* 5, 986-996.
- Akers, J.C., Gonda, D., Kim, R., Carter, B.S., and Chen, C.C. (2013). Biogenesis of extracellular vesicles (EV): exosomes, microvesicles, retrovirus-like vesicles, and apoptotic bodies. *J Neurooncol* 113, 1-11.
- Allaire, P.D., Seyed Sadr, M., Chaineau, M., Seyed Sadr, E., Konefal, S., Fotouhi, M., Maret, D., Ritter, B., Del Maestro, R.F., and McPherson, P.S. (2013). Interplay between Rab35 and Arf6 controls cargo recycling to coordinate cell adhesion and migration. *J Cell Sci* 126, 722-731.
- Alonso, R., Mazzeo, C., Rodriguez, M.C., Marsh, M., Fraile-Ramos, A., Calvo, V., Avila-Flores, A., Merida, I., and Izquierdo, M. (2011). Diacylglycerol kinase alpha regulates the formation and polarisation of mature multivesicular bodies involved in the secretion of Fas ligand-containing exosomes in T lymphocytes. *Cell Death Differ* 18, 1161-1173.

Anastasiadou, E., and Slack, F.J. (2014). Cancer. Malicious exosomes. *Science* 346, 1459-1460.

Anderson, E.C., and Wong, M.H. (2010). Caught in the Akt: regulation of Wnt signaling in the intestine. *Gastroenterology* 139, 718-722.

Anne-Marie Marzesco, T.G., Daniel Louvard, and Ahmed Zahraou (1998). The Rod cGMP Phosphodiesterase  $\alpha$  Subunit Dissociates the Small GTPase Rab13 from Membranes. *THE JOURNAL OF BIOLOGICAL CHEMISTRY*.

Ariel Savina, M.V., and Maria I. Colombo (2002). The exosome pathway in K562 cells is regulated by Rab11. *Journal of Cell Science*.

Arroyo, J.D., Chevillet, J.R., Kroh, E.M., Ruf, I.K., Pritchard, C.C., Gibson, D.F., Mitchell, P.S., Bennett, C.F., Pogosova-Agadjanyan, E.L., Stirewalt, D.L., *et al.* (2011). Argonaute2 complexes carry a population of circulating microRNAs independent of vesicles in human plasma. *Proc Natl Acad Sci U S A* 108, 5003-5008.

Aucher, A., Rudnicka, D., and Davis, D.M. (2013). MicroRNAs transfer from human macrophages to hepato-carcinoma cells and inhibit proliferation. *J Immunol* 191, 6250-6260.

Baietti, M.F., Zhang, Z., Mortier, E., Melchior, A., Degeest, G., Geeraerts, A., Ivarsson, Y., Depoortere, F., Coomans, C., Vermeiren, E., *et al.* (2012). Syndecan-syntenin-ALIX regulates the biogenesis of exosomes. *Nat Cell Biol* 14, 677-685.

Balkom, B.W.M.v., Eisele, A.S., Pegtel, D.M., Bervoets, S., and Verhaar, M.C. (2015). Quantitative and qualitative analysis of small RNAs in human endothelial cells and exosomes provides insights into localized RNA processing, degradation and sorting. *Journal of extracellular vesicles* 4.

Bartel, D.P., and Chen, C.Z. (2004). Micromanagers of gene expression: the potentially widespread influence of metazoan microRNAs. *Nat Rev Genet* 5, 396-400.

Batagov, A.O., and Kurochkin, I.V. (2013). Exosomes secreted by human cells transport largely mRNA fragments that are enriched in the 3'-untranslated regions. *Biology direct* 8, 12.

Becker, A., Thakur, B.K., Weiss, J.M., Kim, H.S., Peinado, H., and Lyden, D. (2016). Extracellular Vesicles in Cancer: Cell-to-Cell Mediators of Metastasis. *Cancer Cell* 30, 836-848.

Beckett, K., Monier, S., Palmer, L., Alexandre, C., Green, H., Bonneil, E., Raposo, G., Thibault, P., Le Borgne, R., and Vincent, J.P. (2013). Drosophila S2 cells secrete wingless on exosome-like vesicles but the wingless gradient forms independently of exosomes. *Traffic* 14, 82-96.

Behm-Ansmant, I., Rehwinkel, J., Doerks, T., Stark, A., Bork, P., and Izaurralde, E. (2006). mRNA degradation by miRNAs and GW182 requires both CCR4:NOT deadenylase and DCP1:DCP2 decapping complexes. *Genes & Development* 20, 1885-1898.

Bellingham, S.A., Coleman, B.M., and Hill, A.F. (2012). Small RNA deep sequencing reveals a distinct miRNA signature released in exosomes from prion-infected neuronal cells. *Nucleic Acids Res.*

Bénédicte Hugel, M.C.M., Corinne Kunzelmann, and Jean-Marie Freyssinet (2005). Membrane Microparticles: Two Sides of the Coin. *PHYSIOLOGY*.

Bernstein, E., Caudy, A., Hammond, S., Hannon, G. (2001). Role for a bidentate ribonuclease in the initiation step of RNA interference. *Nature* 409, 363-366.

Berrondo, C., Flax, J., Kucherov, V., Siebert, A., Osinski, T., Rosenberg, A., Fucile, C., RICHHEIMER, S., and Beckham, C.J. (2016). Expression of the Long Non-Coding RNA HOTAIR Correlates with Disease Progression in Bladder Cancer and Is Contained in Bladder Cancer Patient Urinary Exosomes. *PLOS ONE* 11, e0147236.

Bertotti, A., Papp, E., Jones, S., Adleff, V., Anagnostou, V., Lupo, B., Sausen, M., Phallen, J., Hruban, C.A., Tokheim, C., *et al.* (2015). The genomic landscape of response to EGFR blockade in colorectal cancer. *Nature* 526, 263-267.

Bhuin, T., and Roy, J.K. (2014). Rab proteins: the key regulators of intracellular vesicle transport. *Exp Cell Res* 328, 1-19.

Bobrie, A., Colombo, M., Krumeich, S., Raposo, G., and Thery, C. (2012). Diverse subpopulations of vesicles secreted by different intracellular mechanisms are present in exosome preparations obtained by differential ultracentrifugation. *J Extracell Vesicles* 1.

Booth, A.M., Fang, Y., Fallon, J.K., Yang, J.M., Hildreth, J.E., and Gould, S.J. (2006). Exosomes and HIV Gag bud from endosome-like domains of the T cell plasma membrane. *J Cell Biol* 172, 923-935.

Cha, D.J., Franklin, J.L., Dou, Y., Liu, Q., Higginbotham, J.N., Beckler, M.D., Weaver, A.M., Vickers, K., Prasad, N., Levy, S., *et al.* (2015a). KRAS-dependent sorting of miRNA to exosomes. *eLife* 4, 1-22.

Cha, D.J., Franklin, J.L., Dou, Y., Liu, Q., Higginbotham, J.N., Demory Beckler, M., Weaver, A.M., Vickers, K., Prasad, N., Levy, S., *et al.* (2015b). KRAS-dependent sorting of miRNA to exosomes. *Elife* 4, e07197.

Chen, G., Huang, A.C., Zhang, W., Zhang, G., Wu, M., Xu, W., Yu, Z., Yang, J., Wang, B., Sun, H., *et al.* (2018). Exosomal PD-L1 contributes to immunosuppression and is associated with anti-PD-1 response. *Nature* 560, 382-386.

Chen, X., Liang, H., Zhang, J., Zen, K., and Zhang, C.Y. (2012). Horizontal transfer of microRNAs: molecular mechanisms and clinical applications. *Protein & cell* 3, 28-37.

Chevillet, J.R., Kang, Q., Ruf, I.K., Briggs, H.A., Vojtech, L.N., Hughes, S.M., Cheng, H.H., Arroyo, J.D., Meredith, E.K., Gallichotte, E.N., *et al.* (2014). Quantitative and stoichiometric analysis of the microRNA content of exosomes. *Proc Natl Acad Sci U S A* 111, 14888-14893.

Chin, A.R., Yan, W., Cao, M., Liu, X., and Wang, S.E. (2018). Polarized Secretion of Extracellular Vesicles by Mammary Epithelia. *J Mammary Gland Biol Neoplasia* 23, 165-176.

Christoforides, S., McBride, H., Burgoyne, R.D., and Zerial, M. (1999). The Rab5 effector EEA1 is a core component of endosome docking. *Nature*.

Christoph Hess, S.S., Andreas Hefti, Regine Landmann, and Juerg-Alfred Schifferli (1999). Ectosomes Released by Human Neutrophils Are Specialized Functional Units. *The Journal of Immunology*.

Ciravolo, V., Huber, V., Ghedini, G.C., Venturelli, E., Bianchi, F., Campiglio, M., Morelli, D., Villa, A., Della Mina, P., Menard, S., *et al.* (2012). Potential role of HER2-overexpressing exosomes in countering trastuzumab-based therapy. *J Cell Physiol* 227, 658-667.

Clayton, A., Mitchell, J.P., Court, J., Mason, M.D., and Tabi, Z. (2007). Human tumor-derived exosomes selectively impair lymphocyte responses to interleukin-2. *Cancer Res* 67, 7458-7466.

Cocucci, E., Racchetti, G., and Meldolesi, J. (2009). Shedding microvesicles: artefacts no more. *Trends Cell Biol* 19, 43-51.

Colombo, M., Moita, C., van Niel, G., Kowal, J., Vigneron, J., Benaroch, P., Manel, N., Moita, L.F., Thery, C., and Raposo, G. (2013). Analysis of ESCRT functions in exosome biogenesis, composition and secretion highlights the heterogeneity of extracellular vesicles. *J Cell Sci* 126, 5553-5565.

Colombo, M., Raposo, G., and Thery, C. (2014a). Biogenesis, secretion, and intercellular interactions of exosomes and other extracellular vesicles. *Annu Rev Cell Dev Biol* 30, 255-289.

Colombo, M., Raposo, G., and Thery, C. (2014b). Biogenesis, Secretion, and Intercellular Interactions of Exosomes and Other Extracellular Vesicles. *Annu Rev Cell Dev Biol* 30, 255-289.

Costa-Silva, B., Aiello, N.M., Ocean, A.J., Singh, S., Zhang, H., Thakur, B.K., Becker, A., Hoshino, A., Mark, M.T., Molina, H., *et al.* (2015). Pancreatic cancer exosomes initiate pre-metastatic niche formation in the liver. *Nat Cell Biol* 17, 816-826.



Creemers, E.E., Tijssen, A.J., and Pinto, Y.M. (2012). Circulating MicroRNAs Novel Biomarkers and Extracellular Communicators in Cardiovascular Disease? *Circulation Research* 110, 483-495.

Crescitelli, R., Lasser, C., Szabo, T.G., Kittel, A., Eldh, M., Dinzani, I., Buzas, E.I., and Lotvall, J. (2013). Distinct RNA profiles in subpopulations of extracellular vesicles: apoptotic bodies, microvesicles and exosomes. *J Extracell Vesicles* 2.

de Renzis, S., Sonnichsen, B., and Zerial, M. (2002). Divalent Rab effectors regulate the sub-compartmental organization and sorting of early endosomes. *Nat Cell Biol* 4, 124-133.

Delprato, A., Merithew, E., and Lambright, D.G. (2004). Structure, exchange determinants, and family-wide rab specificity of the tandem helical bundle and Vps9 domains of Rabex-5. *Cell* 118, 607-617.

Demory Beckler, M., Higginbotham, J.N., Franklin, J.L., Ham, A.J., Halvey, P.J., Imasuen, I.E., Whitwell, C., Li, M., Liebler, D.C., and Coffey, R.J. (2013). Proteomic analysis of exosomes from mutant KRAS colon cancer cells identifies intercellular transfer of mutant KRAS. *Mol Cell Proteomics* 12, 343-355.

DeRita, R.M., Sayeed, A., Garcia, V., Krishn, S.R., Shields, C.D., Sarker, S., Friedman, A., McCue, P., Molugu, S.K., Rodeck, U., *et al.* (2019). Tumor-Derived Extracellular Vesicles Require beta1 Integrins to Promote Anchorage-Independent Growth. *iScience* 14, 199-209.

Ding, L., and Han, M. (2007). GW182 family proteins are crucial for microRNA-mediated gene silencing. *Trends Cell Biol* 17, 411-416.

DIRK FASSHAUER, R.B.S., AXEL T. BRUNGER, AND REINHARD JAHN (1998). Conserved structural features of the synaptic fusion complex: SNARE proteins reclassified as Q- and R-SNAREs. *Proc Natl Acad Sci U S A*.

Djuranovic, S., Nahvi, A., and Green, R. (2012). miRNA-mediated gene silencing by translational repression followed by mRNA deadenylation and decay. *Science* 336, 237-240.

Dou, Y., Cha, D.J., Franklin, J.L., Higginbotham, J.N., Jeppesen, D.K., Weaver, A.M., Prasad, N., Levy, S., Coffey, R.J., Patton, J.G., *et al.* (2016). Circular RNAs are down-regulated in KRAS mutant colon cancer cells and can be transferred to exosomes. *Sci Rep* 6, 37982.

EBERHARD G. TRAMS, C.J.L., NORMAN SALEM, Jr., URSULA HEINE (1981). EXFOLIATION OF MEMBRANE ECTO-ENZYMES IN THE FORM OF MICRO-VESICLES. *Biochimica et Biophysica Acta* 645.

Edouard M. Bevers, P.C., David W.C. Dekkers, Robert F.A. Zwaal (1999). Lipid translocation across the plasma membrane of mammalian cells. *Biochimica et Biophysica Acta*.

Ellis, B.C., Molloy, P.L., and Graham, L.D. (2012). CRNDE: A Long Non-Coding RNA Involved in Cancer, Neurobiology, and Development. *Front Genet* 3, 270.

Emmrich, S., Streltsov, A., Schmidt, F., Thangapandi, V.R., Reinhardt, D., and Klusmann, J.H. (2014). LincRNAs MONC and MIR100HG act as oncogenes in acute megakaryoblastic leukemia. *Mol Cancer* 13, 171.

Eulalio, A., Huntzinger, E., and Izaurralde, E. (2008). GW182 interaction with Argonaute is essential for miRNA-mediated translational repression and mRNA decay. *Nat Struct Mol Biol* 15, 346-353.

Fabbri, M., Paone, A., Calore, F., Galli, R., and Croce, C.M. (2013). A new role for microRNAs, as ligands of Toll-like receptors. *RNA Biol* 10, 169-174.

Fabbri, M., Paone, A., Calore, F., Galli, R., Gaudio, E., Santhanam, R., Lovat, F., Fadda, P., Mao, C., Nuovo, G.J., *et al.* (2012). MicroRNAs bind to Toll-like receptors to induce prometastatic inflammatory response. *Proc Natl Acad Sci U S A* 109, E2110-2116.

Fader, C.M., Sanchez, D.G., Mestre, M.B., and Colombo, M.I. (2009). TI-VAMP/VAMP7 and VAMP3/cellubrevin: two v-SNARE proteins involved in specific steps of the autophagy/multivesicular body pathways. *Biochim Biophys Acta* 1793, 1901-1916.

Fang, S., Xu, C., Zhang, Y., Xue, C., Yang, C., Bi, H., Qian, X., Wu, M., Ji, K., Zhao, Y., *et al.* (2016). Umbilical Cord-Derived Mesenchymal Stem Cell-Derived Exosomal MicroRNAs Suppress Myofibroblast Differentiation by Inhibiting the Transforming Growth Factor-beta/SMAD2 Pathway During Wound Healing. *Stem Cells Transl Med* 5, 1425-1439.

Freedman, J.E., Gerstein, M., Mick, E., Rozowsky, J., Levy, D., Kitchen, R., Das, S., Shah, R., Danielson, K., Beaulieu, L., *et al.* (2016). Diverse human extracellular RNAs are widely detected in human plasma. *Nat Commun* 7, 11106.

Fritz, J.V., Heintz-Buschart, A., Ghosal, A., Wampach, L., Etheridge, A., Galas, D., and Wilmes, P. (2016). Sources and Functions of Extracellular Small RNAs in Human Circulation. *Annu Rev Nutr* 36, 301-336.

Fu, Q., Zhang, Q., Lou, Y., Yang, J., Nie, G., Chen, Q., Chen, Y., Zhang, J., Wang, J., Wei, T., *et al.* (2018). Primary tumor-derived exosomes facilitate metastasis by regulating adhesion of circulating tumor cells via SMAD3 in liver cancer. *Oncogene* 37, 6105-6118.

Futter, C.E., Pearse, A., Hewlett, L.J., and Hopkins, C.R. (1996). Multivesicular endosomes containing internalized EGF-EGF receptor complexes mature and then fuse directly with lysosomes. *J Cell Biol* 132, 1011-1023.

Gibbins, D.J., Ciaudo, C., Erhardt, M., and Voinnet, O. (2009). Multivesicular bodies associate with components of miRNA effector complexes and modulate miRNA activity. *Nat Cell Biol* 11, 1143-1149.

Gopal, A., Zhou, Z.H., Knobler, C.M., and Gelbart, W.M. (2012). Visualizing large RNA molecules in solution. *RNA* 18, 284-299.

Gregory, R.I., Chendrimada, T.P., Cooch, N., and Shiekhattar, R. (2005). Human RISC couples microRNA biogenesis and posttranscriptional gene silencing. *Cell* 123, 631-640.

Gregory, R.I., Yan, K.P., Amuthan, G., Chendrimada, T., Doratotaj, B., Cooch, N., and Shiekhattar, R. (2004). The Microprocessor complex mediates the genesis of microRNAs. *Nature* 432, 235-240.

Griffiths-Jones, S. (2004). The microRNA Registry. *Nucleic Acids Res* 32 *Database issue*, D109-111.

Griffiths-Jones, S., Grocock, R.J., van Dongen, S., Bateman, A., and Enright, A.J. (2006). miRBase: microRNA sequences, targets and gene nomenclature. *Nucleic Acids Res* 34, D140-144.

Gross, J.C., Chaudhary, V., Bartscherer, K., and Boutros, M. (2012). Active Wnt proteins are secreted on exosomes. *Nat Cell Biol* 14, 1036-1045.

Guadamillas, M.C., Cerezo, A., and Del Pozo, M.A. (2011). Overcoming anoikis--pathways to anchorage-independent growth in cancer. *J Cell Sci* 124, 3189-3197.

Ha, M., and Kim, V.N. (2014). Regulation of microRNA biogenesis. *Nat Rev Mol Cell Biol* 15, 509-524.

Haas, A.K., Yoshimura, S., Stephens, D.J., Preisinger, C., Fuchs, E., and Barr, F.A. (2007). Analysis of GTPase-activating proteins: Rab1 and Rab43 are key Rabs required to maintain a functional Golgi complex in human cells. *J Cell Sci* 120, 2997-3010.

HAI-LI LANG, G.-W.H., BO ZHANG, WEI KUANG, YONG CHEN, LEI WU and GUO-HAI XU (2017). Glioma cells enhance angiogenesis and inhibit endothelial cell apoptosis through the release of exosomes that contain long non-coding RNA CCAT2. *Oncology Reports*.

Hamidi, H., and Ivaska, J. (2018). Every step of the way: integrins in cancer progression and metastasis. *Nat Rev Cancer* 18, 533-548.

Hammond, S.M., Bernstein, E., Beach, D., and Hannon, G.J. (2000). An RNA-directed nuclease mediates post-transcriptional gene silencing in *Drosophila* cells. *Nature* 404, 293-296.

Han, J., Pluhackova, K., and Bockmann, R.A. (2017). The Multifaceted Role of SNARE Proteins in Membrane Fusion. *Front Physiol* 8, 5.

Hangauer, M.J., Vaughn, I.W., and McManus, M.T. (2013). Pervasive transcription of the human genome produces thousands of previously unidentified long intergenic noncoding RNAs. *PLoS Genet* 9, e1003569.

Harada, T., Yamamoto, H., Kishida, S., Kishida, M., Awada, C., Takao, T., and Kikuchi, A. (2017). Wnt5b-associated exosomes promote cancer cell migration and proliferation. *Cancer science* 108, 42-52.

Haraszti, R.A., Didiot, M.C., Sapp, E., Leszyk, J., Shaffer, S.A., Rockwell, H.E., Gao, F., Narain, N.R., DiFiglia, M., Kiebish, M.A., *et al.* (2016). High-resolution proteomic and lipidomic analysis of exosomes and microvesicles from different cell sources. *J Extracell Vesicles* 5, 32570.

Heneghan, H.M., Miller, N., Lowery, A.J., Sweeney, K.J., Newell, J., and Kerin, M.J. (2010). Circulating microRNAs as novel minimally invasive biomarkers for breast cancer. *Annals of surgery* 251, 499-505.

Hessvik, N.P., and Llorente, A. (2018). Current knowledge on exosome biogenesis and release. *Cell Mol Life Sci* 75, 193-208.

Higginbotham, J.N., Demory Beckler, M., Gephart, J.D., Franklin, J.L., Bogatcheva, G., Kremers, G.J., Piston, D.W., Ayers, G.D., McConnell, R.E., Tyska, M.J., *et al.* (2011). Amphiregulin exosomes increase cancer cell invasion. *Curr Biol* 21, 779-786.

Hinger, S.A., Cha, D.J., Franklin, J.L., Higginbotham, J.N., Dou, Y., Ping, J., Shu, L., Prasad, N., Levy, S., Zhang, B., *et al.* (2018). Diverse Long RNAs Are Differentially Sorted into Extracellular Vesicles Secreted by Colorectal Cancer Cells. *Cell Rep* 25, 715-725 e714.

Hirotsugu Matsuo, J.C., Nathalie Mayran, Isabelle Le Blanc, Charles Ferguson, Julien Faure, Nathalie Sartori Blanc, Stefan Matile, Jacques Dubochet, Re´my Sadoul, Robert G. Parton, Francis Vilbois, Jean Gruenberg (2004). Role of LBPA and Alix in Multivesicular Liposome Formation and Endosome Organization. *Science*.

Hon, K.W., Ab-Mutalib, N.S., Abdullah, N.M.A., Jamal, R., and Abu, N. (2019). Extracellular Vesicle-derived circular RNAs confers chemoresistance in Colorectal cancer. *Sci Rep* 9, 16497.

Hoshino, A., Costa-Silva, B., Shen, T.L., Rodrigues, G., Hashimoto, A., Tesic Mark, M., Molina, H., Kohsaka, S., Di Giannatale, A., Ceder, S., *et al.* (2015). Tumour exosome integrins determine organotropic metastasis. *Nature* 527, 329-335.

Hoshino, D., Kirkbride, K.C., Costello, K., Clark, E.S., Sinha, S., Grega-Larson, N., Tyska, M.J., and Weaver, A.M. (2013). Exosome Secretion Is Enhanced by Invadopodia and Drives Invasive Behavior. *Cell Reports* 5, 1159-1168.

Hsu, C., Morohashi, Y., Yoshimura, S., Manrique-Hoyos, N., Jung, S., Lauterbach, M.A., Bakhti, M., Gronborg, M., Mobius, W., Rhee, J., *et al.* (2010). Regulation of exosome secretion by Rab35 and its GTPase-activating proteins TBC1D10A-C. *J Cell Biol* 189, 223-232.

Hu, C., Chen, M., Jiang, R., Guo, Y., Wu, M., and Zhang, X. (2018). Exosome-related tumor microenvironment. *Journal of Cancer* 9, 3084-3092.

Huang, Z., and Feng, Y. (2017). Exosomes Derived From Hypoxic Colorectal Cancer Cells Promote Angiogenesis Through Wnt4-Induced beta-Catenin Signaling in Endothelial Cells. *Oncol Res* 25, 651-661.

Huang, Z., Huang, D., Ni, S., Peng, Z., Sheng, W., and Du, X. (2010). Plasma microRNAs are promising novel biomarkers for early detection of colorectal cancer. *Int J Cancer* 127, 118-126.

Huber, V., Fais, S., Iero, M., Lugini, L., Canese, P., Squarcina, P., Zaccheddu, A., Colone, M., Arancia, G., Gentile, M., *et al.* (2005). Human colorectal cancer cells induce T-cell death

through release of proapoptotic microvesicles: role in immune escape. *Gastroenterology* 128, 1796-1804.

Hurwitz, S.N., and Meckes, D.G., Jr. (2019). Extracellular Vesicle Integrins Distinguish Unique Cancers. *Proteomes* 7.

Hyenne, V., Apaydin, A., Rodriguez, D., Spiegelhalter, C., Hoff-Yoessle, S., Diem, M., Tak, S., Lefebvre, O., Schwab, Y., Goetz, J.G., *et al.* (2015). RAL-1 controls multivesicular body biogenesis and exosome secretion. *J Cell Biol* 211, 27-37.

Ikeda, M., and Longnecker, R. (2007). Cholesterol is critical for Epstein-Barr virus latent membrane protein 2A trafficking and protein stability. *Virology* 360, 461-468.

Ioannou, M.S., Bell, E.S., Girard, M., Chaineau, M., Hamlin, J.N., Daubaras, M., Monast, A., Park, M., Hodgson, L., and McPherson, P.S. (2015). DENND2B activates Rab13 at the leading edge of migrating cells and promotes metastatic behavior. *J Cell Biol* 208, 629-648.

Jae, N., McEwan, D.G., Manavski, Y., Boon, R.A., and Dimmeler, S. (2015). Rab7a and Rab27b control secretion of endothelial microRNA through extracellular vesicles. *FEBS Lett* 589, 3182-3188.

Jaiswal, J.K., Andrews, N.W., and Simon, S.M. (2002). Membrane proximal lysosomes are the major vesicles responsible for calcium-dependent exocytosis in nonsecretory cells. *J Cell Biol* 159, 625-635.

Jakobsen, K.R., Sørensen, E., Brøndum, K.K., Daugaard, T.F., Thomsen, R., and Nielsen, A.L. (2013). Direct RNA sequencing mediated identification of mRNA localized in protrusions of human MDA-MB-231 metastatic breast cancer cells. *Journal of Molecular Signaling* 8, 9.

Jeppesen, D.K., Fenix, A.M., Franklin, J.L., Higginbotham, J.N., Zhang, Q., Zimmerman, L.J., Liebler, D.C., Ping, J., Liu, Q., Evans, R., *et al.* (2019). Reassessment of Exosome Composition. *Cell* 177, 428-445 e418.

Ji, H., Chen, M., Greening, D.W., He, W., Rai, A., Zhang, W., and Simpson, R.J. (2014). Deep sequencing of RNA from three different extracellular vesicle (EV) subtypes released from the human LIM1863 colon cancer cell line uncovers distinct miRNA-enrichment signatures. *PLoS One* 9, e110314.

Jia, P., Cai, H., Liu, X., Chen, J., Ma, J., Wang, P., Liu, Y., Zheng, J., and Xue, Y. (2016). Long non-coding RNA H19 regulates glioma angiogenesis and the biological behavior of glioma-associated endothelial cells by inhibiting microRNA-29a. *Cancer letters* 381, 359-369.

Jiang, L., Dong, H., Cao, H., Ji, X., Luan, S., and Liu, J. (2019). Exosomes in Pathogenesis, Diagnosis, and Treatment of Alzheimer's Disease. *Med Sci Monit* 25, 3329-3335.

Kahlert, C., and Kalluri, R. (2013). Exosomes in tumor microenvironment influence cancer progression and metastasis. *Journal of molecular medicine* 91, 431-437.

Kajimoto, T., Okada, T., Miya, S., Zhang, L., and Nakamura, S. (2013). Ongoing activation of sphingosine 1-phosphate receptors mediates maturation of exosomal multivesicular endosomes. *Nat Commun* 4, 2712.

Kalluri, R. (2016). The biology and function of exosomes in cancer. *J Clin Invest* 126, 1208-1215.

Kalra, H., Simpson, R.J., Ji, H., Aikawa, E., Altevogt, P., Askenase, P., Bond, V.C., Borrás, F.E., Breakefield, X., Budnik, V., *et al.* (2012). Vesiclepedia: a compendium for extracellular vesicles with continuous community annotation. *PLoS Biol* 10, e1001450.

Kanda, I., Nishimura, N., Nakatsuji, H., Yamamura, R., Nakanishi, H., and Sasaki, T. (2008). Involvement of Rab13 and JRAB/MICAL-L2 in epithelial cell scattering. *Oncogene* 27, 1687-1695.



Ketting, R.F., Fischer, S., Bernstein, E., Sijen, T., Hannon, G.J., and Plasterk, R. (2001). Dicer functions in RNA interference and in synthesis of small RNA involved in developmental timing in *C. elegans*. *Genes & Dev* 15, 2654-2659.

Kirkland, S.C. (1985). Dome Formation by a Human Colonie Adenocarcinoma Cell Line (HCA-7). *Cancer Research*.

Klumperman, J., and Raposo, G. (2014). The complex ultrastructure of the endolysosomal system. *Cold Spring Harb Perspect Biol* 6, a016857.

Kogure, T., Yan, I.K., Lin, W.L., and Patel, T. (2013). Extracellular Vesicle-Mediated Transfer of a Novel Long Noncoding RNA TUC339: A Mechanism of Intercellular Signaling in Human Hepatocellular Cancer. *Genes & cancer* 4, 261-272.

Kohler, K., Louvard, D., and Zahraoui, A. (2004). Rab13 regulates PKA signaling during tight junction assembly. *J Cell Biol* 165, 175-180.

Koles, K., Nunnari, J., Korkut, C., Barria, R., Brewer, C., Li, Y., Leszyk, J., Zhang, B., and Budnik, V. (2012). Mechanism of evenness interrupted (Evi)-exosome release at synaptic boutons. *J Biol Chem* 287, 16820-16834.

Koppers-Lalic, D., Hackenberg, M., Bijnsdorp, I.V., van Eijndhoven, M.A., Sadek, P., Sie, D., Zini, N., Middeldorp, J.M., Ylstra, B., de Menezes, R.X., *et al.* (2014). Nontemplated nucleotide additions distinguish the small RNA composition in cells from exosomes. *Cell Rep* 8, 1649-1658.

Korpal, M., Lee, E.S., Hu, G., and Kang, Y. (2008). The miR-200 family inhibits epithelial-mesenchymal transition and cancer cell migration by direct targeting of E-cadherin transcriptional repressors ZEB1 and ZEB2. *J Biol Chem* 283, 14910-14914.

Kosaka, N., Iguchi, H., Yoshioka, Y., Takeshita, F., Matsuki, Y., and Ochiya, T. (2010). Secretory mechanisms and intercellular transfer of microRNAs in living cells. *J Biol Chem* **285**, 17442-17452.

Kowal, J., Arras, G., Colombo, M., Jouve, M., Morath, J.P., Primdal-Bengtson, B., Dingli, F., Loew, D., Tkach, M., and Thery, C. (2016). Proteomic comparison defines novel markers to characterize heterogeneous populations of extracellular vesicle subtypes. *Proc Natl Acad Sci U S A* **113**, E968-977.

Kroh, E.M., Parkin, R.K., Mitchell, P.S., and Tewari, M. (2010). Analysis of circulating microRNA biomarkers in plasma and serum using quantitative reverse transcription-PCR (qRT-PCR). *Methods* **50**, 298-301.

Lamber, E.P., Siedenburg, A.C., and Barr, F.A. (2019). Rab regulation by GEFs and GAPs during membrane traffic. *Curr Opin Cell Biol* **59**, 34-39.

Lan, J., Sun, L., Xu, F., Liu, L., Hu, F., Song, D., Hou, Z., Wu, W., Luo, X., Wang, J., *et al.* (2019). M2 Macrophage-Derived Exosomes Promote Cell Migration and Invasion in Colon Cancer. *Cancer Res* **79**, 146-158.

Langemeyer, L., and Barr, F.A. (2012). Analysis of rab GTPases. *Curr Protoc Cell Biol* *Chapter 15*, Unit 15 18.

Langemeyer, L., Nunes Bastos, R., Cai, Y., Itzen, A., Reinisch, K.M., and Barr, F.A. (2014). Diversity and plasticity in Rab GTPase nucleotide release mechanism has consequences for Rab activation and inactivation. *Elife* **3**, e01623.

Lee, R.C., Feinbaum, R.L., and Ambros, V. (1993). The *C. elegans* heterochronic gene *lin-4* encodes small RNAs with antisense complementarity to *lin-14*. *Cell* **75**, 843-854.

Lee, Y., Ahn, C., Han, J., Choi, H., Kim, J., Yim, J., Lee, J., Provost, P., Radmark, O., Kim, S., *et al.* (2003). The nuclear RNase III Drosha initiates microRNA processing. *Nature* 425, 415-419.

Lee, Y.S., Nakahara, K., Pham, J.W., Kim, K., He, Z., Sontheimer, E.J., and Carthew, R.W. (2004). Distinct roles for *Drosophila* Dicer-1 and Dicer-2 in the siRNA/miRNA silencing pathways. *Cell* 117, 69-81.

Li, C., Ma, H., Wang, Y., Cao, Z., Graves-Deal, R., Powell, A.E., Starchenko, A., Ayers, G.D., Washington, M.K., Kamath, V., *et al.* (2014). Excess PLAC8 promotes an unconventional ERK2-dependent EMT in colon cancer. *J Clin Invest* 124, 2172-2187.

Li, Y.Y., Tao, Y.W., Gao, S., Li, P., Zheng, J.M., Zhang, S.E., Liang, J., and Zhang, Y. (2018). Cancer-associated fibroblasts contribute to oral cancer cells proliferation and metastasis via exosome-mediated paracrine miR-34a-5p. *EBioMedicine* 36, 209-220.

Lippincott-Schwartz, G.W.G.a.J. (2009). New roles for endosomes: from vesicular carriers to multi-purpose platforms. *Molecular Cell Biology*.

Liu, J., Carmell, M.A., Rivas, F.V., Marsden, C.G., Thomson, J.M., Song, J.J., Hammond, S.M., Joshua-Tor, L., and Hannon, G.J. (2004). Argonaute2 is the catalytic engine of mammalian RNAi. *Science* 305, 1437-1441.

Lu, Y., Zhao, X., Liu, Q., Li, C., Graves-Deal, R., Cao, Z., Singh, B., Franklin, J.L., Wang, J., Hu, H., Yang, M., *et al.* (2017). lncRNA MIR100HG-derived miR-100 and miR-125b mediate Cetuximab resistance via Wnt/beta catenin signaling. *Nature Medicine* *in press*.

Lund, E., Guttinger, S., Calado, A., Dahlberg, J.E., and Kutay, U. (2004). Nuclear export of microRNA precursors. *Science* 303, 95-98.

Lv, M.M., Zhu, X.Y., Chen, W.X., Zhong, S.L., Hu, Q., Ma, T.F., Zhang, J., Chen, L., Tang, J.H., and Zhao, J.H. (2014). Exosomes mediate drug resistance transfer in MCF-7 breast cancer cells and a probable mechanism is delivery of P-glycoprotein. *Tumour Biol* 35, 10773-10779.

Maas, S.L.N., Breakefield, X.O., and Weaver, A.M. (2016). Extracellular Vesicles: Unique Intercellular Delivery Vehicles. *Trends in Cell Biology*.

Majidi, M., Hubbs, A., and Lichy, J. (1998). Activation of Extracellular Signal-regulated Kinase 2 by a Novel Abl-binding Protein, ST5. *The Journal of Biological Chemistry*.

Marc Ruiz-Martinez, A.N., Ramón M. Marrades, Sandra Santasusagna, Carmen Muñoz, Josep Ramírez, Nuria Viñolas, Laureano Molins, Mariano Monzo (2016). YKT6 expression, exosome release, and survival in non-small cell lung cancer. *Oncotarget*.

Martin, T.A., and Jiang, W.G. (2009). Loss of tight junction barrier function and its role in cancer metastasis. *Biochim Biophys Acta* 1788, 872-891.

Marzesco, A.M., Dunia, I., Pandjaitan, R., Recouvreur, M., Dauzonne, D., Benedetti, E.L., Louvard, D., and Zahraoui, A. (2002). The small GTPase Rab13 regulates assembly of functional tight junctions in epithelial cells. *Mol Biol Cell* 13, 1819-1831.

Mateescu, B., Kowal, E.J., van Balkom, B.W., Bartel, S., Bhattacharyya, S.N., Buzas, E.I., Buck, A.H., de Candia, P., Chow, F.W., Das, S., *et al.* (2017). Obstacles and opportunities in the functional analysis of extracellular vesicle RNA - an ISEV position paper. *J Extracell Vesicles* 6, 1286095.

Matsumura, T., Sugimachi, K., Inuma, H., Takahashi, Y., Kurashige, J., Sawada, G., Ueda, M., Uchi, R., Ueo, H., Takano, Y., *et al.* (2015). Exosomal microRNA in serum is a novel biomarker of recurrence in human colorectal cancer. *Br J Cancer* 113, 275-281.

McConnell, R.E., Higginbotham, J.N., Shifrin, D.A., Jr., Tabb, D.L., Coffey, R.J., and Tyska, M.J. (2009). The enterocyte microvillus is a vesicle-generating organelle. *J Cell Biol* 185, 1285-1298.

McGrath JP, C.D., Smith DH, Chen EY, Seeburg PH, Goeddel DV, Levinson AD. (1983). Structure and organization of the human Ki-ras proto-oncogene and a related processed pseudogene. *Nature* 304.

McKenzie, A.J., Hoshino, D., Cha, D.J., Franklin, J.L., Coffey, R.J., Patton, J.G., and Weaver, A.M. (2016). KRAS-MEK signaling controls Ago2 and miRNA sorting into exosomes. *Cell Reports* 15: 978-987.

McPherson, M.S.I.a.P.S. (2016). Regulation of Cancer Cell Behavior by the Small GTPase Rab13. *The Journal of Biological Chemistry*.

Melo, S.A., Sugimoto, H., O'Connell, J.T., Kato, N., Villanueva, A., Vidal, A., Qiu, L., Vitkin, E., Perelman, L.T., Melo, C.A., *et al.* (2014). Cancer exosomes perform cell-independent microRNA biogenesis and promote tumorigenesis. *Cancer Cell* 26, 707-721.

Mercer, T.R., Dinger, M.E., Bracken, C.P., Kolle, G., Szubert, J.M., Korbie, D.J., Askarian-Amiri, M.E., Gardiner, B.B., Goodall, G.J., Grimmond, S.M., *et al.* (2010). Regulated post-transcriptional RNA cleavage diversifies the eukaryotic transcriptome. *Genome Res* 20, 1639-1650.

Misale, S., Di Nicolantonio, F., Sartore-Bianchi, A., Siena, S., and Bardelli, A. (2014). Resistance to anti-EGFR therapy in colorectal cancer: from heterogeneity to convergent evolution. *Cancer Discov* 4, 1269-1280.

Mittelbrunn, M., Gutierrez-Vazquez, C., Villarroya-Beltri, C., Gonzalez, S., Sanchez-Cabo, F., Gonzalez, M.A., Bernad, A., and Sanchez-Madrid, F. (2011). Unidirectional transfer of microRNA-loaded exosomes from T cells to antigen-presenting cells. *Nat Commun* 2, 282.

Miyake, K., Shibata, T., Ohto, U., Shimizu, T., Saitoh, S.I., Fukui, R., and Murakami, Y. (2018). Mechanisms controlling nucleic acid-sensing Toll-like receptors. *Int Immunol* 30, 43-51.

Montecalvo, A., Larregina, A.T., Shufesky, W.J., Stolz, D.B., Sullivan, M.L., Karlsson, J.M., Baty, C.J., Gibson, G.A., Erdos, G., Wang, Z., *et al.* (2012). Mechanism of transfer of functional microRNAs between mouse dendritic cells via exosomes. *Blood* 119, 756-766.

Moreno-Gonzalo, O., Villarroya-Beltri, C., and Sınchez-Madrid, F. (2014). Post-Translational Modifications of Exosomal Proteins. *Frontiers in Immunology* 5.

Muralidharan-Chari, V., Clancy, J., Plou, C., Romao, M., Chavrier, P., Raposo, G., and D'Souza-Schorey, C. (2009). ARF6-regulated shedding of tumor cell-derived plasma membrane microvesicles. *Curr Biol* 19, 1875-1885.

Nabhan, J.F., Hu, R., Oh, R.S., Cohen, S.N., and Lu, Q. (2012). Formation and release of arrestin domain-containing protein 1-mediated microvesicles (ARMs) at plasma membrane by recruitment of TSG101 protein. *Proc Natl Acad Sci U S A* 109, 4146-4151.

Nakayama, M.S.a.K.I. (2006). Protrudin Induces Neurite Formation by Directional Membrane Trafficking. *Science*.

Neeft M, W.M., de Jong AS, Negroiu G, Metz CHG, van Loon A, Griffith J, Krijgsveld J, Wulfraat N, Koch H, Heck AJR, Brose N, Kleijmeer M, van der Sluijs P (2005). Munc13-4 is an Effector of Rab27a and Controls Secretion of Lysosomes in Hematopoietic Cells. *Molecular Biology of the Cell*.

Noerholm, M., Balaj, L., Limperg, T., Salehi, A., Zhu, L.D., Hochberg, F.H., Breakefield, X.O., Carter, B.S., and Skog, J. (2012). RNA expression patterns in serum microvesicles from patients with glioblastoma multiforme and controls. *BMC cancer* 12, 22.

Nokes, R.L., Fields, I.C., Collins, R.N., and Folsch, H. (2008). Rab13 regulates membrane trafficking between TGN and recycling endosomes in polarized epithelial cells. *J Cell Biol* 182, 845-853.

Nolte-'t Hoen, E.N., Buermans, H.P., Waasdorp, M., Stoorvogel, W., Wauben, M.H., and t Hoen, P.A. (2012). Deep sequencing of RNA from immune cell-derived vesicles uncovers the selective incorporation of small non-coding RNA biotypes with potential regulatory functions. *Nucleic Acids Res* 40, 9272-9285.

Ochieng, J., Pratap, S., Khatua, A.K., and Sakwe, A.M. (2009). Anchorage-independent growth of breast carcinoma cells is mediated by serum exosomes. *Exp Cell Res* 315, 1875-1888.

Okoye, I.S., Coomes, S.M., Pelly, V.S., Czieso, S., Papayannopoulos, V., Tolmachova, T., Seabra, M.C., and Wilson, M.S. (2014). MicroRNA-containing T-regulatory-cell-derived exosomes suppress pathogenic T helper 1 cells. *Immunity* 41, 89-103.

Ono, M., Kosaka, N., Tominaga, N., Yoshioka, Y., Takeshita, F., Takahashi, R.U., Yoshida, M., Tsuda, H., Tamura, K., and Ochiya, T. (2014). Exosomes from bone marrow mesenchymal stem cells contain a microRNA that promotes dormancy in metastatic breast cancer cells. *Sci Signal* 7, ra63.

Orban, T.I., and Izaurralde, E. (2005). Decay of mRNAs targeted by RISC requires XRN1, the Ski complex, and the exosome. *RNA* 11, 459-469.

Ortega-Carrion, A., and Vicente-Manzanares, M. (2016). Concerning immune synapses: a spatiotemporal timeline. *F1000Res* 5.

Ostrowski, M., Carmo, N.B., Krumeich, S., Fanget, I., Raposo, G., Savina, A., Moita, C.F., Schauer, K., Hume, A.N., Freitas, R.P., *et al.* (2010). Rab27a and Rab27b control different steps of the exosome secretion pathway. *Nat Cell Biol* 12, 19-30; sup pp 11-13.

Paolillo, M., and Schinelli, S. (2017). Integrins and Exosomes, a Dangerous Liaison in Cancer Progression. *Cancers (Basel)* 9.

Pasquinelli, A.E., Reinhart, B.J., Slack, F., Martindale, M.Q., Kuroda, M.I., Maller, B., Hayward, D.C., Ball, E.E., Degan, B., Muller, P., *et al.* (2000). Conservation of the sequence and temporal expression of let-7 heterochronic regulatory RNA. *Nature* *408*, 86-89.

Pegtel, D.M., Cosmopoulos, K., Thorley-Lawson, D.A., Eijndhoven, M.A.J.v., Hopmans, E.S., Lindenberg, J.L., Gruijl, T.D.d., Würdinger, T., and Middeldorp, J.M. (2010). Functional delivery of viral miRNAs via exosomes. *Proceedings of the National Academy of Sciences* *107*, 6328-6333.

Peinado, H., Aleckovic, M., Lavotshkin, S., Matei, I., Costa-Silva, B., Moreno-Bueno, G., Hergueta-Redondo, M., Williams, C., Garcia-Santos, G., Ghajar, C., *et al.* (2012). Melanoma exosomes educate bone marrow progenitor cells toward a pro-metastatic phenotype through MET. *Nat Med* *18*, 883-891.

Pfeffer, S.R. (2017). Rab GTPases: master regulators that establish the secretory and endocytic pathways. *Mol Biol Cell* *28*, 712-715.

Pfriege, F.W., and Vitale, N. (2018). Cholesterol and the journey of extracellular vesicles. *J Lipid Res* *59*, 2255-2261.

Phuyal, S., Skotland, T., Hessvik, N.P., Simolin, H., Overbye, A., Brech, A., Parton, R.G., Ekroos, K., Sandvig, K., and Llorente, A. (2015). The ether lipid precursor hexadecylglycerol stimulates the release and changes the composition of exosomes derived from PC-3 cells. *J Biol Chem* *290*, 4225-4237.

Plebanek, M.P., Angeloni, N.L., Vinokour, E., Li, J., Henkin, A., Martinez-Marin, D., Filleur, S., Bhowmick, R., Henkin, J., Miller, S.D., *et al.* (2017). Pre-metastatic cancer exosomes induce immune surveillance by patrolling monocytes at the metastatic niche. *Nat Commun* *8*, 1319.



Poliseno, L., Salmena, L., Zhang, J., Carver, B., Haveman, W.J., and Pandolfi, P.P. (2010). A coding-independent function of gene and pseudogene mRNAs regulates tumour biology. *Nature* **465**, 1033-1038.

Qu, L., Ding, J., Chen, C., Wu, Z.J., Liu, B., Gao, Y., Chen, W., Liu, F., Sun, W., Li, X.F., *et al.* (2016). Exosome-Transmitted IncARSR Promotes Sunitinib Resistance in Renal Cancer by Acting as a Competing Endogenous RNA. *Cancer Cell* **29**, 653-668.

Quinn, J.F., Patel, T., Wong, D., Das, S., Freedman, J.E., Laurent, L.C., Carter, B.S., Hochberg, F., Van Keuren-Jensen, K., Huentelman, M., *et al.* (2015). Extracellular RNAs: development as biomarkers of human disease. *J Extracell Vesicles* **4**, 27495.

Rahajeng, J., Giridharan, S.S., Cai, B., Naslavsky, N., and Caplan, S. (2012). MICAL-L1 is a tubular endosomal membrane hub that connects Rab35 and Arf6 with Rab8a. *Traffic* **13**, 82-93.

Rai, A., Greening, D.W., Chen, M., Xu, R., Ji, H., and Simpson, R.J. (2019). Exosomes Derived from Human Primary and Metastatic Colorectal Cancer Cells Contribute to Functional Heterogeneity of Activated Fibroblasts by Reprogramming Their Proteome. *Proteomics* **19**, e1800148.

Raposo, G., Nijman, H.W., Stoorvogel, W., Liejendekker, R., Harding, C.V., Melief, C.J., and Geuze, H.J. (1996). B lymphocytes secrete antigen-presenting vesicles. *J Exp Med* **183**, 1161-1172.

Raposo, G., and Stoorvogel, W. (2013). Extracellular vesicles: exosomes, microvesicles, and friends. *J Cell Biol* **200**, 373-383.

Ratajczak, J., Miekus, K., Kucia, M., Zhang, J., Reca, R., Dvorak, P., and Ratajczak, M.Z. (2006a). Embryonic stem cell-derived microvesicles reprogram hematopoietic progenitors: evidence for horizontal transfer of mRNA and protein delivery. *Leukemia* **20**, 847-856.

Ratajczak, J., Wysoczynski, M., Hayek, F., Janowska-Wieczorek, A., and Ratajczak, M.Z. (2006b). Membrane-derived microvesicles: important and underappreciated mediators of cell-to-cell communication. *Leukemia* 20, 1487-1495.

Redzic, J.S., Kendrick, A.A., Bahmed, K., Dahl, K.D., Pearson, C.G., Robinson, W.A., Robinson, S.E., Graner, M.W., and Eisenmesser, E.Z. (2013). Extracellular vesicles secreted from cancer cell lines stimulate secretion of MMP-9, IL-6, TGF-beta1 and EMMPRIN. *PLoS One* 8, e71225.

Rehwinkel, J.A.N., Behm-Ansmant, I., Gatfield, D., and Izaurralde, E. (2005). A crucial role for GW182 and the DCP1:DCP2 decapping complex in miRNA-mediated gene silencing. *RNA* 11, 1640-1647.

Ridder, K., Keller, S., Dams, M., Rupp, A.K., Schlaudraff, J., Del Turco, D., Starmann, J., Macas, J., Karpova, D., Devraj, K., *et al.* (2014). Extracellular vesicle-mediated transfer of genetic information between the hematopoietic system and the brain in response to inflammation. *PLoS Biol* 12, e1001874.

Rinn, J.L., and Chang, H.Y. (2012). Genome Regulation by Long Noncoding RNAs. *Annu Rev Biochem* 81, 145-166.

Robbins, P.D., and Morelli, A.E. (2014). Regulation of immune responses by extracellular vesicles. *Nature reviews* 14, 195-208.

Rose M. Johnstone, M.A., James R. Hammond, Linda Orr, and Claire Turbide (1987). Vesicle Formation during Reticulocyte Maturation

ASSOCIATION OF PLASMA MEMBRANE ACTIVITIES WITH RELEASED VESICLES (EXOSOMES). *The Journal of Biological Chemistry* 262, 9412-9420.

Sahgal S, A.J., Icha J, Paatero I, Hamidi H, Arjonen A, Pietila M, Rokka A, Ivaska J (2019). GGA2 and RAB13 promote activity-dependent B1-integrin recycling. *Journal of Cell Science*.

Sakha, S., Muramatsu, T., Ueda, K., and Inazawa, J. (2016). Exosomal microRNA miR-1246 induces cell motility and invasion through the regulation of DENND2D in oral squamous cell carcinoma. *Sci Rep* 6, 38750.

Santangelo, L., Giurato, G., Cicchini, C., Montaldo, C., Mancone, C., Tarallo, R., Battistelli, C., Alonzi, T., Weisz, A., and Tripodi, M. (2016). The RNA-Binding Protein SYNCRIP Is a Component of the Hepatocyte Exosomal Machinery Controlling MicroRNA Sorting. *Cell Rep* 17, 799-808.

Sato, Y., Goto, Y., Narita, N., and Hoon, D.S. (2009). Cancer Cells Expressing Toll-like Receptors and the Tumor Microenvironment. *Cancer Microenviron* 2 *Suppl* 1, 205-214.

Schlienger, S., Campbell, S., and Claing, A. (2014). ARF1 regulates the Rho/MLC pathway to control EGF-dependent breast cancer cell invasion. *Mol Biol Cell* 25, 17-29.

Schmausser, B., Andrulis, M., Endrich, S., Muller-Hermelink, H.K., and Eck, M. (2005). Toll-like receptors TLR4, TLR5 and TLR9 on gastric carcinoma cells: an implication for interaction with *Helicobacter pylori*. *Int J Med Microbiol* 295, 179-185.

Schmidt, O., and Teis, D. (2012). The ESCRT machinery. *Curr Biol* 22, R116-120.

Schooley, A.M., Andrews, N.M., Zhao, H., and Addison, C.L. (2012). beta1 integrin is required for anchorage-independent growth and invasion of tumor cells in a context dependent manner. *Cancer letters* 316, 157-167.

Schorey, J.S., Cheng, Y., Singh, P.P., and Smith, V.L. (2015). Exosomes and other extracellular vesicles in host-pathogen interactions. *EMBO Rep* 16, 24-43.

Schwarz, D.S., Hutvagner, G., Du, T., Xu, Z., Aronin, N., and Zamore, P.D. (2003). Asymmetry in the assembly of the RNAi enzyme complex. *Cell* 115, 199-208.

Sharma, P., Mesci, P., Carromeu, C., McClatchy, D.R., Schiapparelli, L., Yates, J.R., 3rd, Muotri, A.R., and Cline, H.T. (2019). Exosomes regulate neurogenesis and circuit assembly. *Proc Natl Acad Sci U S A* *116*, 16086-16094.

Shechner, D.M., Hacısuleyman, E., Younger, S.T., and Rinn, J.L. (2015). Multiplexable, locus-specific targeting of long RNAs with CRISPR-Display. *Nat Methods* *12*, 664-670.

Shifrin, D.A., Jr., Demory Beckler, M., Coffey, R.J., and Tyska, M.J. (2013). Extracellular vesicles: communication, coercion, and conditioning. *Mol Biol Cell* *24*, 1253-1259.

Shirasawa, S., Furuse, M., Yokoyama, N., and Sasazuki, T. (1993). Altered growth of human colon cancer cell lines disrupted at activated Ki-ras. *Science* *260*, 85-88.

Shurtleff, M.J., Temoche-Diaz, M.M., Karfilis, K.V., Ri, S., and Schekman, R. (2016). Y-box protein 1 is required to sort microRNAs into exosomes in cells and in a cell-free reaction. *Elife* *5*.

Simons, M., and Raposo, G. (2009). Exosomes--vesicular carriers for intercellular communication. *Curr Opin Cell Biol* *21*, 575-581.

Singh, B., and Coffey, R.J. (2014). Trafficking of epidermal growth factor receptor ligands in polarized epithelial cells. *Annu Rev Physiol* *76*, 275-300.

Skog, J., Würdinger, T., van Rijn, S., Meijer, D.H., Gainche, L., Sena-Esteves, M., Curry, W.T., Carter, B.S., Krichevsky, A.M., and Breakefield, X.O. (2008). Glioblastoma microvesicles transport RNA and proteins that promote tumour growth and provide diagnostic biomarkers. *Nature cell biology* *10*, 1470-1476.

Sotelo, J.R., and Porter, K.R. (1959). An electron microscope study of the rat ovum. *J Biophys Biochem Cytol* *5*, 327-342.

Squadrito, Mario L., Baer, C., Burdet, F., Maderna, C., Gilfillan, Gregor D., Lyle, R., Ibberson, M., and De Palma, M. (2014). Endogenous RNAs Modulate MicroRNA Sorting to Exosomes and Transfer to Acceptor Cells. *Cell Reports* *8*, 1432-1446.

Statello, L., Maugeri, M., Garre, E., Nawaz, M., Wahlgren, J., Papadimitriou, A., Lundqvist, C., Lindfors, L., Collen, A., Sunnerhagen, P., *et al.* (2018). Identification of RNA-binding proteins in exosomes capable of interacting with different types of RNA: RBP-facilitated transport of RNAs into exosomes. *PLoS One* *13*, e0195969.

Stenmark, H. (2009). Rab GTPases as coordinators of vesicle traffic. *Nat Rev Mol Cell Biol* *10*, 513-525.

Sung, B.H., and Weaver, A.M. (2017). Exosome secretion promotes chemotaxis of cancer cells. *Cell adhesion & migration* *11*, 187-195.

Szczepanski, M.J., Szajnik, M., Welsh, A., Whiteside, T.L., and Boyiadzis, M. (2011). Blast-derived microvesicles in sera from patients with acute myeloid leukemia suppress natural killer cell function via membrane-associated transforming growth factor-beta1. *Haematologica* *96*, 1302-1309.

Tabet, F., Vickers, K.C., Cuesta Torres, L.F., Wiese, C.B., Shoucri, B.M., Lambert, G., Catherinet, C., Prado-Lourenco, L., Levin, M.G., Thacker, S., *et al.* (2014). HDL-transferred microRNA-223 regulates ICAM-1 expression in endothelial cells. *Nature communications* *5*.

Takahashi, K., Yan, I.K., Kogure, T., Haga, H., and Patel, T. (2014a). Extracellular vesicle-mediated transfer of long non-coding RNA ROR modulates chemosensitivity in human hepatocellular cancer. *FEBS Open Bio* *4*, 458-467.

Takahashi, K., Yan, I.K., Wood, J., Haga, H., and Patel, T. (2014b). Involvement of extracellular vesicle long noncoding RNA (linc-VLDLR) in tumor cell responses to chemotherapy. *Mol Cancer Res* *12*, 1377-1387.

Takahashi, S., Kubo, K., Waguri, S., Yabashi, A., Shin, H.W., Katoh, Y., and Nakayama, K. (2012). Rab11 regulates exocytosis of recycling vesicles at the plasma membrane. *J Cell Sci* *125*, 4049-4057.

Tamai, K., Tanaka, N., Nakano, T., Kakazu, E., Kondo, Y., Inoue, J., Shiina, M., Fukushima, K., Hoshino, T., Sano, K., *et al.* (2010). Exosome secretion of dendritic cells is regulated by Hrs, an ESCRT-0 protein. *Biochem Biophys Res Commun* 399, 384-390.

Tambini, A., Ketz, N., and Davachi, L. (2010). Enhanced brain correlations during rest are related to memory for recent experiences. *Neuron* 65, 280-290.

Tauro, B.J., Greening, D.W., Mathias, R.A., Mathivanan, S., Ji, H., and Simpson, R.J. (2013). Two distinct populations of exosomes are released from LIM1863 colon carcinoma cell-derived organoids. *Mol Cell Proteomics* 12, 587-598.

Temoche-Diaz, M.M., Shurtleff, M.J., Nottingham, R.M., Yao, J., Fadadu, R.P., Lambowitz, A.M., and Schekman, R. (2019). Distinct mechanisms of microRNA sorting into cancer cell-derived extracellular vesicle subtypes. *Elife* 8.

They, C. (2011). Exosomes: secreted vesicles and intercellular communications. *F1000 biology reports* 3, 15.

They, C., Boussac, M., Veron, P., Ricciardi-Castagnoli, P., Raposo, G., Garin, J., and Amigorena, S. (2001). Proteomic analysis of dendritic cell-derived exosomes: a secreted subcellular compartment distinct from apoptotic vesicles. *J Immunol* 166, 7309-7318.

They, C., Regnault, A., Garin, J., Wolfers, J., Zitvogel, L., Ricciardi-Castagnoli, P., Raposo, G., and Amigorena, S. (1999). Molecular characterization of dendritic cell-derived exosomes. Selective accumulation of the heat shock protein hsc73. *J Cell Biol* 147, 599-610.

They, C., Witwer, K.W., Aikawa, E., Alcaraz, M.J., Anderson, J.D., Andriantsitohaina, R., Antoniou, A., Arab, T., Archer, F., Atkin-Smith, G.K., *et al.* (2018). Minimal information for studies of extracellular vesicles 2018 (MISEV2018): a position statement of the International Society for Extracellular Vesicles and update of the MISEV2014 guidelines. *J Extracell Vesicles* 7, 1535750.

Tkach, M., and They, C. (2016). Communication by Extracellular Vesicles: Where We Are and Where We Need to Go. *Cell* 164, 1226-1232.

Trajkovic, K., Hsu, C., Chiantia, S., Rajendran, L., Wenzel, D., Wieland, F., Schwille, P., Brugger, B., and Simons, M. (2008). Ceramide triggers budding of exosome vesicles into multivesicular Endosomes. *Science* 319, 1244-1247.

Turchinovich, A., Weiz, L., Langheinz, A., and Burwinkel, B. (2011). Characterization of extracellular circulating microRNA. *Nucleic Acids Res* 39, 7223-7233.

Valadi, H., Ekstrom, K., Bossios, A., Sjostrand, M., Lee, J.J., and Lotvall, J.O. (2007). Exosome-mediated transfer of mRNAs and microRNAs is a novel mechanism of genetic exchange between cells. *Nat Cell Biol* 9, 654-659.

Valenti, R., Huber, V., Filipazzi, P., Pilla, L., Sovena, G., Villa, A., Corbelli, A., Fais, S., Parmiani, G., and Rivoltini, L. (2006). Human tumor-released microvesicles promote the differentiation of myeloid cells with transforming growth factor-beta-mediated suppressive activity on T lymphocytes. *Cancer Res* 66, 9290-9298.

van der Grein, S.G., and Nolte-'t Hoen, E.N. (2014). "Small Talk" in the Innate Immune System via RNA-Containing Extracellular Vesicles. *Front Immunol* 5, 542.

Van, I.S.C., Van Der Wouden, J.M., Liebisch, G., Schmitz, G., and Hoekstra, D. (2004). Polarized membrane traffic and cell polarity development is dependent on dihydroceramide synthase-regulated sphinganine turnover. *Mol Biol Cell* 15, 4115-4124.

van Niel, G., Raposo, G., Candalh, C., Boussac, M., Hershberg, R., Cerf-Bensussan, N., and Heyman, M. (2001). Intestinal epithelial cells secrete exosome-like vesicles. *Gastroenterology* 121, 337-349.

Vickers, K.C., Palmisano, B.T., Shoucri, B.M., Shamburek, R.D., and Remaley, A.T. (2011). MicroRNAs are transported in plasma and delivered to recipient cells by high-density lipoproteins. *Nat Cell Biol* 13, 423-433.

Villarroya-Beltri, C., Gutierrez-Vazquez, C., Sanchez-Cabo, F., Perez-Hernandez, D., Vazquez, J., Martin-Cofreces, N., Martinez-Herrera, D.J., Pascual-Montano, A., Mittelbrunn, M., and Sanchez-Madrid, F. (2013a). Sumoylated hnRNPA2B1 controls the sorting of miRNAs into exosomes through binding to specific motifs. *Nat Commun* 4, 2980.

Villarroya-Beltri, C., Gutiérrez-Vázquez, C., Sánchez-Cabo, F., Pérez-Hernández, D., Vázquez, J., Martin-Cofreces, N., Martinez-Herrera, D.J., Pascual-Montano, A., Mittelbrunn, M., and Sánchez-Madrid, F. (2013b). Sumoylated hnRNPA2B1 controls the sorting of miRNAs into exosomes through binding to specific motifs. *Nature communications* 4, 2980.

Vitale, G., Rybin, V., Christoforides, S., P., T., McCaffrey, M., Stenmark, H., and Zerial, M. (1998). Distinct Rab-binding domains mediate the interaction of Rabaptin-5 with GTP-bound rab4 and rab5. *EMBO J*.

Vu, L.T., Peng, B., Zhang, D.X., Ma, V., Mathey-Andrews, C.A., Lam, C.K., Kiomourtzis, T., Jin, J., McReynolds, L., Huang, L., *et al.* (2019). Tumor-secreted extracellular vesicles promote the activation of cancer-associated fibroblasts via the transfer of microRNA-125b. *J Extracell Vesicles* 8, 1599680.

Walsh, R.B., Becalska, A.N., Zunitch, M.J., Wang, S., Isaac, B., Yeh, A., Koles, K., and Rodal, A.A. (2019). Opposing functions for retromer and Rab11 in extracellular vesicle cargo traffic at synapses. *bioRxiv*, 645713.

Wang, J., Vasaikar, S., Shi, Z., Greer, M., and Zhang, B. (2017). WebGestalt 2017: a more comprehensive, powerful, flexible and interactive gene set enrichment analysis toolkit. *Nucleic Acids Res*.



Webber, J.P., Spary, L.K., Sanders, A.J., Chowdhury, R., Jiang, W.G., Steadman, R., Wymant, J., Jones, A.T., Kynaston, H., Mason, M.D., *et al.* (2015). Differentiation of tumour-promoting stromal myofibroblasts by cancer exosomes. *Oncogene* *34*, 290-302.

Wei, Z., Batagov, A.O., Schinelli, S., Wang, J., Wang, Y., El Fatimy, R., Rabinovsky, R., Balaj, L., Chen, C.C., Hochberg, F., *et al.* (2017). Coding and noncoding landscape of extracellular RNA released by human glioma stem cells. *Nat Commun* *8*, 1145.

White, I.J., Bailey, L.M., Aghakhani, M.R., Moss, S.E., and Futter, C.E. (2006). EGF stimulates annexin 1-dependent inward vesiculation in a multivesicular endosome subpopulation. *EMBO J* *25*, 1-12.

Williams, C., Royo, F., Aizpurua-Olaizola, O., Pazos, R., Boons, G.J., Reichardt, N.C., and Falcon-Perez, J.M. (2018). Glycosylation of extracellular vesicles: current knowledge, tools and clinical perspectives. *J Extracell Vesicles* *7*, 1442985.

Wilusz, J.E., Freier, S.M., and Spector, D.L. (2008). 3' end processing of a long nuclear-retained noncoding RNA yields a tRNA-like cytoplasmic RNA. *Cell* *135*, 919-932.

Wong, R., and Cunningham, D. (2008). Using predictive biomarkers to select patients with advanced colorectal cancer for treatment with epidermal growth factor receptor antibodies. *J Clin Oncol* *26*, 5668-5670.

Worst, T.S., Meyer, Y., Gottschalt, M., Weis, C.A., von Hardenberg, J., Frank, C., Steidler, A., Michel, M.S., and Erben, P. (2017). RAB27A, RAB27B and VPS36 are downregulated in advanced prostate cancer and show functional relevance in prostate cancer cells. *International journal of oncology* *50*, 920-932.

Wortzel, I., Dror, S., Kenific, C.M., and Lyden, D. (2019). Exosome-Mediated Metastasis: Communication from a Distance. *Dev Cell* *49*, 347-360.

Wu, C., Agrawal, S., VasANJI, A., Drazba, J., Sarkaria, S., Xie, J., Welch, C.M., Liu, M., Anand-Apte, B., and Horowitz, A. (2011a). Rab13-dependent trafficking of RhoA is required for directional migration and angiogenesis. *J Biol Chem* 286, 23511-23520.

Wu, X., Bradley, M.J., Cai, Y., Kummel, D., De La Cruz, E.M., Barr, F.A., and Reinisch, K.M. (2011b). Insights regarding guanine nucleotide exchange from the structure of a DENN-domain protein complexed with its Rab GTPase substrate. *Proc Natl Acad Sci U S A* 108, 18672-18677.

Yamamura, R., Nishimura, N., Nakatsuji, H., Arase, S., and Sasaki, T. (2008). The interaction of JRAB/MICAL-L2 with Rab8 and Rab13 coordinates the assembly of tight junctions and adherens junctions. *Mol Biol Cell* 19, 971-983.

Yi, R., Qin, Y., Macara, I.G., and Cullen, B.R. (2003). Exportin-5 mediates the nuclear export of pre-microRNAs and short hairpin RNAs. *Genes Dev* 17, 3011-3016.

Yoshimura, S., Egerer, J., Fuchs, E., Haas, A.K., and Barr, F.A. (2007). Functional dissection of Rab GTPases involved in primary cilium formation. *J Cell Biol* 178, 363-369.

Yoshimura, S., Gerondopoulos, A., Linford, A., Rigden, D.J., and Barr, F.A. (2010). Family-wide characterization of the DENN domain Rab GDP-GTP exchange factors. *J Cell Biol* 191, 367-381.

Yuan, T., Huang, X., Woodcock, M., Du, M., Dittmar, R., Wang, Y., Tsai, S., Kohli, M., Boardman, L., Patel, T., *et al.* (2016). Plasma extracellular RNA profiles in healthy and cancer patients. *Sci Rep* 6, 19413.

Zerial, M., and McBride, H. (2001). Rab Proteins as Membrane Organizers. *Nature Reviews Molecular Cell Biology*.

Zhang, H., Freitas, D., Kim, H.S., Fabijanic, K., Li, Z., Chen, H., Mark, M.T., Molina, H., Martin, A.B., Bojmar, L., *et al.* (2018). Identification of distinct nanoparticles and subsets of extracellular vesicles by asymmetric flow field-flow fractionation. *Nat Cell Biol* 20, 332-343.

Zhang, H.G., and Grizzle, W.E. (2011). Exosomes and cancer: a newly described pathway of immune suppression. *Clin Cancer Res* 17, 959-964.

Zhang, J., Li, S., Li, L., Li, M., Guo, C., Yao, J., and Mi, S. (2015). Exosome and exosomal microRNA: trafficking, sorting, and function. *Genomics Proteomics Bioinformatics* 13, 17-24.

Zhang, Q., Higginbotham, J.N., Jeppesen, D.K., Yang, Y.P., Li, W., McKinley, E.T., Graves-Deal, R., Ping, J., Britain, C.M., Dorsett, K.A., *et al.* (2019). Transfer of Functional Cargo in Exomeres. *Cell Rep* 27, 940-954 e946.

Zhang, S., Zhang, Y., Qu, J., Che, X., Fan, Y., Hou, K., Guo, T., Deng, G., Song, N., Li, C., *et al.* (2017). Exosomes promote cetuximab resistance via the PTEN/Akt pathway in colon cancer cells. *Braz J Med Biol Res* 51, e6472.

Zhang, Y., Yang, L., and Chen, L.L. (2014). Life without A tail: new formats of long noncoding RNAs. *Int J Biochem Cell Biol* 54, 338-349.

Zhou, W., Fong, M.Y., Min, Y., Somlo, G., Liu, L., Palomares, M.R., Yu, Y., Chow, A., O'Connor, S.T., Chin, A.R., *et al.* (2014). Cancer-secreted miR-105 destroys vascular endothelial barriers to promote metastasis. *Cancer Cell* 25, 501-515.

Zomer, A., Maynard, C., Verweij, F.J., Kamermans, A., Schafer, R., Beerling, E., Schiffelers, R.M., de Wit, E., Berenguer, J., Ellenbroek, S.I., *et al.* (2015). In Vivo imaging reveals extracellular vesicle-mediated phenocopying of metastatic behavior. *Cell* 161, 1046-1057.

Zomer, A., Vendrig, T., Hopmans, E.S., van Eijndhoven, M., Middeldorp, J.M., and Pegtel, D.M. (2010). Exosomes: Fit to deliver small RNA. *Communicative & integrative biology* 3, 447-450.